NEW CONDUCTOMETRIC DETECTION METHODS FOR SENSITIVE ION CHROMATOGRAPHIC MEASUREMENT OF WEAK ELECTROLYTES

by

HONGZHU LIAO

Presented to the Faculty of the Graduate School of

The University of Texas at Arlington in Partial Fulfillment

of the Requirements

for the Degree of

DOCTOR OF PHILOSOPHY

THE UNIVERSITY OF TEXAS AT ARLINGTON

DECEMBER 2015

Acknowledgements

At first, I would like to deeply thank my mentor, Dr. Purnendu K. Dasgupta, for his guidance and support during this long journey of my doctoral program. He accepted me when I had no good background of analytical chemistry. His wide and deep knowledge in science and unyielding spirit inspired me to overcome many barriers. One of the most important lessons I learnt from him is how to solve a problem in a much better way than previous efforts. He also gave me the chances to try something I proposed, even failed in the end. I would not make good achievements without his guidance and support. I would also like to deeply thank my committee members, Dr. Daniel W. Armstrong, Dr. Kevin A. Schug, and Dr. Kannan Srinivasan for their constructive criticism and valuable suggestions in my research. Dr. Armstrong always said 'Life is a balance' in the separation science course. For me, it means health, family, and career. As a young tenured professor, Dr. Schug is an excellent chemist, who inspires our graduate students to move forward. Dr. Srinivasan from Thermo-Scientific Inc. provides good suggestions about my research, supports consumable materials in IC system and builds specific designs in my different projects.

I would like to thank Dr. Charles Phillip Shelor, Dr. Yongjing Chen, and Dr. Abul K. Azad. They just like my second mentors in different times. Especially, Dr. Phillip Shelor gave me a lot of immediate help and suggestions in many of my projects. I would also like to thank the following visiting scholars, post-doctors and transfer students from China. They are Dr. Bingcheng Yang, Dr. Mingli Chen, Dr. Mijun Peng, Dr. Yinhuan Li, Dr. Jianxiu Du, Dr. Hong Shen, Dr. Weixiong Huang, Dr. Min Zhang, Dr. Yong Tian and Dr. Ting (Tina) Yang. They provided many good suggestions about my study, research, and life, even after going back to China. I would also like to thank Brian Stamos, Chuchu

Qing, Akinde Florence Kadjo, and all other group members for their help and support. I also want to thank my dear friends who are in the same PhD program. We encourage each other and help each other.

I also want to thanks Jill Howard, Debbie Cooke, Barbara J. Smith, Dr. William Cleaver, and Jim Garner for their assistance on providing laboratory supplies, research facilities and paperwork. To all the others, though you have not been named, you are no less important.

Especially, I would like to thank my wife Caihong (Rebecca) Chen. She flight over the Pacific with courage and got married with a poor young boy. She trusts me and supports me. Besides, I am thankful to my parents and my grandma (both sides) for their love, trust, and support over the years. I am also so thankful to my dear brothers and sisters, friends, and relatives for their love and support all the time.

November 10, 2015

Abstract

NEW CONDUCTOMETRIC DETECTION METHODS FOR ION CHROMATOGRAPHIC MEASUREMENT OF WEAK ELECTROLYTES

Hongzhu Liao, PhD

The University of Texas at Arlington, 2015

Supervising Professor: Purnendu K. Dasgupta

Since Suppressed conductometric anion chromatography (SCAC) was proposed in the mid-1970s, SCAC has become a widely used tool for the determination of anion species in aqueous samples. Its application ranges from trace analysis in semiconductor manufacture to pharmaceutical analysis. This dissertation primarily focuses on three different projects on the conductometric determination of weak acids. Other work carried out during the same period both involved SCAC for the determination of anion composition of açaí Extracts and on the unusual ion exchange behavior of myo-inositol phosphates.

SCAC responds poorly and nonlinearly to weak acids, because they only ionize partially and the degree of ionization change as a function of pK_a and concentration. Various efforts to improve conductometric detection of weak acids have been proposed. The best results have come from the introduction from a small constant amount of base after the suppressed conductometric detection (D1). The acid form of analyte HA can react with the equivalent base solution to produce the corresponding salt and the

conductivity is measured again (D2). This second signal arises from the difference of the conductance of A^- and OH^- as the overall process is $HA + OH^- \rightarrow A^- + H_2O$.

The use of a readily available commercial ICS-5000 IC system that contains two independently operable ion chromatographs provided facile implementation of such a scheme. SCAC was carried out in the analytical channel to separate different anions. After D1, LiOH generated by a capillary scale electrodialytic generator was introduced into the main stream by different mixers designed and built in-house, including a back-flow tee mixer (BT), an end-blocked membrane tee mixer (EMT), and a tubular membrane mixer (TM). Based on its mixing efficiency and small dispersion, the BT design was found to be the best to perform sensitive determination of weak acids at D2.

Using the same principle of reacting HA with OH^-, a volatile analyte transfer device (VATD) of annular tubular design was fabricated to assist the transfer and enrichment of volatile weak acids. Volatile weak acids can transfer across a gas permeable membrane from the outer annular channel of VATD to the central channel. As this scheme is dilutionless and does not involve mixing of two liquids, the baseline noise at D2 reduced ≥100x, compared with previous efforts, resulting in a proportionate improvement in the limits of detection. The VATD is a robust low-noise device providing highly sensitive conductometric detection of volatile weak acids like sulfide and cyanide.

The third project provided complementarity to the second one. Because the majority of weak acids are not volatile, this time a permeative amine introduction device (PAID) was used to introduce a volatile base into the effluent weak acid stream. Diethylamine was chosen as the amine source due to its low pK_b value (3.0) and high vapor pressure. The eluites were thus detected against a low diethylammonium hydroxide background (5-31 μS/cm) as negative peaks. The PAID as described here is a robust low-noise design to allow sensitive conductometric detection of weak acids.

Table of Contents

List of Illustrations

List of Tables

Chapter 1

Introduction

1.1 Background

Ion chromatography (IC) has become the benchmark for anion analysis in aqueous samples. Its application ranges from trace analysis in semiconductor manufacture[1] to pharmaceutical analysis.[2] IC is a term used to describe three different liquid chromatography techniques, including ion-exchange chromatography, ion-exclusion chromatography, and ion-interaction chromatography (also termed ion-pair chromatography or paired-ion chromatography).[3] The typical analytes of these methods include common inorganic anions, low molecular weight organic acids, alkali metal cations, alkaline-earth metal cations, and amines.[3,4] In recent years, the application of IC has extended to the analysis of other analyte groups, like carbohydrate and amino acids,[5,6,7] carbohydrates are very weak acids that ionize significantly at pH $\geq$12. The common detection methods in IC include conductivity (suppressed[8] and non-suppressed[9]), amperometry[10,11] and spectrophotometry (direct[12] and indirect[13]). Post-column reactions for signal enhancement are also applied with these methods.[14,15]

1.2 ion-exchange chromatography

1.2.1 Ion exchanger resin

Ion exchanger resin consists of three different parts. The first is the substrate, the most widely used is styrene based organic polymers. Early on, silica-based exchanges were used in chromatography but their limited pH stability have long led to such substrates being abandoned. The second component are the fixed ionic sites, which are typically covalently bonded to the substrates. Finally are the exchangeable counter-ions, which hold on to the fixed ionic sites and exactly neutralize the charge from the fixed sites. These counter-ions can be replaced by other counter-ions of the same charge sign

although one counter-ion may have more or less affinity for the fixed ionic sites; this is indeed the basis of chromatographic separation of different ions on an ion exchanger.

Ion exchanger resins based on poly(styrene-divinylbenzene) (PS-DVB) and poly(ethylvinylbenzene-divinylbenzene) (EVB-DVB) are the most widely used substrates for chromatographic ion exchangers packings. These materials are characterized by their good physical and chemical stabilities. The PS-DVB polymer is schematically represented in Figure 1-1. The ion exchanger is mainly made of polystyrene. Some amount of DVB is added to crosslink the linear chain of styrene polymer. A higher percent of DVB produces a more rigid polymer resin bead. Compared to common gel-type ion exchange resins, a much greater amount of DVB is typically used in chromatographic resins to enable high pressure use. The substrate is then converted to an ion exchanger by introducing suitable functional groups into the polymer substrates.

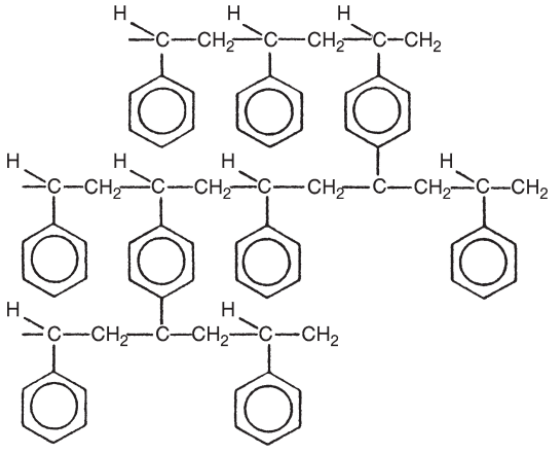

Figure 1-1 Schematic representation of a PS-DVB copolymer. (from ref. [4]).

Ion exchangers are either anion exchangers in which the fixed ionic sites are positively charged, or cation exchangers in which the fixed ionic sites carry a negative charge. Strongly acidic cation exchanger typically contain sulfonic acid groups while weakly acidic cation exchanger typically contain carboxylic acid and/or phosphonic acid

groups. Strongly basic anion exchanger and weakly basic anion exchanger are respectively composed of quaternary amine groups and less substituted amine groups.

1.2.2 Principle of ion exchange

An anion-exchange column contains ion exchange resins with fixed cationic groups, while a cation-exchange column contains ion exchange resins with fixed anion groups. In the following, the ion exchange process is illustrated by an anion-exchange system. The anion exchanger can be represented as R^+E^-, where R^+ is positively-charged resin and E^- is the eluent anion. When a negative-charged analyte (A^-) flows through the anion exchanger, A^- can be attracted by the positively-charged resin R^+ due to electrostatic interaction. There is a competitive relationship between E^- and A^-. Certain amount of E^- will be exchanged by A^- after reaching equilibrium, as shown in Equation 1-1:

$$R^+E^- + A^- \rightleftarrows R^+A^- + E^- \quad (1\text{-}1)$$

The ion exchange is stoichiometric since both eluent solution and ion exchange resin need must remain electroneutral. Even if analyte A^- may have a higher affinity than eluent anion E^-, the analyte A^- can be eluted from the resin bed by applying a high concentration of E^- or flowing E^- for an extended period. The relevant equilibrium constant for this competitive process is referred to as the selectivity coefficient, *K(A,E)*:

$$K(A,E) = \frac{[A_R^-]}{[A_M^-]} \times \frac{[E_M^-]}{[E_R^-]} \quad (1\text{-}2)$$

Where the parentheses indicate the activities of each species, A^- and E^- can be either in the column resin (R) or in the mobile phase (M). This equation can be further generalized to multivalent anions as following:

$$K(A,E) = \frac{[A_R^{x-}]^y}{[A_M^{x-}]^y} \times \frac{[E_M^{y-}]^x}{[E_R^{y-}]^x} \quad (1\text{-}3)$$

Where x^- is the charge on A and y^- is the charge on E.

Different analytes have different selectivity coefficients for a given ion exchange column. The higher the selectivity coefficient of analyte, the more strongly it will be retained and longer will be the retention time. Analyte anions will elute at different retention times and thus be separated due to different degrees of affinity for the column resin. The separation mechanism for cation exchange is similar.

1.2.3 Non-suppressed conductivity detection

When two electrodes are inserted into an electrolyte solution and an ac potential is applied across the electrodes, an electrical current can results. Based on Ohm's Law, the resistance of solution between the electrodes can be given by Equation 1-4:

$$R=U/I \quad (1\text{-}4)$$

Where R is the resistance in ohm (Ω), U is the applied voltage in volt (V), and I is the current in ampere (A). The conductance of a solution, G, has the SI unit Siemens (S). It is simply the reciprocal of the resistance of the solution:

$$G=1/R \quad (1\text{-}5)$$

Given a particular measurement cell, the conductance of the solution is determined by the type and the concentration of ionic species in the solution, and the temperature of solution. The conductivity detector is the most widely used universal detector in IC, because conductivity is a universal property of all ions and only ions. Due to temperature effect, the conductivity detector applied in IC systems need to be well temperature-controlled. Generally, a temperature sensor containing the conductivity cell is used to measure and correct for the temperature dependence of the conductance. A typical correction coefficient of conductivity is +1.7% per °C.

All ions in the solution contribute the conductance. The total conductance signal depends on the all ionic species present and their limiting equivalent conductance (λ) in cm^2*S/mol. The tables of λ for different ionic species are available in publications.[3,16]

Frist, let us consider the background conductance of the eluent in an anion chromatography system. For simplicity let us assume that the eluent is fully dissociated and contains only one type of cation (E^+) and one type of anion (E^-). The background conductance of the eluent (E) can be given as:

$$G_{Background} = \frac{(\lambda_E{}^+ + \lambda_E{}^-)\, C_E}{10^{-3} K} \quad (1\text{-}6)$$

Where C_E is the formal concentration of eluent in mol/L, $\lambda_E{}^+$ and $\lambda_E{}^-$ are the respective limiting equivalent conductance of E^+ and E^-, K in cm^{-1} is the cell constant of conductivity detector (equal to the distance between two electrodes (in cm) divided by the surface area of each identical electrodes (in cm^2). Now consider that our analyte A^- is fully ionized. Whatever cation it is associated with when it is injected, the cation will not be retained by the anion exchange column and will rapidly exit the system. When the analyte anion A^- eventually elutes, let us assume that the peak concentration is C_A. Before analyte elution eluent cation and anion concentration were both C_E; nothing has happened to affect the eluent cation concentration. So if an anion A^- of concentration C_A has now appeared, the concentration of the eluent anion must have decreased to C_E-C_A to maintain electroneutrality. The total conductance now will thus be given by:

$$G_{Total} = \frac{\lambda_E{}^+ C_E + \lambda_E{}^-(C_E - C_A) + \lambda_A{}^- C_A}{10^{-3} K} \quad (1\text{-}7)$$

Where $\lambda_A{}^-$ is the limiting equivalent conductance of A^-. The change of conductance corresponding to the elution of analyte is the signal and is equal then to the difference of expressions in equations 1-6 and 1-7:

$$G_{Signal} = G_{Total} - G_{Background} = \frac{(\lambda_A{}^- - \lambda_E{}^-)\, C_A}{10^{-3} K} \quad (1\text{-}8)$$

If eluent E is only partially dissociated, Equation 1-6 can be easily modified as:

$$G_{Background} = \frac{(\lambda_E{}^+ + \lambda_E{}^-)\ C_E f_E}{10^{-3}K} \quad (1\text{-}9)$$

Where f_E is the degree of dissociation of eluent. The lower the f_E value, the lower the background signal and thus the lower the baseline noise. If both eluent and analyte are only partly dissociated, then the modified form can be given by Equation 1-10[17]:

$$G_{Signal} = \left(\frac{(\lambda_E{}^+ - \lambda_A{}^-) - (\lambda_E{}^+ + \lambda_E{}^-) f_E}{10^{-3}K}\right) f_A C_A \quad (1\text{-}10)$$

Where f_A is the degree of dissociation of analyte. The conductance signal G_{Signal} is directly related to f_A value. The conductivity signal G_{Signal} increases as f_E decreases. A low f_E value is desirable in non-suppressed conductivity detection for both reducing the background signal and increasing analyte signal.

1.2.4 Suppressed conductivity detection

1.2.4.1 Principle of suppression

Eluent suppression is a post-column reaction which can reduce the eluent background while enhancing the analyte signal of an anionic analyte by converting them to the corresponding acids (for all but very weak acids with $pK_a \geq 7.0$). As a result, detection limits are largely improved. The concept of suppression was first proposed by Small et al. in 1975.[8] The first version was a packed-column suppressor. The reaction in the suppressor for anion chromatography can be summarized as the following equations:

$$R\text{-}SO_3H + NaOH\ (eluent) \rightarrow R\text{-}SO_3Na + H_2O \quad (1\text{-}11)$$

$$R\text{-}SO_3H + NaA\ (analyte) \rightarrow R\text{-}SO_3Na + HA \quad (1\text{-}12)$$

Where R is the resin substrates, $-SO_3H$ is sulfonic acid group. The ion exchange between Na^+ and H^+ converts eluent NaOH into H_2O and thus the background is largely reduced, and converts analyte NaA into HA and thus the signal is enhanced due to the highest limiting equivalent conductance of hydronium ion $\lambda_{H}{}^+$. If total suppression occurs, the background conductance from water dissociation is <0.1 μS/cm. Since eluent has

converted into water, the conductance of an eluting analyte is only contributed by H^+ and A^-, given by Equation 1-13:

$$G_{Signal} = \frac{(\lambda_H^+ + \lambda_A^-)\, C_A f_A}{10^{-3} K} \quad (1\text{-}13)$$

1.2.4.2 Developments in suppressor technology

Chemical suppressor for IC was first introduced in 1975 by Small et al.[8] It is an ion exchange resin packed-column originally referred to as “stripper”. The two principal limitations of the packed-column suppressor were: (a) the requirement of frequent offline regeneration with a stream of strong acid when its capacity had been exhausted, followed by copious washing with water to remove the residual acid, and (b) considerable peak dispersion due to its large volume. Variations in retention times of weak acids as a function of the degree of suppressor exhaustion was also observed.

A multi-bundle hollow fiber suppressor with a jacket tube was introduced in 1981 by Stevens et al.[18] The eluent flowed through the lumen of a bundle of tubular ion exchange membranes while the regenerant, sulfuric acid, flowed through the outer jacket continuously, in a countercurrent mode. The hollow fiber suppressor allows continuous operation without offline regeneration. However, these early hollow fiber suppressors had very limited capacity, high pressure drops and caused very substantial peak broadening. Stevens et al. later found that the mass transfer of ions was improved when inert beads were packed into the fiber.[19] By reducing the void volume of hollow fiber suppressor, the band dispersion was reduced and resolution was improved. This was the first commercialized form of the fiber suppressor. However, its performance related to band broadening, dead volume, and backpressure became worse with time. In use, the initially uniformly placed beads packed in a single file became non-uniform because of the elastomeric nature of the membrane fiber and the propensity of the beads to move down

to form clumps in places while leaving voids in others, exacerbated by pulsating reciprocating pumps then in use. Eventually they will rupture where the beads have formed a significant clump, stretching the membrane locally and thus weakening it. Dasgupta proposed the annular helical suppressor in 1984.[20,21] A nylon monofilament was inserted into a Nafion cation exchange membrane (CEM) tube and then the whole was coiled into a small diameter helical form and thermoset to maintain the shape. The efficiency of mass transfer of ions from eluent stream to the regenerant stream was greatly improved. It provided high efficient exchange and low dispersion volume for anion chromatography. In 1985, Dasgupta et al. introduced a dual membrane annular helical suppressor with a high ion exchange capacity and low dispersion volume.[22] One filament-filled CEM tube was inserted into a second closely fitting CEM tube in the same type. The whole was coiled into a small diameter helical shape and the shape was kept by the filament after thermosetting. The eluent stream flows in the annular space between the two membranes while regenerant flows through the innermost channel and the outer jacket tube. This device can provide a larger available membrane surface area per unit flow-through volume of suppressor, relative to the previous designs.

Planar membrane suppressor was proposed in 1985 by Stillian.[23] Rather than fibers, flat sheets of ion exchange membranes were used, permitting a greater area for ion exchange for a given device length. The commercialized planar membrane suppressor, called a MicroMembrane Suppressor (MMS), was introduced in 1991 by Dionex.[24] This type of suppressor has large ion exchange capacity, minimal void volume (<50 μL) and thus results in good peak efficiency and small band dispersion. As in previous designs, a chemical regenerant need to be supplied continuously. Without careful choice of the regenerant, it can penetrate through the ion exchange membrane

into the eluent stream, which increases the eluent background and reduces the detection sensitivity, especially for weak acid analytes.

The ion exchange process of both fiber suppressor and planar membrane suppressor is based on diffusion transport that is driven by the proton gradient across the membrane. Electric field acceleration of the ion exchange process was proposed by Tian et al.[25] However, in practice their devices still required a relatively high concentration of sulfuric acid as the regenerant. The first electrodialytic membrane suppressor, using only water as regenerant, was introduced by Dasgupta et al. in 1989.[26] A platinum-wire-filled Nafion perfluorosulfonate membrane tube was inserted into another perfluorosulfonate membrane tube and then the whole was coiled into a helical design. The whole helical assembly was inserted into an outer jacket (stainless still tube) packed with granular conductive carbon. An alkaline eluent, e.g., Na_2CO_3 or NaOH flowed in the annular space between the two membranes and pure water flowed in the outer jacket and the inner membrane channels, both countercurrent to the eluent stream. A DC voltage (typically 3-8 V) was applied between the carbon bed and the central platinum wire. H^+ and oxygen gas was produced by water electrolysis at the anode side as follows:

$$H_2O - 2e^- \rightarrow 2H^+ + 1/2O_2 \quad (1\text{-}15)$$

Similarly, a corresponding amount OH^- was produced at the cathode side:

$$2H_2O + 2e^- \rightarrow H_2 + 2OH^- \quad (1\text{-}16)$$

The electrical field direction promotes the migration of anodically generated H^+ through the CEM into the annular eluent channel, thus neutralizing eluent anion OH^- into water while eluent cation Na^+ migrates through the other CEM to the cathode side. The ion replacement of Na^+ by H^+ converted eluent Na_2CO_3 or NaOH into H_2CO_3 or H_2O. At the same time, the analyte was converted from the sodium salt to the corresponding acid

form. The regenerant water flows can carry out hydrogen gas and oxygen gas produced in the innermost and outermost channels to waste.

Based on the same principle, Dionex Corp introduced a commercially available electrodialytic membrane suppressor, termed as “Self Regenerating Suppressor”(SRS) .[27] No external acid regenerant was required to achieve the suppression purpose. Basically, the SRS is very similar to previous MMS design, but a Platinum screen electrode was added in each external channel as cathode and anode, respectively. The eluent flowed through the middle channel between two CEMs, while an external water source was fed into the regenerant channels to carry the electrodialytically produced base and the electrolytic H_2 and O_2 gas to the waste as shown in Figure 1-2, in a direction countercurrent to that of the eluent flow. Eluent NaOH was converted into H_2O and analyte NaA is converted into HA. The SRS addressed the limitations of the previous chemical suppressor by achieving continuous suppression only using water as regenerant. The “recycle mode”, where the suppressed eluent stream is fed back as the regenerant source, is commonly used due to simplify the operation and eliminates the need for a separate regenerant pump. However, for trace analysis using fresh water as the regenerant, termed as “external water mode”, is the method of choice for providing lower baseline noise levels, relative to the “recycle mode”. The use of “gas-augmented recycle mode” can allow rapid removal of the liquid and electrolytic gases assisted by inert gas, such as helium or nitrogen, offering noise performance similar to the “external water mode”.[28] In an SRS anion suppressor, the transport of hydronium ions to the cathode determines the current efficiency. The ion exchange capacity of the central eluent screen plays an important role in determining the current efficiency of a given electrolytic suppressor device. The higher the ion exchange capacity of the eluent screen,

the lower the current efficiency. The noise performance was improved by applying only the current required for full suppression.

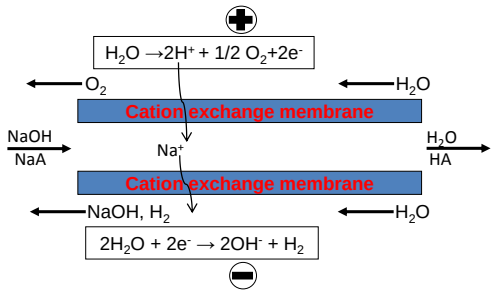

Figure 1-2 An Anion Self Regenerating Suppressor (ASRS) schematic.

After a series of SRS versions,[29] Dionex Corporation introduced a commercially available electrolytically regenerated packed-bed suppressor, termed as “Atlas electrolytic suppressor (AES) in 2001.[30] The AES contains six cation exchange monolith disks and five flow distributor disks. The monolith disks and flow distributor disks are alternately sandwiched between two CEMs. The placement of these disks is such that a serpentine flow pathway is created to increase the effective residence time of the eluent in the suppression bed. As a consequence, the current efficiency and the dynamic suppression capacity of the suppressor are increased.

In 2013, the Thermo Scientific Dionex introduced the new generation suppressor, termed as “Electrolytically Regenerated Suppressor” (ERS) 500.[31] ERS 500 can tolerate at least 500 psi backpressure, which is good for adding post-suppressor devices. The eluent chamber is filled with a planar packed-bed of ion-exchange resin instead of a piece of cation exchange screen to improve start-up time and static capacity. There are many other different types of suppressors, like packed-column mini-suppressor[32] and continuously regenerated packed-column suppressor[33], etc. These have been reviewed by Haddad et al.[17]

1.3 Conductivity signal enhancement of weak acids in previous efforts

As discussed earlier, suppressed anion chromatography provides poor sensitivity to weak acids. Very weak acids with $pK_a \geq 7.0$ can be hardly detected by SCAC. However, the determination of weak acids is important in many fields, including food analysis, environmental analysis, and pharmaceutical analysis, etc.

1.3.1 Ion replacement reaction after suppression

Many different efforts to detect these weakly dissociated acids better have been made for some time; this has been reviewed by Karu et al.[34] Tanaka and Fritz proposed the conversion of carbonic acid to $KHCO_3$ and then to KOH by first using a cation exchange column in K^+-form and then an anion exchange column in OH^- form, in the context of ion-exclusion chromatography.[35] Relative to detection as H_2CO_3, the sensitivity of the determination was improved by an order to magnitude. Following the same strategy, Dasgupta et al. described a post-suppression conversion of weak acid HA into NaOH in two sequential ion-exchange steps (HA→NaA→ NaOH) in 1991.[36] A membrane-based converter, consisting of a serially connected a cation-exchanger and an anion-exchanger membrane tube, was woven in a low dispersion design and bathed externally with NaOH solution. The converter was installed after the suppressed conductivity detector of a conventional NaOH eluent suppressed anion chromatography system and followed by a second conductivity detector. However, the HA to NaA conversion was very incomplete for very weak acids. As $[H^+]$ becomes low, a buffer was formed and the intended conversion was not particularly successful. The authors next tried a simultaneous conversion of the H^+ and A^- from the weak acid to Li^+ and F^- by a simultaneous cation/anion exchange step, exchanging H^+ for very labile Li^+ and exchanging the counter anion for very labile F^-.[37] The dual membrane converter device consisted of a cation-exchange membrane and an anion-exchange membrane. The

eluent stream goes through the central channel of the converter while the regenerant LiF goes through both the cation side and the anion side channels. Sensitivity to very weak acid improved relative to the previously described system involving sequential ion exchange to NaOH. However, due to the buffer formation, the overall conversion efficiency of very weak acids was still limited.

In 1997, this ion-replacement method was retried by Caliamanis et al.[38,39] The HA to NaA conversion was carried out in a commercially available anion mimcromembrane suppressor (AMMS) that is composed of two cation exchange membranes. The desired process was the conversion of HA to NaA. The Na^+-donating regenerant that the authors used was Na_2EDTA, the large multiply charged counter ion minimized regenerant penetration even when used at a high concentration. However, as in the previous efforts by Berglund and Dasgupta, the formation of a buffer inhibited ionization of HA, limiting this approach.

1.3.2 Indirect suppressed conductivity detection

Zhu et al. proposed indirect suppressed conductivity technique for weak acid determination.[40] They proposed an eluent containing NaCl with some (~3 mM) NaOH added, the eluent pH was ~11.5. A standard AMMS then exchanged all the Na^+ for H^+:

$$NaCl + NaOH + NaA \rightarrow HCl + H_2O + HA \quad (1\text{-}17)$$

Note that much like what was discussed for nonsuppressed detection, the appearance of A^- has a concomitant decrease in the concentrations of Cl^- and OH^- eluting from the column. On the right side of equation 1-17, the only conducting species is HCl and a decrease in chloride concentration thus appears as a negative dip. If HA is not so weak that its ionization can be completely neglected in the HCl background, the signal will depend not only the concentration of analyte but also the degree of dissociation f_A of analyte at that pH and the difference between λ_{A^-} and λ_{Cl^-}. The analytes included some

common organic acids and amino acids, but very weak acids with $pK_a \geq 7.0$ were not studied. Instead of chloride, sulfate and nitrate were also explored as eluents. The high background conductivity led to significant noise and the LODs of analytes were in the tens of μM. The eluent components and concentrations needed to be adjusted to meet the requirements of the separation and detection for different analytes. This method was thus rather complicated (too many variables) and has not been further developed.

1.3.3 Incomplete chemical suppressed conductivity detection

Huang et al. attempted incomplete suppression in 1999, in which the alkaline eluent was deliberately not completely neutralized by chemical suppression.[41] H_2SO_4 regenerant was provided at a concentration slightly lower than that required for complete suppression. At this incomplete suppression condition, weak acid analytes appeared as negative peaks on an elevated basic background conductivity. Only one commercially available micro-membrane suppressor was needed, so the dilution and band dispersion caused by the converter devices in previous efforts were eliminated. There are many drawbacks of this incomplete suppression method. Even after a long equilibration time (5 hours), it was still difficult to maintain a steady baseline and to achieve a reasonable noise level, even a small change in the environment could disturb the degree of "incompleteness". In addition, gradient eluent is not applicable for this method.

1.3.4 Two-dimensional detection after suppression and base introduction

Dasgupta and co-workers introduced two-dimensional conductivity detection after suppression and base introduction in IC system.[42,43,44] A small constant amount of NaOH (0.1 mM) was introduced into the effluent by a micro-electrodialytic NaOH generator (MENG) as shown in Figure 1-3. When the acid form of analyte HA passes through the MENG device, it can react with the equivalent NaOH to produce NaA. The net signal at

the second conductivity detector (D2), G_{D2}, is the difference between the base-line signal and the signal when the analyte pass through D2. The D2 signal for a monoprotic acid can be expressed as Equation 1-18:

$$G_{Signal} = \frac{(\lambda_{A^-} - \lambda_{OH^-})\, C_A f_A}{10^{-3} K} \quad (1\text{-}18)$$

The addition of a second detector makes this approach attractive. Strong acids produced a linear response on both detectors, but the response was much greater on the first detector. Weak acids with pK_a <9.5 produced a nonlinear and poor response on the first detector, but a good linear response on the second detector. Peak height and peak area ratio values from the two detector signals provided unique fingerprint for each analyte anion. The dual detection method was a useful tool for pK_a value evaluation of acids and peak identification beyond retention characteristics.[42,43] This method can be used to identify the occurrence of coelution. One of the major factors inhibiting the adoption of such a two-dimensional detection system has been the lack of commercially available equipment which will allow one to carry this technique without having to build special devices. One goal in this research was to be able to use commercially available equipment to practice this approach.

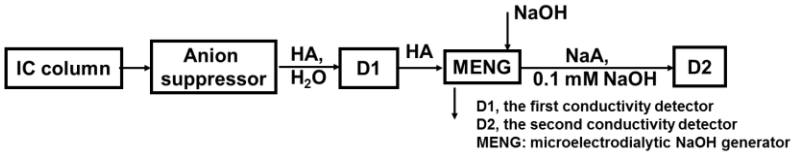

Figure 1-3 Sequential conductometry after suppression and base introduction with MENG device.

1.4 Research presented in this dissertation

IC provides a useful tool for measuring ionic species in aqueous samples. The overall objective in this dissertation is to develop new detection methods for IC and to

provide better conductometric detection of weak acids. Chapter 2 describes a developed method for the anion composition analysis of açaí fruit extract, including organic acid anions and common inorganic acid anions. Chapter 3 is to unveil the abnormal ion-exchange behavior of myo-inositol phosphates, including myo-inositol mono-, di-, tri-, tetra-, pentakis-, and hexakisphosphate. Chapter 4, 5, and 6 are different strategies to better detect weak acids, following the same base introduction technique. The contents of Chapter 2 have been published in *Journal of Agricultural and Food Chemistry* and those of Chapte 3-5 appear as three separate papers in *Analytical Chemistry*. The contents of Chapter 6 have been submitted.

1.4.1 Anion Composition of açaí Extracts

Many products labeled açaí are presently marketed as natural supplements with various claimed health benefits. Authentic açaí is expensive; as a result, numerous products labeled as containing açaí are being sold that actually contain little or no açaí. Authentic açaí samples from Brazil and Florida as well as several reputed açaí products were analyzed by suppressed conductometric anion chromatography. Columns with different selectivities were used to obtain a complete separation of all anions. Tandem mass spectrometry was used for confirmation of the less common ions. Quinate, lactate, acetate, formate, galacturonate, chloride, sulfate, malate, oxalate, phosphate, citrate, isocitrate, and myo-inositol hexakisphosphate (phytate) were found. Only the Florida açaí had detectable levels of hexanoate. No açaí sample had any detectable levels of tartrate, which is present in abundance in grape juice, the most common adulterant. The highly characteristic anion profile and in particular the absence of tartrate can readily be used to identify authentic açaí products. açaí from Florida had a 6 times greater level of phytate. The present analytical approach for phytate may be superior to extant methods.

1.4.2 Enigmatic Ion-Exchange Behavior of myo-Inositol Phosphates

The separation of myo-inositol mono-, di-, tri-, tetra-, pentakis-, and hexakisphosphate ($InsP_1$, $InsP_2$, $InsP_3$, $InsP_4$, $InsP_5$, $InsP_6$) was carried out using hydroxide eluent ion chromatography. Acid hydrolysis of $InsP_6$ (phytate) was used to prepare a distribution of InsP's, ranging from $InsP_1$ to $InsP_5$'s and including unhydrolyzed $InsP_6$. Counting all possible positional isomers (many of which have stereoisomers that will not be separable by conventional ion exchange), 40 chromatographically separable peaks are possible; up to 22 were separated and identified by mass spectrometry. InsP's show unusual ion exchange behavior in two respects: (a) the retention order is not monotonically related with the charge on the ion and (b) at the same hydroxide eluent concentration, retention is greatly dependent on the eluent metal cation. The retention of $InsP_3$ −$InsP_6$ was determined to be controlled by steric factors while elution was influenced by eluent cation complexation. These highly phosphorylated InsP's have a much greater affinity for alkali metals ($Li^+ > Na^+ > K^+$) than quaternary ammonium ions. This difference in cation affinity was exploited to improve separation through the use of a tetramethylammonium hydroxide−sodium hydroxide gradient.

1.4.3 Mixing Characteristics of Mixers in Flow Analysis: Application to Two-Dimensional Detection in Ion Chromatography

Three mixer designs, a back-flow tee mixer (BT), an end-blocked membrane tee mixer (EMT), and a tubular membrane mixer (TM), were fabricated and compared to three commercially available mixers, Visco-Jet Micro mixer (VJM) and HS binary tee mixer with 2 and 10 μL volume (HS-2 and HS-10) mixing cartridges. Internal volumes ranged from 8.3 to 20.3 μL. Performance characteristics were evaluated by the Villermaux−Dushman reaction, noise in baseline conductance upon mixing an electrolyte solution with water, and dispersion/relative dispersion of an injected solute. No single

characteristic would uniquely qualify a particular device. In typical postcolumn use when a small reagent flow is added to a principal flow stream using a low-pulsation high end chromatographic pump, with the worst of these mixers, imperfect mixing accounted for 99.6% of the observed noise. EMT, BT, and TM with asymmetric inlets provided better mixing performances relative to VJM, HS-2, and HS-10 with symmetric inlet ports, especially when the secondary liquid flow rate was much lower than the principal stream-flow rate. Dispersion per unit residence time was singularly large for HS-2. Based on its mixing efficiency and small dispersion, the BT design was found to be the best for practicing postcolumn reaction. As an illustrative application, this was then used to introduce electrogenerated LiOH in a suppressed ion chromatography system to perform sensitive detection of weak acids in a second dimension.

1.4.4 Concurrent High-Sensitivity Conductometric Detection of Volatile Weak Acids in a Suppressed Anion Chromatography System

A suppressed hydroxide eluent anion chromatograph effluent flows through the outside of a gas-permeable membrane tube while electrogenerated 100 −200 μM LiOH flows through the lumen into a second conductivity detector. Undissociated volatile acid eluites (e.g., H_2S, HCN, H_2CO_3, etc., represented as HA) transfer through the membrane and react as $OH^- + HA \rightarrow A^- + H_2O$; the conversion of highmobility OH^- to lower mobility A^- results in a significant negative response for these analytes. With the chromatograph operated at a macroscale (0.3 mL/min), the LiOH flow can be 3 −30-fold lower, resulting in corresponding enrichment of the transferred analyte prior to detection. Because there is no mixing of liquids, the detector noise is very low (<0.1 nS/cm), comparable to the principal chromatographic detector. Thus, despite a background of 25−45 μS/cm, limits of detection for sulfide and cyanide are in the submicromolar level, with a linear dynamic range up to 100 μM. Carbonate/ bicarbonate can also be sensitively detected. We

demonstrate adaptation in a standard commercial system. We also show that Microsoft Excel-based numerical simulations of transport quantitatively predict the observed behavior well.

1.4.5 Permeative Amine Introduction for Very Weak Acid Detection in Ion Chromatography

A permeative amine introduction device (PAID) is placed after a conventional KOH eluent suppressed conductometric anion chromatography (SCAC) system. The PAID converts the suppressed eluites from the acid form to the corresponding ammonium salt ($NR_2H + HA \rightarrow NR_2H_2^+ + A^-$) and allows very weak acids HA ($pK_a \geq 7.0$) that cannot normally be detected by SCAC to be measured by a second conductivity detector following the PAID. Permeative reagent introduction is dilutionless, can be operated without pumps and provides good mixing (baseline noise 0.8 nS/cm for 27 μM diethylamine) with low band dispersion (as small as 30 μL). Diethylamine (DEA) was chosen as the amine source due to its low pK_b value (pK_b 3.0), high vapor pressure, and low toxicity and low odor. The eluites are thus detected against a low diethylammonium hydroxide (DEAOH) background (5-31 μS/cm) as negative peaks, because the equivalent conductance of OH^- is greater than X^-. Reducing the background DEA concentration enhances the detectability of traces of weak acids. Lower background [DEA] will limit the maximum concentration of analyte acids that can be determined; a general concept of peak width measurement as a fixed height is proposed as a solution. Trace impurities formed during electrodialytic suppression play a role in background noise; for the first time we look at the nature of such impurities. Appearance of silicate in a sample put in a glass container as a function of pH can be readily followed. The maximum silica level in high purity type 1 water is 50 nM (1.40 parts per billion Si), which is a measurement

challenge in particular. A large injection volume (1 mL) permits detection limits of 21 nM silicate, 3 nM taurine, 3 nM sulfide, and 13 nM cyanide, respectively.

Chapter 2

Authentication of Açaí Extracts by Ion chromatographic Analysis

2.1 Introduction

Açaí palms (Euterpe oleraceae mart.) are native to Central and South America and grow from Belize to Peru and Brazil.[45] Most of the genuine commercial açaí come from the Brazilian Amazon rainforest; commercial cultivation has also begun in Florida. The berries range from green to dark purple in color and ~90% of the mass of the berry is the pit. The health and wellness benefit claims surrounding açaí straddle the border of fact and fantasy; cure-all claims are all too common. There is, however, credible evidence that it has very high antioxidant content,[46,47] can remove reactive oxygen species,[48] inhibit nitric oxide (NO) synthase[49] and cyclooxygenase (COX) -1 and -2,[50] protect human vascular endothelial cells against oxidative stress and inflammation,[51] and induce apoptosis in HL-60 leukemia cells in-vitro.[52] Indeed, the name açaí sells many products.

Despite many “açaí juice” products being on the market, strictly speaking, no “juice” can really be produced from the berry, if juice is defined as the aqueous product of squeezing the berry. Açaí is similar to olives in being oleaginous, oil, not juice, is produced on pressing. Instead, the outer portion of the fruit is scraped off the relatively large seed; water is then added to the berries to produce a purée that is often sold frozen. Depending on the amount of water added, açaí grosso (thick), médio (middle) or fino (fine) grades are produced, with the following respective amounts of total solids: >14%, 10-14% and <10%.[53] Authentic açaí products or supplements are expensive. They are also often sold in the freeze-dried form. Given the cost of the genuine product, the incentive for adulteration is high and given the perceived benefits, the market is significant. For other high-value products with perceived health benefits, such as

pomegranate juice, international authenticity specifications have been set.[54] There are many cautionary notes on the Web[55] and elsewhere regarding the authenticity of açaí products, and açaí berry scams have been the subjects of lawsuits by several state attorney generals in the US as well as the US Federal Trade Commission.[56]

At this time little data are available for the characteristic composition of açaí. Relative to other analysis techniques, suppressed conductometric anion chromatography (hereinafter called SCAC) provides rapid and sensitive analysis. Whereas reversed phase (RP) or ion-pair (IP) liquid chromatography may determine both ionic and nonionic species, this will make for a more complex chromatogram. On the other hand, with SCAC, the number of anionic analytes (the corresponding acids must have a pKa~<6 to be detected) is obviously more limited. Also, the RP or IP chromatography will obligatorily require an expensive mass spectrometer as a detector; as many of the analytes of interest (e.g., organic acids without unsaturated linkages) absorb poorly in the UV to be sensitively detected by optical absorption. In contrast, virtually all carboxylic acids ionize sufficiently in SCAC to be detected. In SCAC, the retention behavior of most of the anions is known for a number of different commercially available ion exchange columns, at least under some particular elution conditions, and can be predicted under most others.[57] If there are ions not identifiable on the basis of known retention behavior, they can be identified by tandem mass spectrometry (MS/MS). Once they are identified, further use of a mass spectrometer is not essential.

The ionic composition of açaí in general and its organic acid profile in particular have never previously been described. General approaches to the characterization of organic acid content of fruit (primarily grape) juices were reviewed some time ago.[58] This review tabulated conditions of liquid chromatographic (HPLC) and electrophoretic methods. Several gas chromatography (GC) methods were described early.[59,60]

Attractive techniques were developed to trap the analytes on anion exchange resins, methylate them in-situ and perform supercritical fluid extraction prior to GC analysis.[61] The general availability of GC-MS in many laboratories makes this particularly attractive; direct analysis without derivatization is possible in many cases.[62] Infrared spectroscopy, both in mid-IR[63,64] and near-IR,[19] have proven useful in determining major organic acids (and often other constituents) in a production setting.

These approaches are not without problems, many acids are thermally labile at GC temperatures and IR spectrometry is too insensitive to determine the acids present in lower levels. Liquid phase separations, especially HPLC, have therefore been primarily used for fingerprinting.[65] Capillary electrophoresis (CE) has been used for this analysis with[66] or without[67,68] prior derivatization but the use of HPLC has dominated this application.[69,70,71,72,73,74,75] Although some approaches use pre-derivatization prior to a reverse phase (RP) separation,[76] most do not.

Most reported approaches use reverse phase columns with a low pH eluent to keep the analyte acids significantly in the unionized form; the basic separation mechanism is ion exclusion[77,78] with stronger acids eluting first. Some approaches directly use strong acid form cation exchangers and a mineral acid eluent to accomplish the same ends.[79,80,81] Ion pairing agents such as tetrabutylammonium are applicable[70] but have not been commonly used. UV absorbance measurement singly[82] or simultaneously/sequentially at multiple wavelengths has been used[77,83,84,85,86,87,88,89] but suppressed conductivity and mass spectrometry provide much better limits of detection (LODs).

We aim in this work to characterize the anion profile of both Brazilian and Floridian açaí and thence to determine if this can be used for authentication.

2.2 Materials and Methods

Brazilian açaí berries were bought directly in a market in Belém, Pará, Brazil. They were washed and disinfected with chlorinated water, then transferred to pulping apparatus to obtain the edible portion (pulp + peel). Water was added to obtain "açaí médio", followed by freezing. The frozen pulp (including added water) was lyophilized in the author's laboratory in Rio de Janeiro to obtain a powder. Lyophilized açaí powder was also obtained from an açaí cultivation farm in Florida. Both samples were sent to the Kansas City district laboratories of the US Food and Drug Administration (FDA). Various other characterizations of these samples (e.g., lipid composition), not discussed here, were carried out at the FDA. Ion chromatographic analysis was conducted at the University of Texas at Arlington. In addition, a sample of white grape juice (brand W), a beverage sample labeled açaí (brand S, did not claim to be a juice and contained undissolved settled solids, only the decantate was used for analysis) and another labeled açaí-pomegranate juice (brand O) were bought from local grocery stores in Arlington, TX. Both the açaí-and the açaí-pomegranate juice were dark purple in color.

Accurately weighed samples (~28 mg) of the lyophilized açaí powders were transferred to a 25 mL volumetric flask, Milli-Q deionized water added to the mark, and the contents sonicated for 20 min. The liquid was divided into two equal portions and was then centrifuged at 7650 rpm for 20 min, followed by filtration through a 0.2 µm nylon syringe filter (13 mm). The filtered sample was diluted four-fold before IC analysis.

The store-bought "juice" samples were filtered through a Hi-Load C-18 Sep-Pak column (www.waters.com) and then a 0.2 µm syringe filter. The açaí-pomegranate juice and grape juice were diluted 200-fold while the açaí extract was diluted 100-fold prior to IC analysis.

Chromatography was conducted on an ICS2000 ion chromatograph, equipped with an ASRS Ultra II 2 mm anion self-regenerating SRS Suppressor and a CD 25 conductivity detector with a DS3-1 detector cell. Three different sets of guard and separator columns were examined for the desired separation: AG11+AS11, AG24+AS24, and AG15+AS15, all 2 mm in diameter. All of the above were from www.dionex.com. The sample injection volume was 20 µL. Gradients used on each column were optimized for the best separation; the KOH gradient elution programs used with each column set is presented in Table 2-1. The background conductivity was usually 0.8 to <3 µS/cm for gradients of 2.5-80 mM KOH.

Table 2-1. KOH gradient progams with IonPac AS11, AS15 and AS24 columns.

Time (min)	KOH (mM) on AS24	KOH (mM) on AS15	KOH (mM) on AS11	Suppressor Current (mA)
0	2.5	2.5	2.5	50
10	2.5	2.5	2.5	50
24	18.0	18.0	18.0	50
40	64.0	64.0	64.0	50
44	70.0	-	-	50
46	2.5	72.0	72.0	50
48	-	2.5	2.5	50
50	-	-	-	50
52	2.5	2.5	2.5	50

IC-MS/MS was performed using the AG24-AS24 column sets and a TSQ Quantum Discovery Max triple quadrupole mass spectrometer equipped with enhanced mass resolution and heated electrospray ionization probes. A model AS autosampler (all MS equipment from www.thermo.com) was used for convenience. The injection volume was 2 µL for selected ion monitoring (SIM) mode, while 25 µL was used to obtain high resolution and fragmentation spectra. Instrument parameters were: Electrospray voltage of 3 kV, vaporizer temperature: 350 °C, capillary temperature: 250 °C, skimmer offset: 0 V, collision gas pressure (fragmentation only): 1.5 mTorr, collision energy: 10 V and

chromatographic filter: 45 seconds. Thomson (Th) units are used for m/z hereinafter. For fragmentation of hexanoic acid in the scan-centroid mode, the parent ion was at 115 Th, the scan range was 30-114 Th over 0.200 s. For fragmentation of phytic acid in the scan-centroid mode, the parent ion was at 218.96 Th, the scan range for segment 1 was 30-218 Th over 0.200 s and that for segment 2 was 221-660 Th over 0.300 s. In both above cases Q1 and Q3 resolutions were 0.7 and 0.3 Th, respectively in full width half maximum (FWHM). The SIM/Profiling mode utilized Q1 and Q3 resolutions of 0.5 and 0.4 Th FWHM, respectively. The high resolution scan for the phytic acid in profile mode used Q1 resolution set at "pass" and the Q3 resolution at 0.04 FWHM. The scan range was 218.5-220 Th over 0.100 s.

2.3 Results and Discussion

2.3.1 Chromatographic Separation.

Standards containing quinate, lactate, acetate, formate, hexanoate, galacturonate, chloride, sulfate, malate, phytate (myo-inositol hexakisphosphate), oxalate, tartrate, phosphate, citrate and isocitrate (hereinafter called the standard mixture), as well as samples of interest were analyzed on all three column sets. The standard mixture contains 20 μM quinate, 10 μM lactate, 10 μM acetate, 10 μM formate, 27 μM hexanoic acid, 10 μM galacturonate, 10 μM chloride, 10 μM sulfate, 10 μM malate, 10 μM tartrate, 10 μM oxalate, 10 μM phosphate, 10 μM citrate, 10 μM isocitrate, 2 μM phytate. The resulting chromatogram on the AS24 column is shown in Figure 2-1 and the 28-40 min region of this chromatogram is shown in magnified view in Figure 2-2. Phytate is the last peak to elute at ~40 min. Figure 2-3 and Figure 2-4 shows the corresponding chromatograms for the AS15 column set.

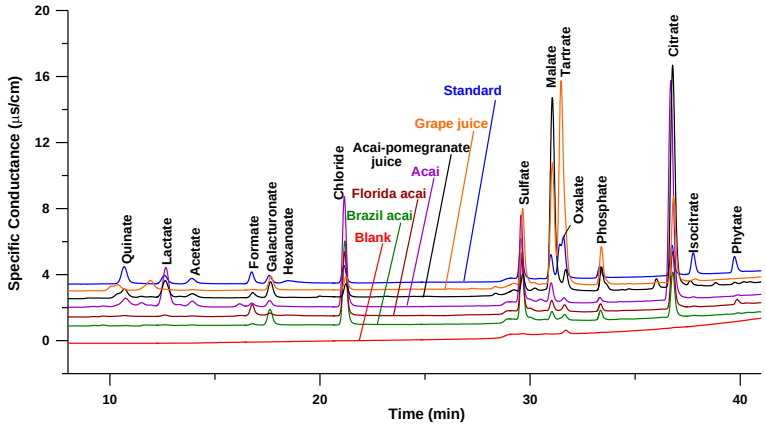

Figure 2-1 Chromatograms of blank, samples and standards on the AG24-AS24 column set.

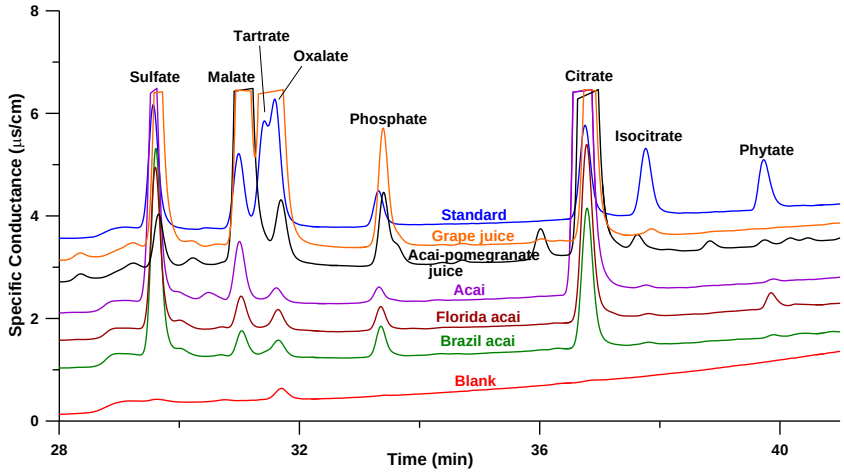

Figure 2-2 Detailed view of the 28 - 41 min region of Figure 2-1.

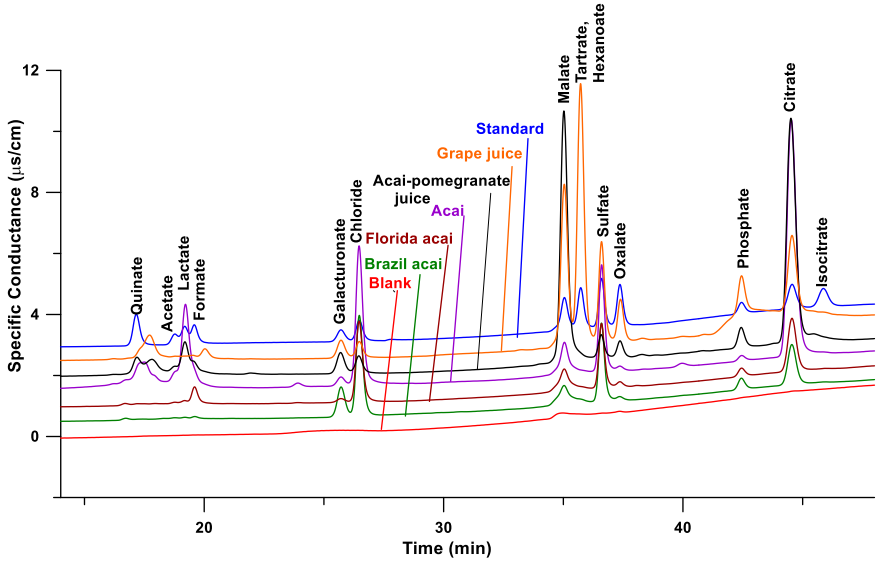

Figure 2-3 Chromatograms of blank, samples and standards on the AS15 column set.

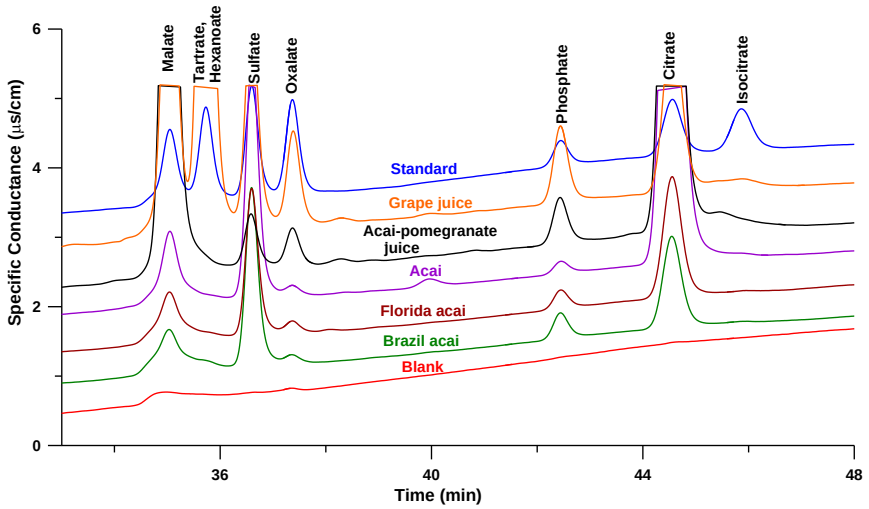

Figure 2-4 Detailed view of the 33 – 48 min region of Figure 2-3.

In this case, phytate does not elute within an hour. Dissolved CO_2 appears as the carbonate peak in all samples; it is a broad peak and can obscure the elution of some peaks of interest. This can be seen in Figure 2-5 for the malate peak on the AS15 column. The standard mixture in Figure 2-5 contains 2 µM lactate, 2 µM acetate, 4 µM formate, 5.4 µM hexanoic acid, 4 µM galacturonate, 20 µM chloride, 10 µM sulfate, 4 µM

malate, 2 μM tartrate, 1 μM oxalate, 4 μM phosphate, 10 μM citrate; 1.5 μM phytate. Blank, standard mix and sample chromatograms on the AS11 column is shown in Figure 2-6. Carbonate and tartrate coelute under these conditions (we also could not separate them on this column under all other conditions we tested) and this peak in turn elutes very close to malate. The separation from malate shown here was the best separation observed.

Although a relatively low eluent concentration (2.5 mM KOH) was used for all three columns for the first 10 min, the early eluting ions lactate, acetate and formate were well separated only on the AS24 column (Figure 2-7). But tartrate and oxalate elute too close to each other on this column under this condition; accurate quantitation will be impossible if both are present. One critical question (see below), if tartrate is present at all, can likely be answered nevertheless, especially if a standard containing both is run at the same time (compare the traces for the standard mix and the açaí sample traces in Figure 2-2). However, Tartrate was well separated from all other anions (except for hexanoate) only on the AS15 column. Hexanoate was observed in only the Floridian açaí and that in trace amounts. Accurate determination of tartrate should thus be possible by the stated method on the AS 15 column. Tartrate was not detected in any of the açaí samples, but it was one of the dominant components in grape juice (Figure 2-1, 2-2, 2-4), at a concentration of 1.92 mg/g.

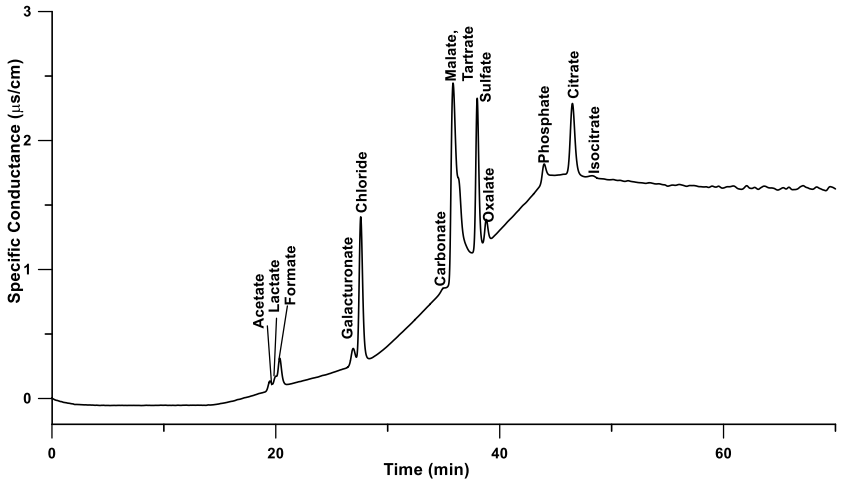

Figure 2-5 Chromatograms of the standard mixture on the AS15 column.

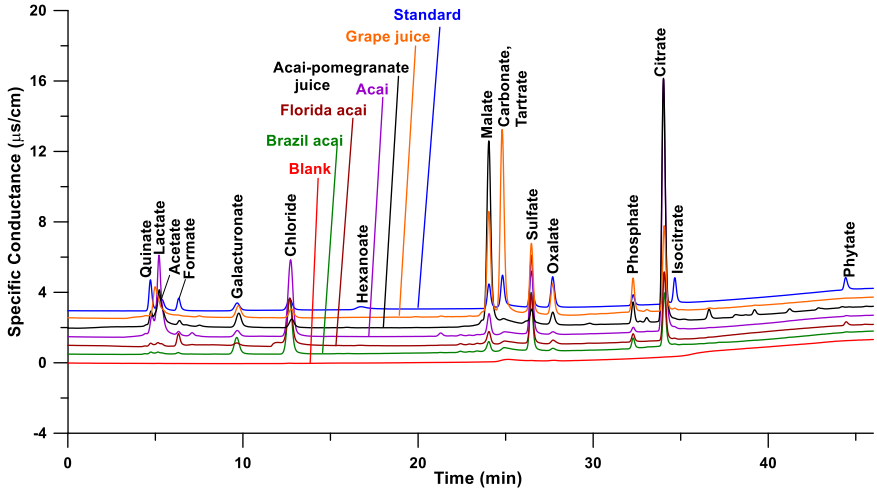

Figure 2-6 Chromatograms of blank, samples and standards on the AS11column.

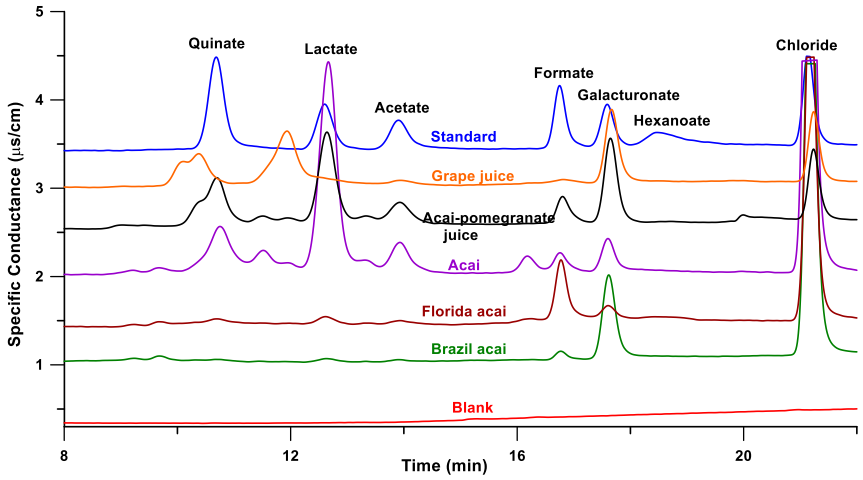

Figure 2-7 Detailed view of the 8-22 mins in Figure 2-1.

Concentrations of all the anions, determined using the AS24 column, are listed in Table 2-2. The calibration plots for these analyte ions are given in Figures 2-8, 2-9, 2-10, and 2-11. The calibration range ranged from 0.2 μM at the low end to 100 μM at the high end, depending on the analyte. The calibration equations are listed in Table 2-3 for the stated ranges; even for the weak acids, at the low concentrations examined, the peak area response was acceptably linear. The linear determination coefficient (r^2) ranged from 0.9914 for hexanoate to 0.9996 for phytate; these are listed in the Table 2-3. Also given therein are the limits of detection (LOD) for each ion under these chromatographic conditions based on the S/N=3 criterion; these ranged from 3 nM for the hexaprotic acid anion phytate to 200 nM for monoprotic weak acid anion hexanoate.

Table 2-2 Concentrations of Anions in Açaí, mg/g.

Sample/ Analyte ion	Floridian açaí	Brazilian açaí	Açaí	Açaí-pomegranate juice	Grape juice
Quinate	0.555±0.012[a]	0.192±0.034	0.185±0.006	0.366±0.013	<0.003
Lactate	0.413±0.022	0.202±0.015	0.308±0.006	0.251±0.005	<0.001
Acetate	0.260±0.012	0.136±0.003	0.046±0.002	0.067±0.005	0.014±0.002
Formate	1.58±0.01	0.228±0.014	0.012±0.001	0.038±0.003	0.007±0.001
Galacturonate	1.83±0.14	12.3±0.2	0.126±0.001	0.661±0.026	0.565±0.014
Hexanoate	1.55±0.12	<0.108	<0.003	<0.006	<0.006
Chloride	4.09±0.01	5.52±0.04	0.200±0.000	0.048±0.002	0.047±0.001
Sulfate	4.18±0.07	5.44±0.12	0.190±0.001	0.067±0.001	0.322±0.002
Malate	2.01±0.08	1.81±0.13	0.103±0.004	2.52±0.03	1.44±0.02
Tartrate	<0.016	<0.016	<0.001	<0.001	1.92±0.05
Oxalate	0.38±0.02	0.214±0.020	0.013±0.001	0.072±0.002	0.184±0.006
Phosphate	1.92±0.05	2.75±0.72	0.042±0.001	0.406±0.007	0.576±0.007
Citrate	15.7±0.1	13.1±0.8	1.90±0.03	3.67±0.02	1.31±0.02
Isocitrate	0.255±0.016	0.278±0.008	0.009±0.0001	<0.002	0.036±0.002
Phytate	1.34±0.01	0.229±0.010	0.007±0.0003	0.025±0.001	<0.003

[a] All results listed as average ± standard deviation (n=3). The ions are listed in order of elution.

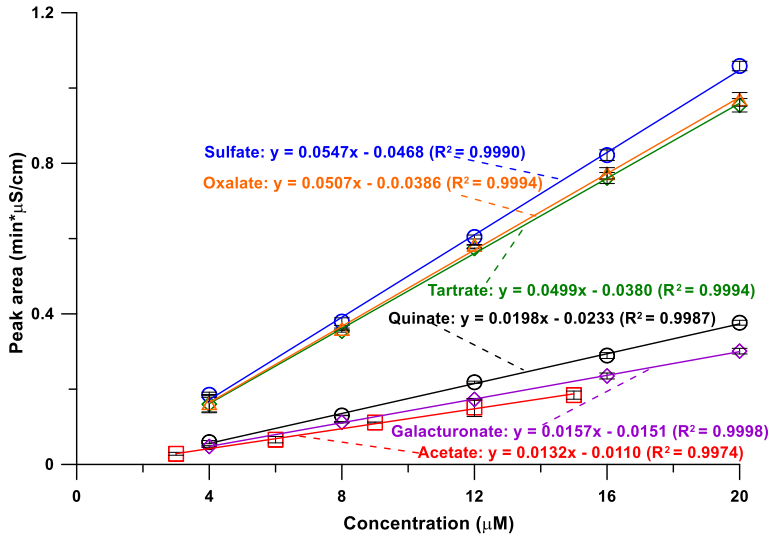

Figure 2-8 Calibration curves for quinate, acetate, galacturonate, and sulfate, using the AS24 column set and tartrate and oxalate using AS15 column set.

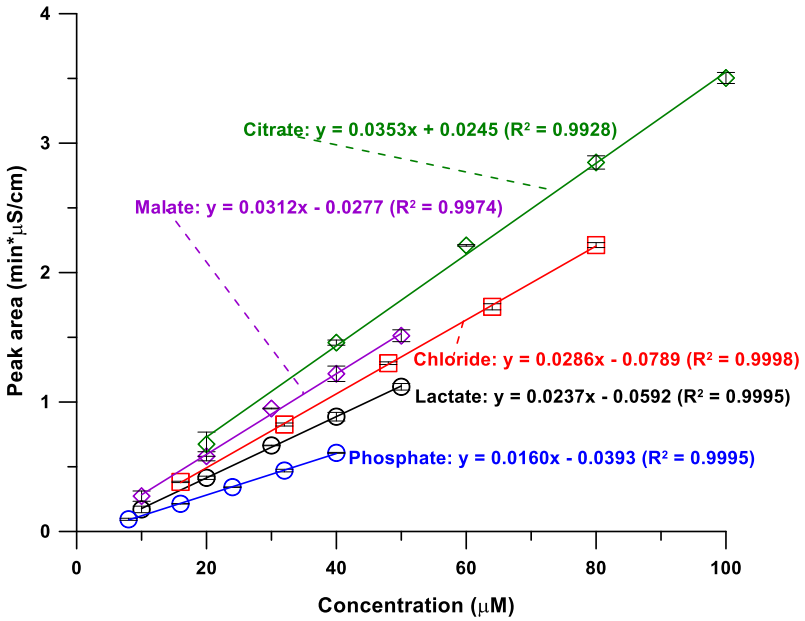

Figure 2-9 Calibration curves for lactate, chloride, malate, phosphate and citrate, using the AS24 column.

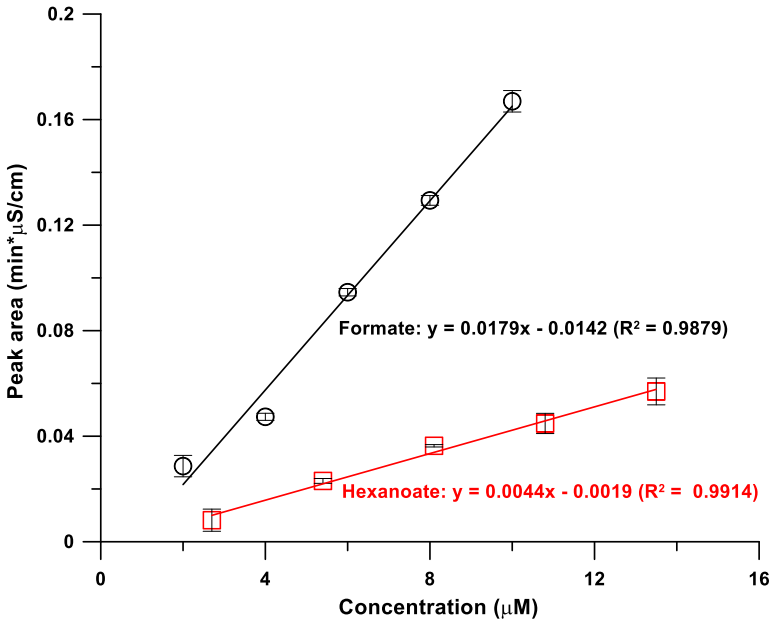

Figure 2-10 Calibration curves for formate and hexanoate, using the AS24 column set.

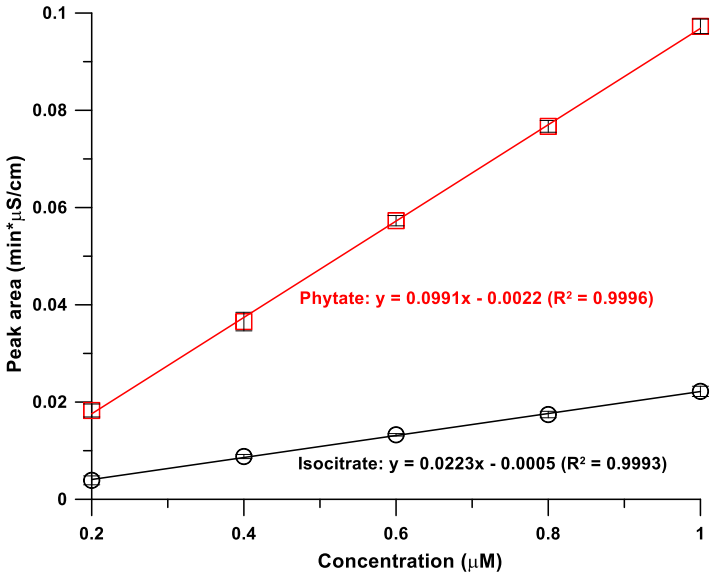

Figure 2-11 Calibration curves for isocitrate and phytate, using the AS24 column.

There is no particular column that is uniquely better than all others to perform juice/extract analysis either for authentication, or differentiate between different strains of açaí. While AS24 can separate most anions, it cannot separate tartrate and oxalate. The latter separation is facile on AS15 but it cannot separate early eluting ions, e.g., acetate, formate and lactate or elute phytate in an hour. Thus, quantitation of all but oxalate and tartrate was done on the AS24 column while oxalate and tartrate were separated and quantitated on the AS15 (See Figure 2-8).

Table 2-3 Calibration equation, range, and LOD.

	Calibration Equation (Y: Peak area, min*μS/cm)	Linear r^2	Calibration Range, μM	Limit of Detection, nM
Quinate	Y = 0.0198 *(C, μM) - 0.0233	0.9987	4 - 20	32
Lactate	Y = 0.0237 *(C, μM) - 0.0592	0.9995	10 -50	29
Acetate	Y = 0.0132 *(C, μM) - 0.0110	0.9974	3 - 15	54
Formate	Y = 0.0179 *(C, μM) - 0.0142	0.9879	2 -10	25
Galacturonate	Y = 0.0157 *(C, μM) - 0.0151	0.9998	4 - 20	32
Hexanoate	Y = 0.0044 *(C, μM) - 0.0019	0.9914	2.7 - 13.5	200
Chloride	Y = 0.0286 *(C, μM) - 0.0789	0.9998	16 - 80	14
Sulfate	Y = 0.0547 *(C, μM) - 0.0468	0.999	4 - 20	7
Malate	Y = 0.0312 *(C, μM) - 0.0277	0.9974	10 - 50	15
Tartrate[a]	Y = 0.0499 *(C, μM) - 0.0380	0.9994	4 - 20	4
Oxalate[a]	Y = 0.0507 *(C, μM) - 0.0386	0.9994	4 - 20	6
Phosphate	Y = 0.0160 *(C, μM) - 0.0393	0.9995	8 - 40	24
Citrate	Y = 0.0353 *(C, μM) + 0.0245	0.9928	20 - 100	9
Isocitrate	Y = 0.0223 *(C, μM) - 0.0005	0.9993	0.2 - 1	14
Phytate	Y = 0.0991 *(C, μM) - 0.0022	0.9996	0.2 - 1	3

2.3.2 Mass Spectrometric Identification of Galacturonate, Hexanoate and Phytate.

Some peaks were not initially identifiable based on known chromatographic retention behavior. The gradient described for the AS24 column was stretched out some over time in order to better elucidate the nature of these peaks. The chromatogram of the Floridian açaí extract under these conditions is shown in Figure 2-12. The black trace uses the right ordinate while the green, orange, and blue traces are the single ion monitoring counts for hexanoate, galactouranate, and phytate, respectively, and use the left ordinate. The virtually co-eluting peaks at 21 min revealed, on negative ion mode mass spectrometric selected ion monitoring study, ions at 115 and 193 Th. The 193 Th signal was ascribed to galacturonate. The retention time and the fragmentation pattern matched exactly with a standard.

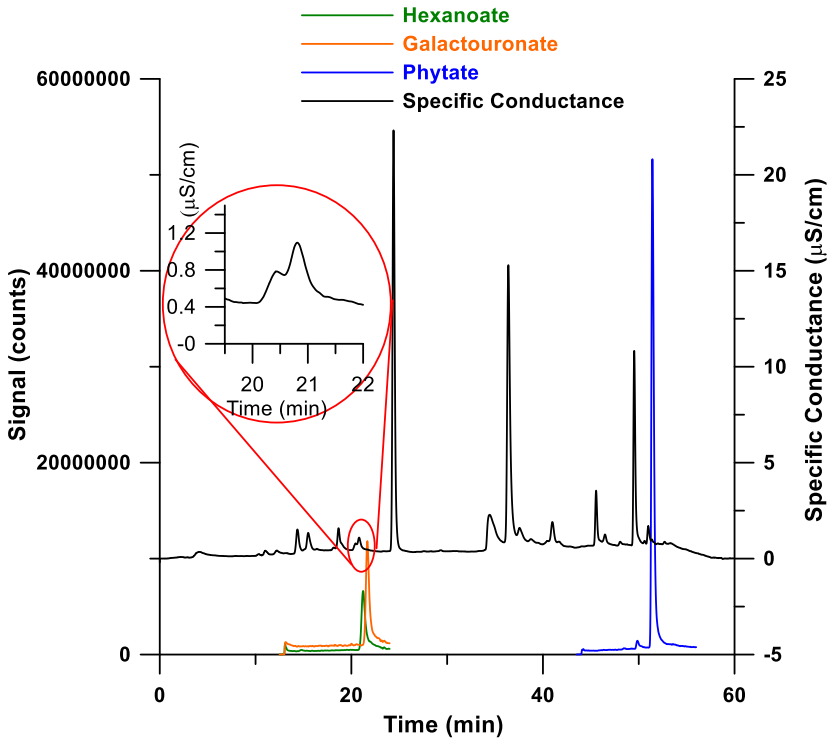

Figure 2-12 Chromatogram of Floridian acai with mass spectrometry detection on AS24 column set.

The 115 Th response was ascribed to hexanoate. A hexanoate standard was used for confirmation; the retention time was within 0.02 min of that in the sample, this is well within the reproducibility of retention times under these conditions. The hexanoate concentration in the sample was too low to quantitatively compare the relative peak intensities in the fragmentation pattern in the sample and the standard. However, the Th values of all the fragment peaks were identical in the sample and the standard, within the mass resolution of the instrument. The relevant data are shown in Figure 2-13a, b.

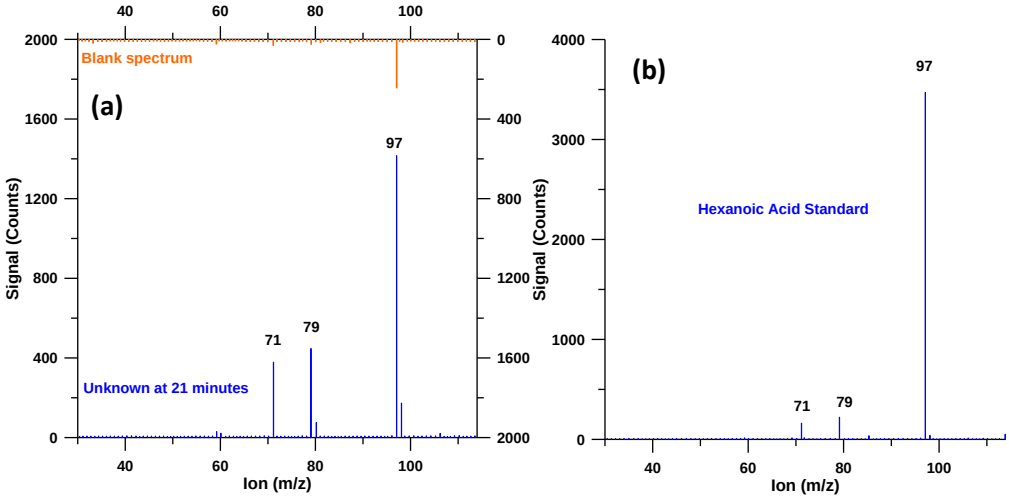

Figure 2-13 Fragmentation pattern of (a) the 115 Th peak eluting at 21 min and (b) 135 μM hexanoic acid standard.

The peak that eluted after citrate at ~52 min was also initially not identified. This peak produced an intense signal at 219 Th. The peak was asymmetric and tailed into the higher Th range, often a characteristic of multiply charged ions that fragment into a less charged ion at a higher Th. Reinvestigation of the full spectrum scan showed the presence of a weaker signal at 329 Th. Both the signals at 219 and 329 Th would be consistent with being derived from a neutral species of 660 mass units: the above two signals resulting respectively from loss of three and two protons. As the singly charged species was not observed, we suspected the parent compound to be a multiprotic strong acid.

A clear isotope distribution, separated by ~0.33 Th, is observed for the 219 Th peak (Figure 2-14), indicating a triply charged ion. Higher resolution spectra were used for confirmation and are shown in Figure 2-15. Fragmentation was performed from 30-218 and 220-659 Th; the results are shown in Figure 2-15. The parent mass and isotope distribution suggested a possible chemical formula of $C_6P_6O_{24}H_{18}$. Nominal Th values of

all of the major ions seen are consistent with fragments that will logically be generated from the triply charged phytate ion (Table 2-4). Additionally, given that the chromatographic retention time matched exactly with an authentic standard of phytate (myo-inositol hexakisphosphate), we positively identified this chromatographic peak as phytate. Table 2-4 contains a list of all major fragments ions listed in the order of their intensity along with their origin.

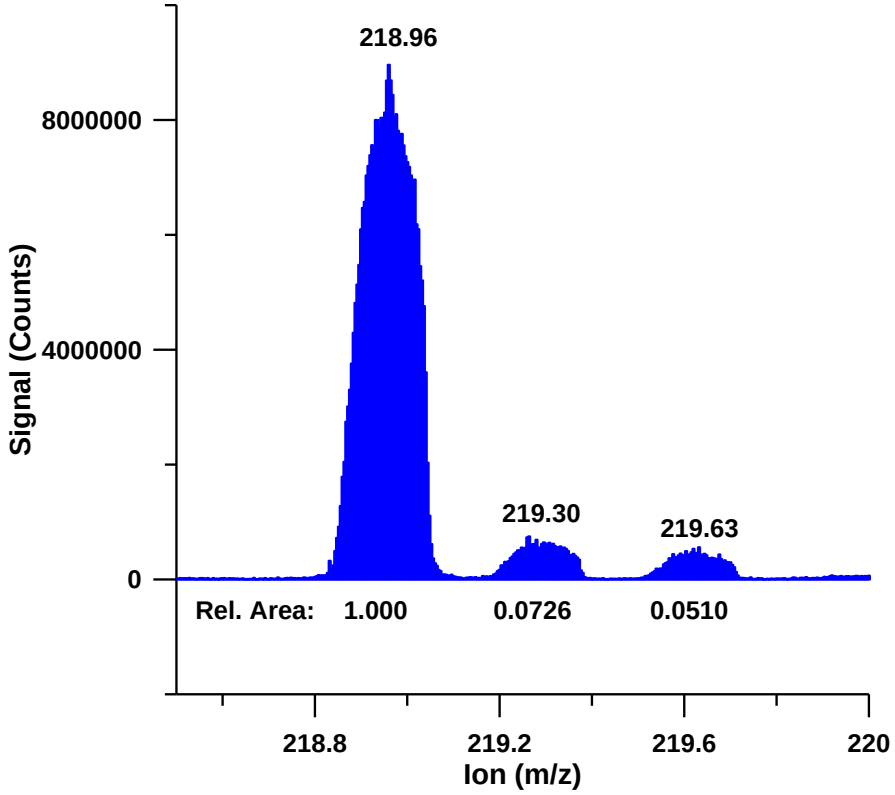

Figure 2-14 Mass spectrum of the peak eluting at 52 min in Figure 2-12.

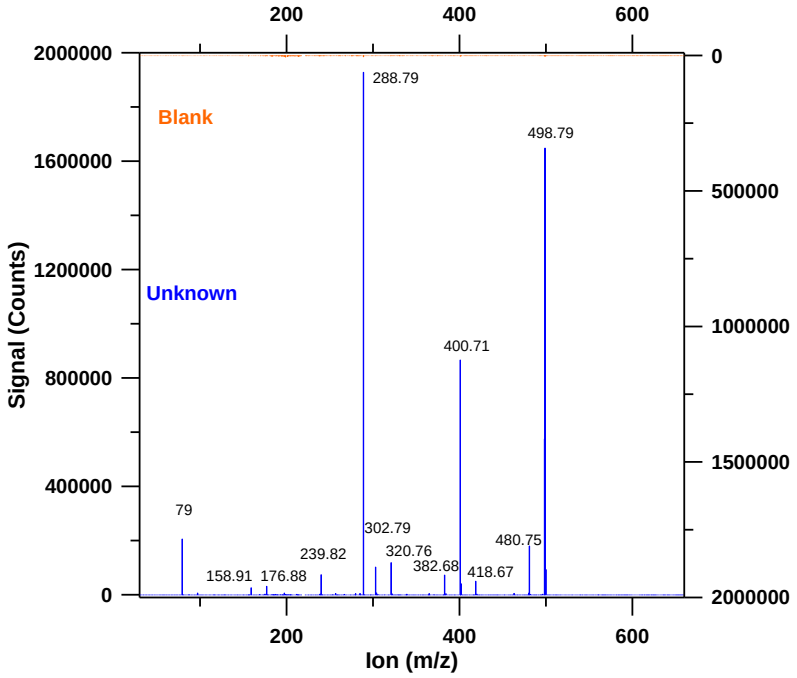

Figure 2-15 Fragmentation spectrum produced upon fragmenting the 219 Th peak.

Table 2-4 Putative Ion Identifi cation of Parent and Daughter

Ions of the Triply Charged Phytate Peak.

m/z (Th)	Ion	Loss
219	$C_6P_6O_{24}H_{15}^{3-}$	*Parent ion*
289	$C_6P_5O_{21}H_{15}^{2-}$	PO_3^-
499	$C_6P_4O_{18}H_{15}^-$	$2*PO_3^-$
401	$C_6P_3O_{14}H_{12}^-$	$2*PO_3^-+HPO_3^-+H_2O$
79	PO_3^-	Ejected ion
481	$C_6P_4O_{17}H_{13}^-$	$2*PO_3^-+H_2O$
321	$C_6P_2O_{11}H_{11}^-$	$2*PO_3^-+2HPO_3^-+H_2O$
303	$C_6P_2O_{10}H_9^-$	$2*PO_3^-+2HPO_3^-+2H_2O$
240	$C_6P_4O_{17}H_{12}^{2-}$	$PO_3^-+HPO_3^-+H_2O$
383	$C_6P_3O_{13}H_{10}^-$	$2*PO_3^-+HPO_3^-+2H_2O$
419	$C_6P_3O_{15}H_{14}^-$	$2*PO_3^-+HPO_3^-$
177	$H_3P_2O_7^-$	Possible gas phase recombination
159	$HP_2O_6^-$	Possible gas phase recombination

2.3.3 Significance of Phytic Acid.

The structure of phytic acid is shown in Figure 2-16. It is found in soil, cereals, legumes, nuts, oil seeds, pollen and spores.[90] Reported health effects of phytic acid are somewhat contradictory. While it has been called an anti-nutrient for several decades (it removes metals like calcium as water-insoluble complexes preventing absorption in the gut) but it is now known that it also act as an antioxidant and anti-cancer agent.[91] Phytate may also help prevent Alzheimer's disease and other neurodegenerative diseases by chelating iron (it has greater affinity for iron than calcium) and keeping it from initiating oxidative damage.[92] The main sources of phytate in the daily diet are cereals and legumes, especially oily seeds and nuts with estimated daily intake in the West ranging between 0.3-2.6 g.[91] The recommended daily dosage for açaí powder formulated as capsules and taken as supplement is 2 g/day. The Floridian açaí contained a much greater amount of phytate (~6 times) than the Brazilian açaí. However, on an absolute scale, the amount of phytate in the Floridian sample was only 1.34 mg/g; it will not be a significant source for phytate. On the other hand, it is possible that Floridian and Brazilian açaí can be distinguished by their phytate content.

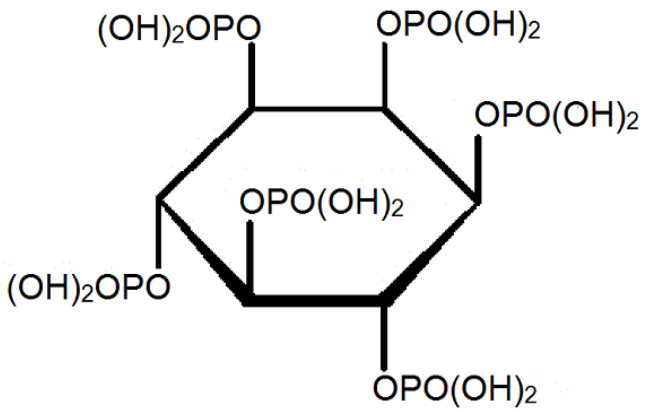

Figure 2-16 Structure of phytic acid (myo-inositol hexakisphosphate).

2.3.4 Implication on Phytate Analysis.

The analysis of phytate is important, the present method provides a superior alternative to extant methods. AOAC method 986.11[93] uses anion exchange separation, then complete hydrolysis and colorimetric phosphate determination. If other inositol phosphates are not completely separated, a positive error results.

In SCAC (obligatorily with an alkaline eluent), phytate will have a charge of -12. The normal expectation will be that it will not elute in a reasonable period, as was presently observed with the AS15 column. Indeed, in previous studies[94] even to elute the triphosphate from an AS4A column required high concentrations of 4-cyanophenolate, an extremely strong eluent. Only the mono and diphosphate could be eluted with a high concentration gradient of NaOH and NaOAc from a PA-10 column.[95] Strong acid eluents with anion exchange columns and post column reactions with Fe^{3+} can separate and detect (by UV absorption) all inositol phosphates.[96],[97],[98] However, unlike the present method, it will not sensitively detect other ions, e.g.; organic acids, or be compatible with mass spectrometry.

The present method can elute phosphate in a reasonable period with a hydroxide eluent. If phytate is the only inositol phosphate analyte of interest, we have found that it can be eluted much sooner using a stronger eluent gradient but without causing coelution with the peaks eluting earlier.

2.3.5 Implications on the Authentication of Açaí.

There is considerable interest in authentication of expensive food and beverages that can be easily adulterated. For example, for pomegranate juice, an international multidimensional authenticity specification algorithm has recently been established.[54] The present work suggests on a preliminary basis that the absence of tartrate may

provide a useful tool to determine the authenticity of pure açaí and/or pomegranate products, especially as the common adulterant juices are all known to contain large to easily detectable levels of tartrate. Of course, many more samples would have to be analyzed to establish the validity of this observation. It is important that any such analysis be done on genuine açaí. For example, it was recently reported that a product labeled "açaí juice" contained 0.6 mg/L nitrate.[53] Nitrate is unlikely to be present inside the fruit and no nitrate was found in any of the açaí samples in the present study. The ability to differentiate between Floridian and Brazilian açaí on the basis of phytate content will also need to be validated by analysis of a much larger number of samples.

The measurement of principal organic acids in fruit juice, especially grape juice (for general characterization and for determination of maturity for harvesting) by SCAC has been previously advocated.[99,100,101] The SCAC technique has grown considerably in power since; presently it is possible to generate an essentially complete anion profile, including that of the organic acids, even those present at low levels. The different selectivities of the multitude of columns presently available permits complete separation, and also aids identification through multidimensional retention mapping as shown in Figure 2-17. For example, lactate elutes before acetate on a AS24 column while the reverse elution order is observed on a AS15. Similarly the elution orders of sulfate and malate are reversed between AS24 and AS11, among many such instances. In most cases, the use of mass spectrometry is not essential. With the açaí products as the focus, we hope to have clearly established the power of this technique.

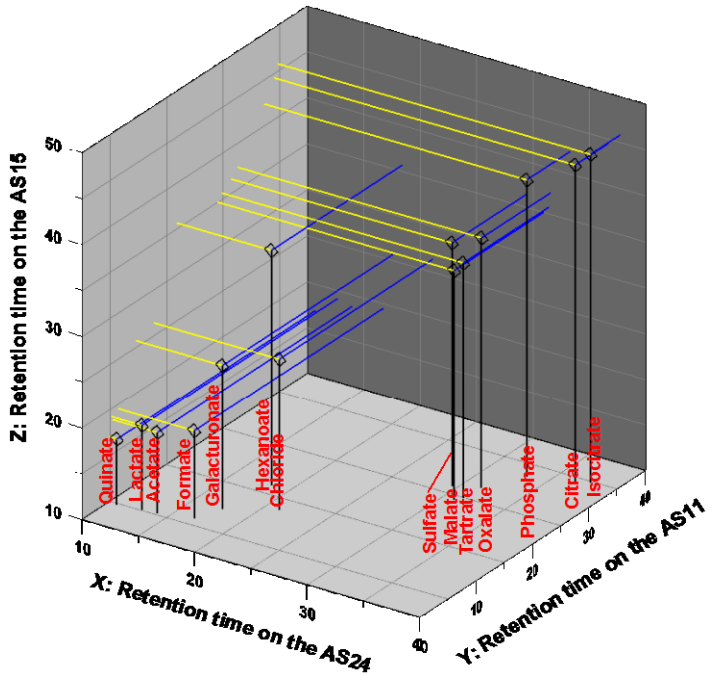

Figure 2-17 3D retention map of different anions on the AS24, AS15 and AS11 three different columns.

2.4 Acknowledgements

We acknowledge valuable discussion with Christopher A. Pohl and Kannan Srinivasan. This chapter has been reprinted with permission from H. Liao, C.P. Shelor, Y. Chen, A.U.O. Sabaa-Srur, R.E. Smith, P.K. Dasgupta. Journal of Agricultural and Food Chemistry. 61 (25) 2013, pp 5928-5935. Copyright 2013 American Chemical Society

I would like to thank C. Phillip Shelor for this chapter, since the IC-MS part was done by him. Three less common ions, including hexanoate, galactouronate, and phyate were confirmed by IC-MS.

Chapter 3

Enigmatic Ion Exchange Behavior of Myo-Inositol Phosphates

3.1 Introduction

Ion exchange retention is commonly thought to be governed by electrostatic interactions. Both electrostatic and hydrophobic interactions control retention, the latter often being dominant: the hydrophobic monovalent ion ClO_4^- often elutes after divalent SO_4^{2-} or even trivalent PO_4^{3-}. True electrostatic selectivity can be achieved only with hydrophilic columns and hydroorganic eluent modifiers.[102] For a given subset of molecules of similar hydrophobicity, however, electrostatic interactions govern the elution order; an increase in charge results in an increase in retention.

There is presently considerable interest in myo-inositol hexakisphosphate (phytate, InsP6, the primary P storage form in many living systems). Phytate is known to form many metal chelates[91,92,103,104,105,106] and was earlier considered an antinutrient because it sequesters calcium,[91] but now its antioxidant and anticancer properties are of greater interest. Phytate chelates iron and prevents it from initiating oxidative damage; it may potentially help prevent Alzheimer's and other neurodegenerative diseases.[92] We recently reported on the determination of phytate in Açaí berry extracts by hydroxide gradient IC.[107] Phytate will have a -12 charge,[106,108] in a strongly alkaline eluent; elution of an ion with a -12 charge is thought to be essentially impossible. Yet we found it to elute before citrate using relatively mild eluent concentrations.

Hydroxide eluent IC determination of phytate has been reported by only one other group,[109,110] using up to 110 -130 mM NaOH containing isopropanol on a multifunctional anion exchanger. IC methods more commonly use concentrated strong acids such as HCl (0.5-0.95 M),[96,97,111] CH_3SO_3H (1.5 M),[98] or HNO_3 (0.155 M)[112] as eluents to suppress ionization for anion exchange separation of InsP's. Ammonium

acetate/acetic acid[113] (75 mM, pH 4.0) and Citrate buffer[114] (1 M, pH 5.0) are only able to elute up to InsP3 and InsP4, respectively. Complete class separation (no isomeric separation) of InsP1-InsP6 was possible with a 0.01 M methylpiperazine buffer (pH 4.0) with a salt gradient up to 0.5 M $NaNO_3$.[115] Postcolumn reaction absorbance detection with $Fe(ClO_4)_3$ is typically used; few other analytes can be sensitively detected in this mode.

Having successfully separated phytate by gradient hydroxide IC, we attempted to separate the variously phosphorylated InsP's ($InsP_{0-6}$) and were surprised to find that $InsP_4$'s and $InsP_5$'s apparently elute after $InsP_6$.[116] It is not logical that $InsP_4$'s and $InsP_5$'s have so much greater hydrophobicity than $InsP_6$ that it even overcomes the considerable differences in the net charge of -12 for $InsP_6$ to -8 for $InsP_4$. Here we unravel reasons for this unusual behavior.

3.2 Experimental section

3.2.1 Preparation of Inositol Phosphates

Phytic acid was acid hydrolyzed according to the method of Cosgrove[117] to produce $InsP_0$ to $InsP_5$. Aliquots were taken from the solution kept at 110 °C every 30 min for the first 14 h, and at longer intervals (6-12 h) thereafter until 48 h; details are given as following. 0.994 g of dipotassium phytate (≥95%, www.sigmaaldrich.com) was dissolved in a minimal amount (~10 mL) of 18.2 MΩ deionized (DI) H_2O (MilliQ, www.emdmillipore.com). A 20 mL polypropylene syringe was filled with ~10 mL of Dowex HCR-W2 high capacity strong acid cation exchange resin (www.sigmaaldrich.com) and washed with DI H_2O. The phytate solution was added to the head of the resin bed and allowed to percolate through the resin by gravity. The effluent was collected and an additional 50 mL of DI H_2O, added in 10 mL aliquots, was used to rinse the remaining phytate from the column. The phytate solution was then adjusted to pH 3.93 using 100

mM KOH (GR ACS, www.emdmillipore.com) before being diluted to a final volume of 260 mL. The solution was then transferred to a stoppered 500 mL inert container and kept in a 110 °C convection oven. One milliliter aliquots of the contents were removed every 30 min for the first 14 h, adjusted to pH 7.0 with 0.1 M KOH, and diluted to 10 mL to produce a final concentration of ~0.5 mM total InsP's. This solution was then diluted 10x and 1 mL placed in a glass autosampler for analysis. Subsequent samples were taken at longer intervals (6-12 h) up to 48 h after the sample was put in the oven. Samples were kept refrigerated until all the desired hydrolyzates were available for analysis.

3.2.2 Ion Chromatographic Analysis

Ion chromatographic studies were conducted on an ICS-5000 ion chromatograph (all chromatographic components below from www.dionex.com). The eluent (0.300 mL/min) was prepared inline using a KOH EGC-III eluent generator and further purified by a continuously regenerated anion trap column. A 10 µL injection volume was used. IonPac AG/AS-24 and IonPac AG/AS-11HC guard and separator columns sets (www.dionex.com) were used in 2 mm format; we have successfully used these before for phytate measurement. After suppression (AERS-500 electrodialytic suppressor), the effluent was conductometrically monitored. All tubing prior to detection were < 0.25 mm in inner diameter. The electrodialytic devices were operated in the recycle mode.

We examined the following eluents: (a) electrogenerated KOH (b) nominally 100 mM NaOH stock prepared from 50% w/w NaOH (www.fishersci.com) and (c) nominally 100 mM tetramethylammonium hydroxide (NMe_4OH) prepared from 1.0 M solution (ACS grade, www.sigmaaldrich.com). Titration with primary standard grade potassium hydrogen phthalate (≥99.95%, www.mallinckrodt.com) indicated exact concentrations of b and c to be 97.9 and 98.5 mM, respectively. Low pressure mixing capabilities of the gradient pump was used to make various concentrations of NaOH and NMe_4OH eluents.

An optimized gradient was used to carry out separations of the InsP's in under an hour on the AS-24 column as listed in Table 3-1 (left part). A mixed hydroxide gradient using NMe_4OH and NaOH was performed using the AS11HC column as listed in Table 3-1 (right part).

Table 3-1 left side for electrogenerated KOH Elution Program using AG/AS24 Columns and right side for Mixed Hydroxide Elution Program using AG/AS11HC Columns.

Time, min	KOH, mM	Time, min	TMAOH, mM	NaOH, mM
0	17.5	0	6	0
5	17.5	7	6	0
15	42	7.5	35	0
30	42	14.5	35	0
50	55	15	65	0
55	55	23	35	30
55.5	17.5	30	0	65
60	17.5	33	0	65
		33.5	6	0
		40	6	0

3.2.3 Mass spectrometry

Mass spectrometric studies were conducted on a TSQ Quantum Discovery Max electrospray ionization (ESI) MS/MS system with a heated ESI probe (www.thermoscientific.com), a different IC system was used with the MS instrument. Instrument parameters were as follows: Electrospray voltage, 500 V; vaporizer temperature, 350 °C; capillary temperature, 250 °C; skimmer offset, 0 V; sheath gas pressure, 50 arbitrary units (AU); auxiliary gas pressure, 50 AU; ion sweep gas pressure,

0 AU; Quadrupole 1 resolution, 0.4 full width half maximum (FWHM); quadrupole 3 resolution 0.5 FWHM. Identical KOH gradient separation was performed on the IC instrument connected to the MS as on the ICS-5000 instrument. This chromatography setup consisted of an IS25 PEEK dual piston isocratic pump, an EG40 eluent generator with an EGC-III KOH cartridge, an LC 30 column oven, and a CD25 conductivity detector with a DS3-1 detector cell, all from Dionex (www.dionex.com). Suppression was performed using an ASRS Ultra II 2mm anion self-regenerating suppressor (www.dionex.com). A 2 µL injection loop was connected to the injection port of a Thermo Finnegan Surveyor autosampler (www.thermoscientific.com). A peristaltic pump delivered ~1 mL/min of DI H_2O for the regeneration of all membrane based devices. The NMe_4OH-NaOH gradient IC analysis required a pump capable of generating gradients through low pressure mechanical mixing. For this, the aforementioned ICS-5000 system was coupled to the MS.

Molecular ions were measured in the single ion monitoring mode (SIM). $InsP_0^{-1}$, $InsP_1^{-1}$, $InsP_2^{-1}$, $InsP_3^{2-}$, $InsP_4^{2-}$, $InsP_5^{2-}$, $InsP_6^{3-}$ or $InsP_6^{2-}$ were measured at nominal mass to charge ratios of 179, 259, 339, 209, 249, 289, and 219 or 329 m/z respectively. A relatively low voltage of 500 V was used for the ESI as preliminary experiments showed that higher ESI voltages resulted in the loss of a phosphate moiety from $InsP_6$ to $InsP_5$ during tuning. Despite the low ESI voltage, because of the high acidity of the phosphate, ionization was still more than adequate as observed from signal counts and even polyvalent molecular ions for the higher substituted InsP's were abundant.

3.3 Results and discussion

3.3.1 Separation of Inositol Phosphates.

The optimized separation of InsP species is shown in Figure 3-1 for selected hydrolysis times between 0.5 – 40.5 hours; the production of intermediate and finally

lower InsP's is clearly visible. The 12.5 hour hydrozylate (selected for its relatively even distribution of all components) was analyzed by MS to identify specific zones (Figure 3-2): 5-8, 17-22, 30-40, and 40-50 min elution windows corresponded to $InsP_1$, $InsP_2$, $InsP_3$, and $InsP_4$ - $InsP_5$ respectively. $InsP_6$ eluted at 42 min. The ultimate product of InsP hydrolysis, inositol and phosphate were detected eluting in the void volume and 15 min, respectively. The rate of phosphate appearance can be used to determine the rate of the reaction at any given time.

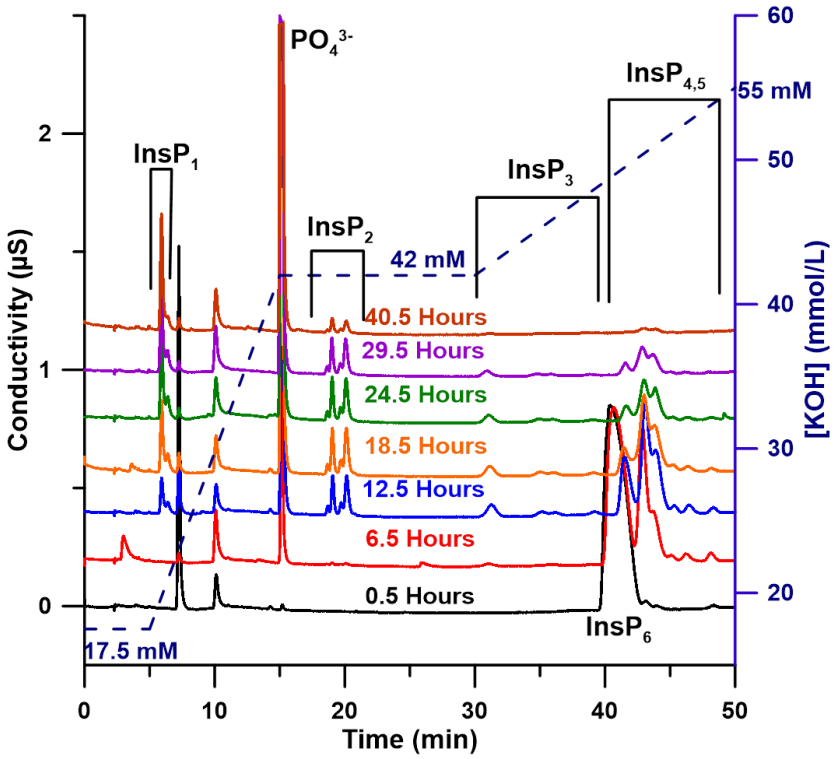

Figure 3-1 Ion Chromatograms of Phytate Hydrozylates from 0.5-40.5 hours.

The dashed blue line is the KOH gradient concentration. Regions of elution for the InsP's are marked.

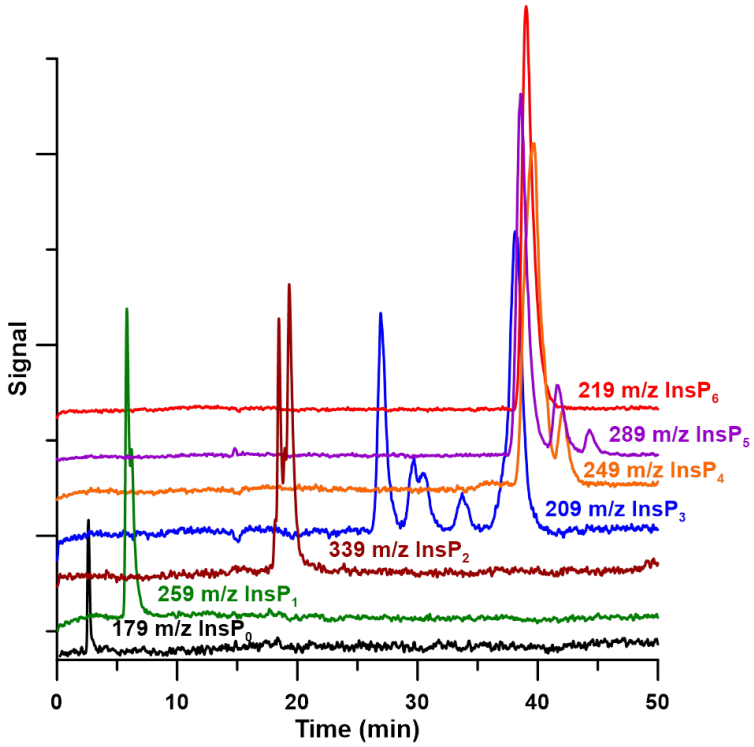

Figure 3-2 Single ion monitoring traces, 12.5 h hydrozylate. Chromatograms have been offset and scaled differently for clarity.

Figure 3-1 indicates (as interpreted by MS analysis, see below) that $InsP_1^{2-}$, PO_4^{3-}, $InsP_2^{4-}$, $InsP_3^{6-}$ elute in the order of their charge but $InsP_4$ – $InsP_6$ do not follow this trend: InsP6 elutes before the majority of $InsP_4$ and $InsP_5$ isomers. The close elution/coelution (Figure 3-2) of these isomers clearly fails the charge-retention predictions. The hydrolysis of $InsP_6$ can theoretically result in 6, 15, 20, 15, and 6 (62 total) possible geometric isomers for $InsP_1$-$InsP_5$ respectively. However, Ins has a plane of symmetry and 4, 12, 16, 12, and 4 of the above positional isomers make up half as many (24 total) enantiomeric pairs which cannot of course be resolved on achiral columns. This makes a total of 40 possible chromatographic peaks including Ins and $InsP_6$. Of these, only 2, 4, 5, 2, and 3 isomers are visually apparent in Fig. 3-2.

3.3.2 Mechanism of Phytate Separation.

Plausible explanations for the retention behavior of $InsP_4$ – $InsP_6$ may include: (a) $InsP_4$ – $InsP_6$ anions do not carry the assigned formal charges, the final protons do not ionize, (b) On a molecular scale, the stationary phase cationic site density is not sufficient to fully interact with all charges on the highly phosphorylated InsP's and (c) the rigid inositol skeleton can at best orient 4 phosphate groups toward the stationary phase, any phosphate groups not interacting with the stationary phase increases eluophilicity (see below).

Successive K_a values for $InsP_6$ have been extensively studied.[106] The pK_a of the final proton varies from >13 in 0.17 M Et_4NClO_4 to 8.29 in 3 M $NaClO_4$. In media closest to our eluent conditions (0.1 M KCl) pK_{12} was reported to be 10.24. The lowest concentration KOH (40 mM) we used for isocratic elution has a pH of ~12.6, sufficient to fully ionize $InsP_6$. Hypothesis (a) must therefore be discarded.

For a hydroxide eluent, the slope of a log (capacity factor (k)) - log [OH^-] equals the charge on the eluite ion.[118] For $InsP_6^{12-}$, the slope should be -12. Figure 3-3 shows such plots for KOH elution on both AS11HC (exchange capacity 140 μeq) and AS24 (290 μeq) columns. Note that within experimental error both columns produced the same effective charge (EC) of -10 with the KOH eluent, given the >2x exchange capacity difference, hypothesis (b) must also be wrong. A closer examination of the log [OH^-] – log k plots suggest, however, that a linear model may be inadequate (see Fig. 3-4 for a plot of the residuals). In Fig. 3-3, the slope between two adjacent data points was plotted vs. the concentration as dashed lines. Here, the EC is seen to decrease with increasing KOH concentration. This also suggests the invalidity of hypothesis (a), especially as it is known that increasing ionic strength actually enhances the dissociation of phytic acid.[106] On the other hand at the lowest eluent concentration, the EC determined for $InsP_6$ was -

11 for the lower capacity column, suggesting strongly that the theoretical -12 will be approached at still lower eluent concentrations, and there is no insufficiency of the resin capacity: hypothesis (b) is untenable.

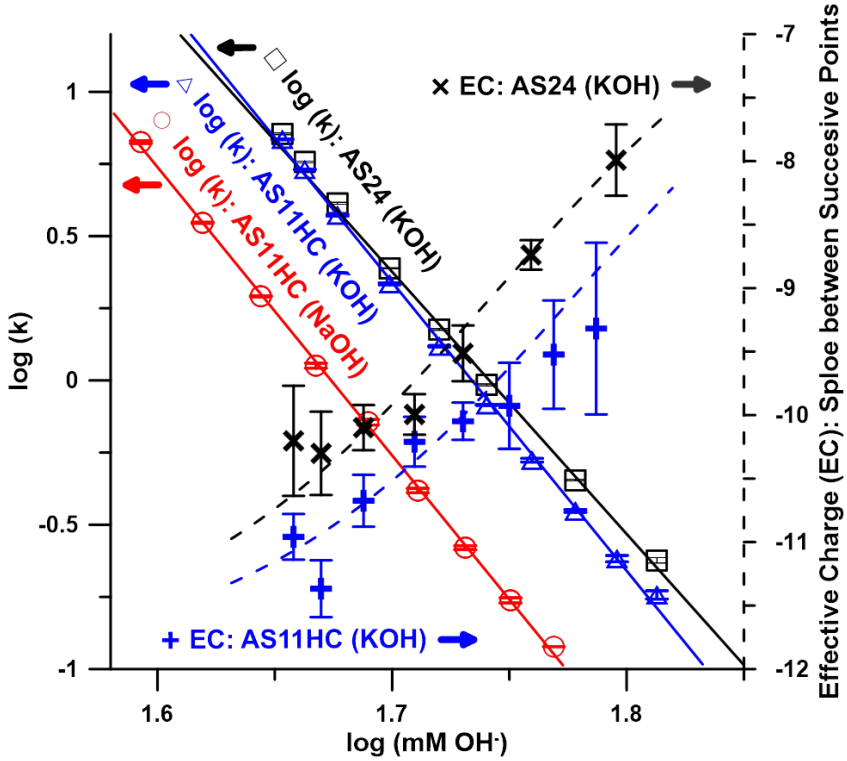

Figure 3-3 Log [OH-] vs Log k for InsP6 anion elution on AG/AS11HC columns using (a) NaOH and (b) KOH; and (c) AG/AS-24 columns using KOH.

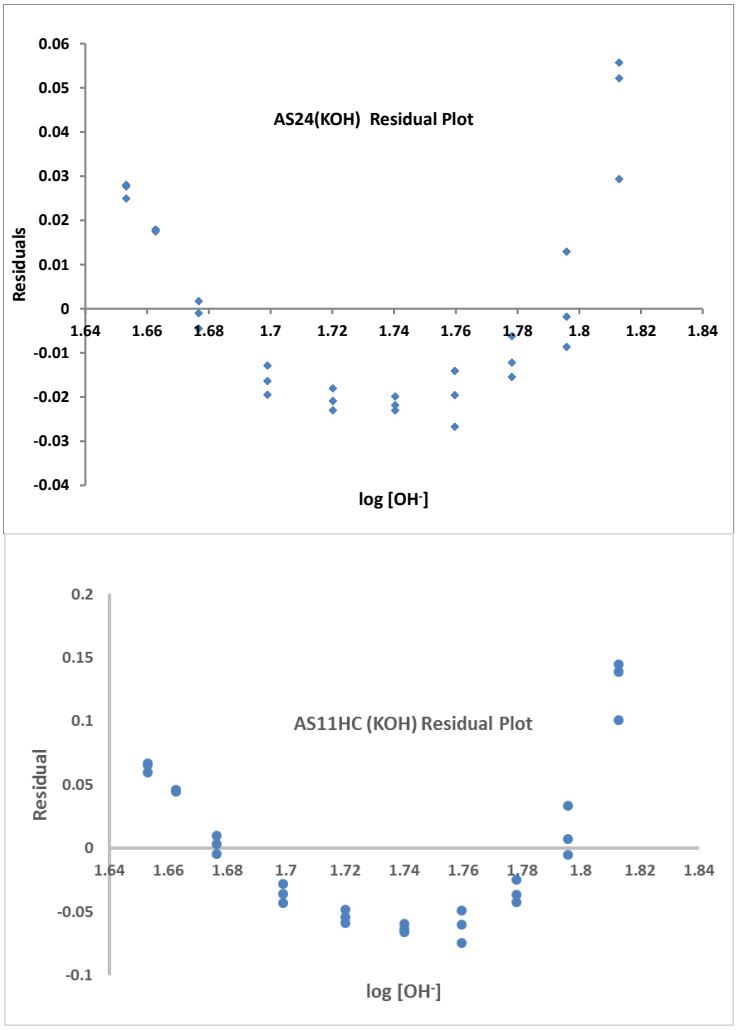

Figure 3-4 Residual plots for the KOH eluent regression plots in Fig. 3-3.

The slope generally indicates the effective charge of $InsP_6$; this ranges between -9.3 and -10 in these plots. The respective slopes and linear correlation coefficients are: (a) -9.98 ± 0.05, r^2 = 0.9994, (b) -10.00 ± 0.08, r^2 = 0.9982, and (c) -9.34± 0.10, r^2 = 0.9977. The interpoint slope is plotted vs the log of the hydroxide concentration. The effective charge of phytate decreases with increasing KOH. The dashed lines are the predicted charge states based on the fits of the complexation constants.

Alternative (c) suggests that the charges on a multiply charged rigid molecule are sterically arranged on opposite sides, the solvation affinity of charged sites not bound to the stationary phase will lead to an eluophilic effect. For stainless steel open tubular columns bearing anion exchange sites, Mo reported that while 2,6-naphthalenedisulfonate elutes after 2-naphthalenesulfonate as expected, 1,3,(6 or 7)-naphthalenetrisulfonate elutes in between the two.[119] While this may provide an explanation for the elution behavior of $InsP_{4-6}$, this cannot explain why there is such a large difference in retention behavior of $InsP_6$ between the same concentrations of KOH and NaOH as eluent and why the EC magnitude of phytate is perceptibly lower with NaOH than with KOH. Indeed our confusion was compounded when we experimented with NMe_4OH: Compared to NaOH or KOH, even a much higher concentration (0.1 M) of NMe_4OH could not elute phytate from either column in 1 h.

3.3.3 The Role of the eluent Cation. Determining Complexation Constants from Effective Charge.

The literature indicates significant alkali metal complexation by phytate. The complexation constants are not available in a straightforward manner. Essentially all the data are reported as potentiometric measurements of the successive K_a values of $InsP_6$ in the presence of various concentrations of NaCl, KCl, etc. and assumptions are made as to charge states that the present experiments will clearly indicate to be invalid. Although direct quantitative comparison with our data is therefore not possible, qualitatively the complexation follows the charge density order $Li^+ > Na^+ > K^+ > Cs^+ >> NR_4^+$.[103,104,106] As eluent cations Na^+ or K^+ will form adducts with phytate, this will reduce EC and increasingly so as the eluent concentration is increased. This is depicted in the dotted line traces (right ordinate) in Figure 3-3. The change in EC with $[M^+]$ ($[M^+]$ being the same as the eluent concentration) can be used in a simple

manner to determine the stepwise complexation constants. If we express the equilibria much like the dissociation of a polyprotic acid, $M_{12}L$ (L being $InsP_6^{12-}$) losing M^+ stepwise to eventually form L^{12-}, the stepwise dissociation constants being K_1 through K_{12}:

$$M_nL^{(12-n)-} \rightleftharpoons M^+ + M_{n-1}L^{(12-(n-1))-} \quad \ldots K_{13-n} \qquad (n = 12\text{-}1) \quad \ldots (3\text{-}1)$$

Much as with polyprotic acids, we express the fraction of the total concentration of each L-bearing species as α-values (K_0 is 1, has no physical meaning, for mathematical convenience)

$$\propto_{M_nL^{(12-n)-}} = \frac{[M^+]^n K_0 \ldots K_{12-n}}{\sum_{n=12-0} [M^+]^n K_0 \ldots K_{12-n}} \quad \ldots(3\text{-}2)$$

EC is then simply the charge-weighted sum of the α-values:

$$EC = -\sum_{n=12-0} (12-n) \propto_{M_nL^{(12-n)-}} \quad \ldots(3\text{-}3)$$

As we have the value of EC as a function of $[M^+]$ (the analyte concentration is so small relative to the eluent concentration that even if 12 M^+ ions were bound to a single ligand molecule, there will be no perceptible change in $[M^+]$. In a given set of experiments, all of the twelve equilibria are not going to be important. For example, in our experiments with KOH with the AS11HC column (Figure 3-3, dashed black trace) EC ranged from -7.4 to -11. Only equilibria involving K_7 through K_{12} plays a significant role; if we have at least 6 EC values as a function of $[M^+]$, the best fit values for K_7 - K_{12} can be calculated by any nonlinear least squares algorithm, e.g. Microsoft Excel Solver.[120,121] The respective best fit values (and their uncertainties from the jackknife approach[122]) were as follows (although the formalism above were for dissociation constants, it is customary to report metal-ligand equilibria in terms of association constants) for -log K_7 through –log K_{12} as measured with the AS11HC column were: (a) For K^+ 6.08±0.35, 3.12±0.12, 2.44±0.11, 1.20±0.04, -0.93±0.02, -4.60 ±0.04 and (b) For Na^+ 6.69±0.02,

2.97±0.00, 2.31±0.00, 1.15±0.00, -0.96±0.00, -4.60±0.01, respectively; consistent with greater binding of Na^+ relative to K^+ by phytate.[103,104,105,106] To our knowledge, this is the first illustration of measurement of successive metal-ionic ligand binding constants through chromatographic measurement of changes in the effective charge on the adduct.

In the only other examples known to us where both the eluent cation and anion play a role in anion exchange separations, the cation provides retention to the analyte ion via adsorption on neutral sites on the stationary phase; this can be a tetralkylammonium ion being adsorbed on a nonpolar phase[21] or alkali cations being adsorbed on a cryptand column.[123,124] A typical gradient run may involve the gradual change from a more to a less adsorbed cation (e.g., NPr_4^+ to NEt_4^+ or Na^+,[21] or Na^+ to Li^+,[123,124] thus leading to reduced column capacity as the gradient progresses. Here, the situation is fundamentally different, the column capacity is unaffected by the eluent; increases in either the cation or anion concentration helps elute the analyte anion. It is also possible to view the effect of the metal ion the same as that of the effect of pH in anion exchange separations, decreasing the pH and converting the analyte to a lower charged form decreases the retention. Variation of the eluent cation in ion exchange chromatography is rarely studied, aside from the alkali metals, the use of Ca, Ba, or quaternary ammonium ions may prove useful in separations between large, highly charged structurally similar ions separated by suppressed conductometric IC.

3.3.4 Practical Consequences.

Because there is a significant difference between the degrees to which different cations are complexed by phytate, in particular the inability of even 0.1 M NMe_4OH to elute phytate in 1 h, whereas even much lower concentrations of NaOH eluted it readily (Figure 3-3), this can be exploited to achieve an extended range of gradient strength in the separation of InsP isomers via an NMe_4OH-NaOH (or even LiOH) gradients. As the

cation is entirely removed in a suppressed system, a low conductivity MS-compatible background will still be attained.

Figure 3-5 shows such a separation of the 12 h phytate hydrozylate with mass spectrometric eluite identification (for comparison, an electrodialytic KOH gradient chromatogram is also shown in Figure 3-6). The first 15.5 minutes uses only an NMe_4OH gradient. Then NMe_4^+ is replaced with Na^+ while $[OH^-]$ is held at 65 mM. As the phosphate groups have little affinity for NMe_4^+, separation is initially purely driven by $[OH^-]$; $InsP_1$'s elute at essentially the same time with KOH or NMe_4OH eluents. While $InsP_2$'s elute after PO_4^{3-} with either KOH or NMe_4OH the retention is less with NMe_4OH, likely because anionic impurities, notably carbonate, in the manually made eluent, the NMe_4OH eluent was also marginally lower in concentration (with a quartic vs quadratic dependence on $[OH^-]$ for the elution of $InsP_2^{4-}$ vs. $InsP_1^{2-}$).

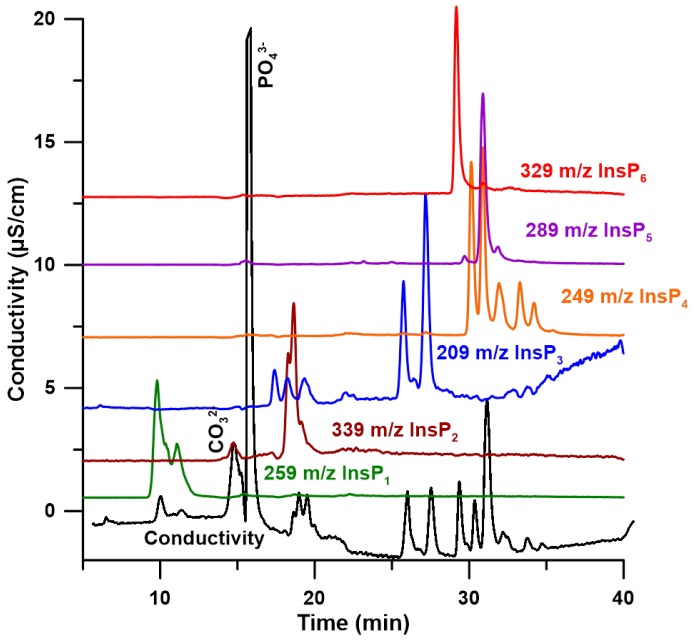

Figure 3-5 NMe_4OH and NaOH gradient separation of 12 hour hydrozylate. MS chromatograms have been rescaled for clarity.

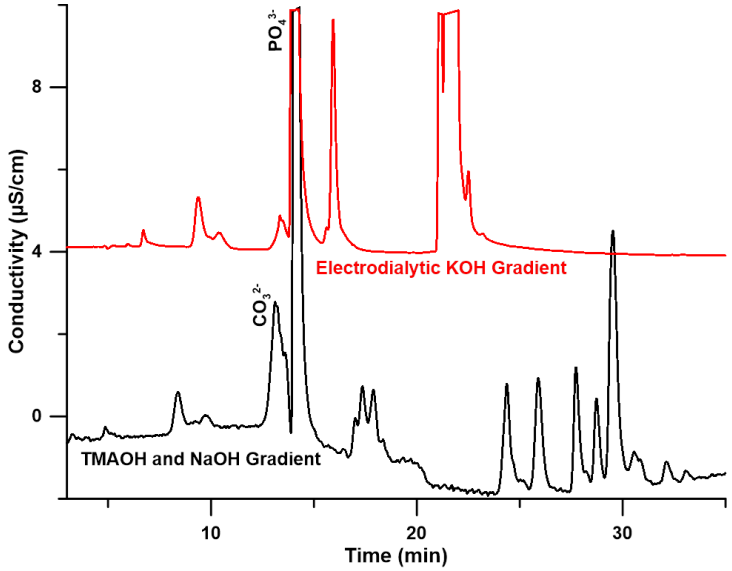

Figure 3-6 Separation of 12 h phytate hydrozylate.

The black trace is the NMe_4OH and NaOH gradient. The red trace is the same hydroxide based gradient but uses entirely KOH. The red trace has been deliberately delayed by 2.2 minutes to compensate for the volume associated with the gradient mixing chamber. This results in an apparent later elution for $InsP_1$ in the red trace.

Although it is not apparent from the conductometrically monitored chromatograms, selected ion monitored MS clearly show $InsP_3$'s elute in two regions. The first group (with at least 3 isomers) elutes with the $InsP_2$'s. Note that higher InsP's can be fragmented to lower ones during electrospray at higher voltages, we have carefully examined the effect of the electrospray voltage and used very low electrospray voltages to minimize this possibility. In any case, during electrospray InsP's can only degrade to a lower phosphorylated state and the earliest eluting $InsP_3$ elutes before any of the $InsP_2$'s (Fig. 3-5). The second $InsP_3$ group elutes only after NaOH is introduced as an eluent. $InsP_3$ has the largest number of structural isomers and spans the largest elution region (also with KOH, see Figure 3-1). In the NMe_4OH-NaOH gradient, however, the InP3's eluting in the first group likely has 2 phosphate groups on one side of the

inositol ring while the third is on the other and the eluophilic behavior of the latter is leading to equal or less retention than $InsP_2$'s. The remaining $InsP_3$'s do not elute with NMe_4OH up to the maximum concentration of 65 mM used and elute only after incorporation of Na^+ in the eluent.

The separation of $InsP_4$ – $InsP_6$ elute after $InsP_3$; $InsP_6$ eluting before any of the $InsP_4$'s or $InsP_5$'s indicating the eluophilic behavior of the largest number of phosphate groups that must remain unbound to the exchanger at a given time. Binding to the exchanger is tantamount to binding with a metal ion and the affinity of the free phosphate groups for complexation must be lower. $InsP_4$ and $InsP_5$ can respectively have 2-4 vs. 3-4 phosphate groups on a single face of the inositol ring, resulting in a narrower elution window for $InsP_5$'s. The NMe_4OH-NaOH gradient clearly provides better separation than a KOH gradient (Fig. 3-5 vs. Figs. 3-1 and 3-2). In Fig. 3-5, 18 peaks are distinguishable in 40 min compared 16 in 60 min using a KOH gradient. With selected ion MS detection and the NMe_4OH-NaOH gradient, the total number of detectable $InsP_{1\text{-}6}$ peaks are 3, 3, 6, 6, 3, 1, respectively accounting for 22 of the 40 possible separable isomers. It is possible to deconvolute the composite responses observed, assuming Gaussian peaks (phytate as a pure compound produces a nearly perfect Gaussian peak) and the maximum number of isomers possible. This is discussed in the next section about deconvolution of peaks.

Cation chromatography is routinely conducted with chelating eluents where the analyte cation is complexed by the eluent anion. The obverse, where the eluent cation is complexed by the analyte anion, is rarely used. Indeed, cation interaction is often ignored in anion-exchange chromatography but may play a critical role in improving separations of highly charged analytes.

3.3.5 Deconvolution of Peaks.

Microsoft Excel Solver was used to fit a series of Gaussian curves to the MS traces to identify potential coelutions. For each InsP's MS trace a number of curves equal to the total number of detectable geometric isomers (n) was fit according to equation (3-4):

$$F_t = \sum_i^n \alpha_i \, e^{\frac{\left(t_i - t_{ri}\right)^2}{2\sigma_i^2}} \qquad (3\text{-}4)$$

F_t is the sum total signal produced from each curve *i* at time *t* in the chromatogram. The constants α, σ, and t_r are representative of the peak height, width, and retention time respectively. Optimization of these parameters through Excel Solver was carried out using a least squares approach according to equation (3-5):

$$M = \sum_t \left(F_t - S_t\right)^2 \quad (3\text{-}5)$$

Where S_t is the background subtracted signal of the mass spectral chromatogram at time *t*. The parameters α, σ, and t_r were iteratively adjusted to produce a minimal value of *M*. It was necessary to constrain the peak width parameter σ to produce fits with widths no larger than the largest observable peak. Figure 3-7 – 3-11 show the fits for InsP1 – InsP5.

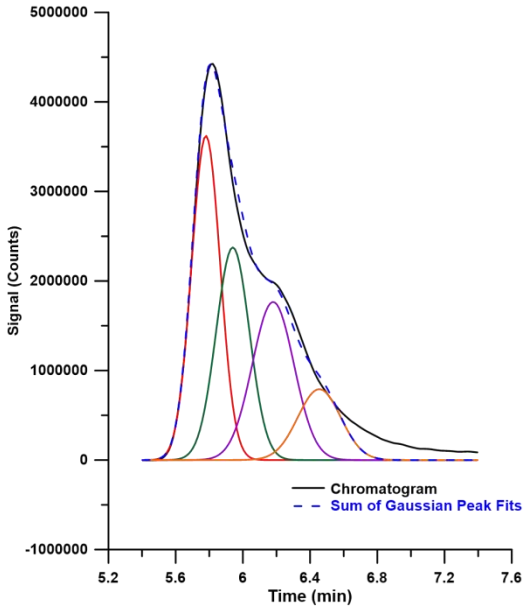

Figure 3-7 Gaussian peak to InsP1. 4 isomers are possible.

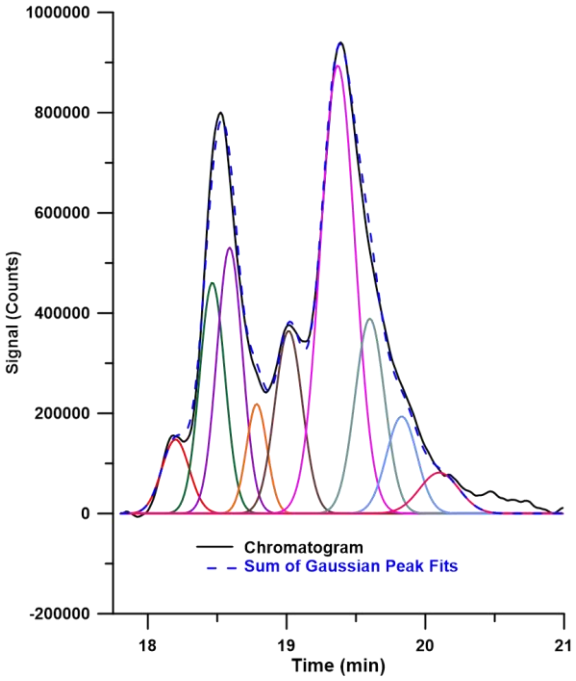

Figure 3-8 Gaussian peak to $InsP_2$. 9 isomers are possible.

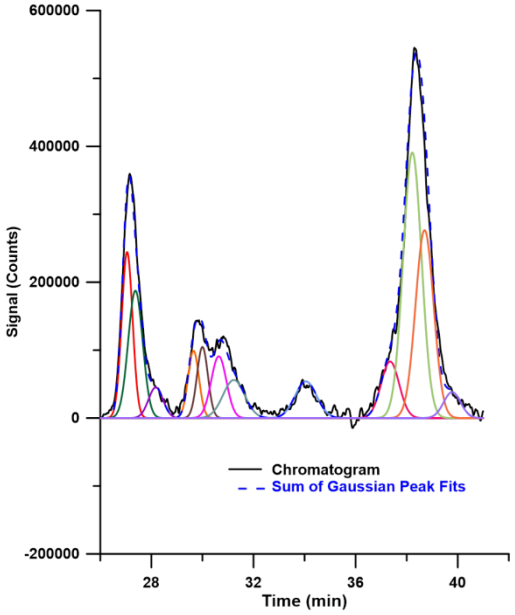

Figure 3-9 Gaussian peak to InsP3. 12 isomers are possible.

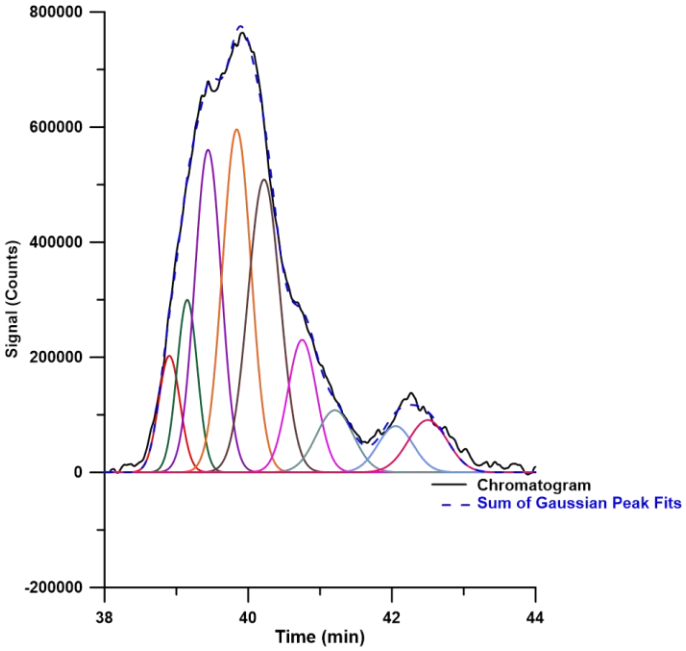

Figure 3-10 Gaussian peak to InsP4. 9 isomers are possible.

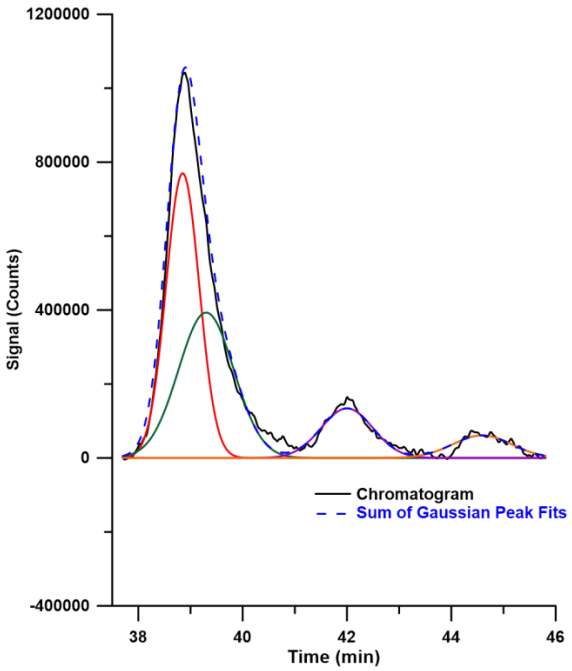

Figure 3-11 Gaussian peak to InsP5. 4 isomers are possible.

3.4 Acknowledgements

We thank Christopher A. Pohl for valuable discussion. We thank an anonymous reviewer for the suggestion to explore the effect of calcium. This research was supported by a grant from Thermo-Fisher Dionex. This chapter has been reprinted with permission from C. P. Shelor, H. Liao, A. F. Kadjo, P. K. Dasgupta. Analytical chemistry. 87 (9) 2015, pp 4851-4855. Copyright 2015 American Chemical Society

This chapter was mainly done by C. Phillip Shelor. I did the acid hydrolysis of phytate and Akinde Florence Kadjo contributed the simulation part in supporting information.

Chapter 4

Mixing Characteristics of Mixers in Flow Analysis. Application to Two-Dimensional Detection in Ion Chromatography

4.1 Introduction

Flow-based reaction detection is widely used in conventional or microfluidic formats and in postcolumn reaction (PCR) mode in liquid chromatography (LC). Moore and Stein's first automated amino acid analyzer used PCR detection with ninhydrin and constituted the basis of the first commercial liquid chromatograph.[125] To the discriminating, this is still preferred over precolumn derivatization and separation.[126]

Occasionally the desired PCR can be induced photochemically or thermally but typically a reagent is introduced to produce a more sensitively detectable compound. The two general cases of interest differ in the speed of the reaction vs. the mixing kinetics. When the former is slow, mixer design is less important: achieving good mixing in a longer timescale is not challenging in analytical situations. But LC-PCR is necessarily limited to relatively fast reactions; providing long reaction times generally lead to unacceptably large dispersion and/or pressure drops. With small volume low residence time mixers, imperfect mixing manifests itself as detector noise.

Commercially available PCR/mixer systems were reviewed some time ago.[127] Although many ingenious microfabricated mixers have since been reported;[128,129,130] none are commercially available. Of two basic mixer types, active mixers require external energy input, e.g., in the form of ultrasonic, acoustic, bubble-induced vibration, electrokinetic instability, piezoelectric vibration, pulsed flow, micro impellers, thermal actuation, magneto-hydrodynamic action, etc.[131,132] In early HPLC, magnetically stirred gradient mixers were common; the volumetric scales used today preclude their use. Passive mixers utilize part of the flow hydrodynamic energy for mixing; herein we are

solely concerned with this type. Beisler et al.[133] designed an ingenious microscale passive mixer for fast reactions that is applicable to capillary HPLC; this inexpensive device can be easily constructed from readily available components.

Turbulent flow is very effective in bringing about mixing. However, with rare exceptions,[129] passive mixers do not operate in this regime. In most analytical scale mixers, flow is not easily characterized as laminar or turbulent; because the passage length in the flow direction is often shorter than the entrance length needed to fully develop either laminar or turbulent flow.[134] In the commercially available Lee Visco-Jet mixers[135] (VJM) and the HypershearTM (HS) mixers,[136] flow is not laminar and pressure drop increases more than linearly with flow rate. The VJM (available in 3-250 μL volumes) consists of 36 serial spin chambers in which the spin direction alternates in every chamber. In the HS mixers (0.5-250 μL volume), cross flow generates vortex shearing for mixing. Diffusive mixing is enhanced by increasing the interfacial area between the streams to be mixed.[131]

Conditions to maintain vertical stratification of (immiscible) fluids in a wide microchannel, i.e., conditions that prevent breaking up of the stratified flow in segments, have been theoretically and experimentally examined.[137] Compared to conventional T- or Y- geometries,[138] structures that involve interdigitation,[139] bifurcation,[140] meandering/zigzag/sinusoidal channels,[141,142] repeated flow division and recombination,[143] patterning on the channel floor (staggered herringbone,[144] sinusoidal modulation[145]), obstacles within the channels e.g. diamond-shaped,[146] which essentially lead to splitting and recombination, or of other geometries to induce stretching and folding,[147] or both,[148] all lead to better mixing.

Although many efficient passive mixers have been demonstrated, there are some shortcomings. Many have three-dimensional features complicated to build. None of the

attractive reported micro mixers[128,129,130] are commercially available. Low Reynolds number (N_{Re}) passive mixers depend on diffusion for mixing and are not particularly efficient. Herein we characterize three easy-to-build and three commercially available mixers. We quantify the mixing efficiencies, and evaluate the overall performance to find an optimum design for reaction detection in flow analysis/PCR-LC.

4.2 Experimental section

An ICS-5000 ion chromatography (IC) system with two independently operable channels, with modifications as shown in Figure 4-1, was used. The principal flow was delivered by pump 1 (10.000 mL/min max, 0.001 mL/min resolution). The nominally minor flow was delivered by pump 2 (3.0000 mL/min max, 0.0001 mL/min resolution). Guard and analytical columns (AG11 and AS11, 2x50 and 2x250 mm) were utilized when mixing an electrolyte with water (see Figure 4-1b). Data collection and analysis were performed using Chromeleon 7.1 software (www.dionex.com). Analyte solutions were prepared with reagent grade chemicals.

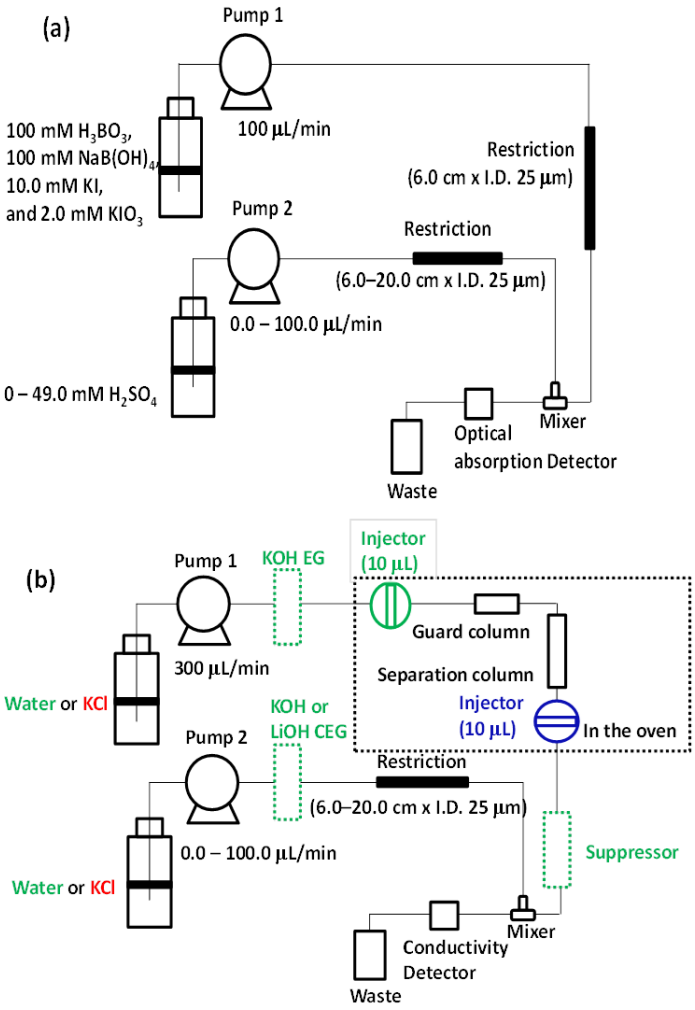

Figure 4-1 All experiments were centered on an ICS-5000 IC system. (a) Villermaux-Dushman reaction system; (b) baseline noise measurement setups and 2-D chromatography setup.

A note about Figure 4-1. EG, Eluent generator; CEG, Capillary eluent generator; (A) Villermaux–Dushman reaction system: Optical absorption detector, 398 nm LED based flow-through detector, restrictors provide adequate backpressure for proper pump operation; the restrictor length after pump 2 was varied with increasing flow rate to keep pump pressure within the optimum range; (B) Dotted enclosure indicates these

components were within a thermostated enclosure at 30 °C System for (1) Baseline noise measurement setup A: KCl or water pumped through pump 1, KCl or water pumped through pump 2; (2) Baseline noise measurement setup B (relevant to chromatography): all green components active, no blue injector, water pumped by both pumps, EG generates 4 mM KOH, goes through column and suppressor (noise at suppressor exit ~1 nS/cm) CEG generates small amount of LiOH or KOH which is introduced through the mixer to generate a final concentration of 0.1 mM base after mixing, (3) Dispersion measurement setup: both pumps pump water, columns or restrictors provide adequate backpressure for properpump operation. Injector (in blue) is used for 0.4 mM KCl injection; (4) 2-D chromatography setup: similar to setup B except a gradient is optionally run in the EG (see e.g., Figure 4-19) and electrogenerated LiOH is introduced before the mixer to obtaina final concentration of 0.1 mM LiOH and on to the detector.

4.2.1 Laboratory-made Mixers.

Backflow tee mixer (BT), end-blocked membrane tee mixer (EMT), and tubular membrane mixer (TM) designs are shown in Figure 4-2 (Figure 4-3 also shows photographs of BT and TM mixers). BT, EMT, and TM have asymmetric inlet ports. When the two flows to be mixed are unequal, exchanging the identity of the inlet ports will significantly affect the mixing performance. The TM architecture most closely resembles a tee, except that the two fluids meet not at a single point but all along the length of a porous tube, representing a multitude of apertures. The EMT design similarly exploits reagent introduction through a microporous fiber, in a different configuration. The BT design effectively uses a much smaller aperture for the smaller flow that meets the larger flow head-on and likely penetrates into it; mixing then continues in the annular space before exiting. The BT mixer was made in two different dimensions, the smaller BT-250

used 250 μm i.d. and the larger BT-330 used 330 μm i.d. PEEK jacket tubes. Unless otherwise stated, BT refers to BT-330. The construction of these three mixers is described as following.

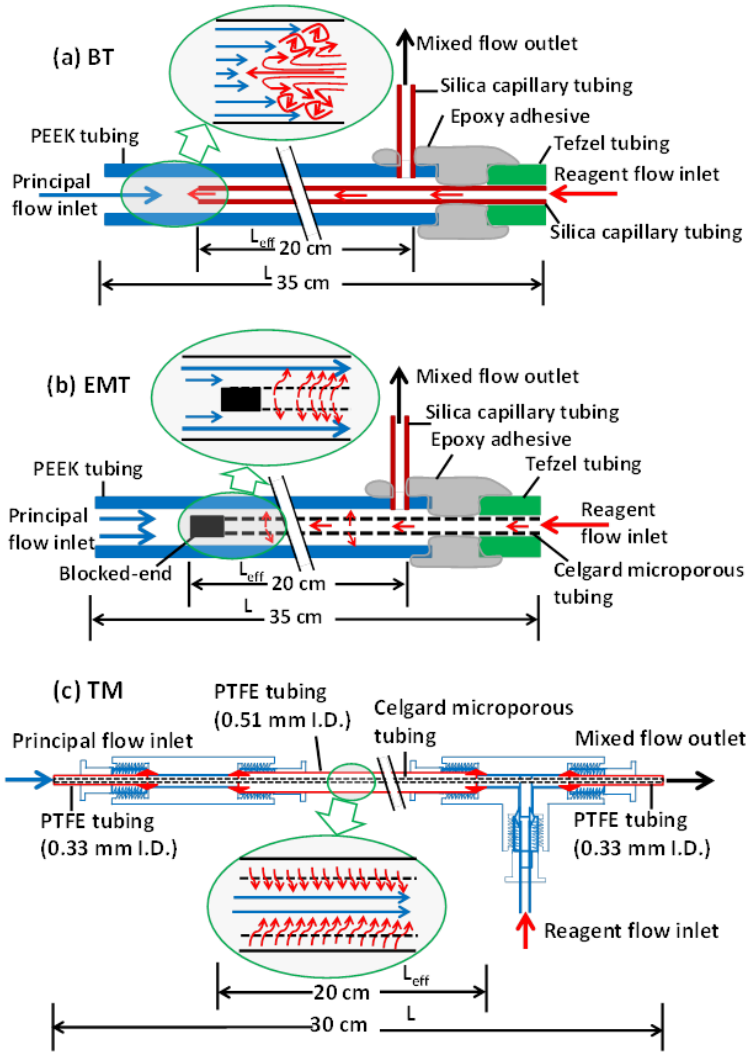

Figure 4-2 Three different laboratory-built mixers: (a) Backflow tee mixer (BT), (b) End-blocked membrane tee mixer (EMT), and (c) Straight tubular membrane mixer (TM).

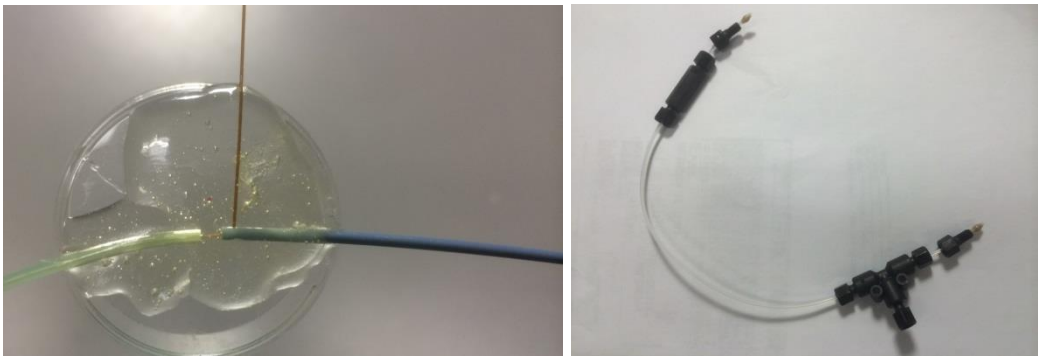

Figure 4-3 Photographs of (a) Left: BT and (b) Right: TM mixers.

(a) Two types of the BT-mixers were constructed. Both used a PEEK jacket tube of 1.59 mm o.d.; in one type, the i.d. was 0.33 mm (BT-330), in the other, the i.d. was 0.25 mm (BT-250). Both were built in different lengths (longest for BT-330: 50 cm, that for BT-250: 100 cm). A 0.41 mm ϕ hole was made into the PEEK tube wall 2.0 mm from one end. A fused silica capillary tubing (100 mm x 0.10 mm i.d. × 0.36 mm o.d.) was epoxied into this hole as the outlet. A second fused silica capillary tubing (0.05 mm i.d. × 0.15 mm o.d.) was inserted from the outlet end of the PEEK jacket (from the end where the outlet capillary was already attached) until it was 5 cm from the open end of the PEEK jacket tube (see Figure 4-2a). The free end of this second silica tubing was then protected with a Tefzel sleeve tubing (1.59 mm o.d., 0.175 mm i.d.). The PEEK-Silica capillary-Tefzel tube joint was affixed together with epoxy, taking care to prevent the epoxy from intruding into the PEEK tube and blocking the exit aperture. For an effective length of 20 cm, the PEEK jacket tube length used was 25 cm and the length of the second silica capillary tube was 30 cm and the length of the PTFE sleeve tubing was 10 cm.

(b) The EMT mixer was constructed very similar to a BT-330 mixer except that a Celgard microporous membrane tube (100 µm i.d.; 150 µm o.d.) was used instead of a silica capillary. One end of the membrane tube was melted shut, this tube was introduced

into the PEEK jacket tube with the closed end first until this was ~5 cm from the end of the PEEK jacket tube. The protruding end of the membrane tube was protected with a Tefzel sleeve as with the BT design and the joint embedded in epoxy.

(c) For the tubular membrane (TM) mixer, a larger Celgard microporous hollow fiber (200 μm i.d.; 290 μm o.d.) was used as the principal flow conduit. A PTFE tube (0.51 mm i.d.; 1.59 mm o.d.) was used as the central jacket as shown in Figure 1c. The termini of the Celgard tube coming though the tee or union was inserted to a PTFE tube (330 μm i.d.; 1.59 mm o.d.) and compression sealed.

4.2.2 Commercial Mixers.

A commercial binary tee “hypershear” mixer available in two volumes (HS 402-0002B and 400-0010B, nominally 2 and 10 μL internal volumes, respectively, hereinafter termed HS-2 and HS-10) containing a mixer cartridge inside (www.triadsci.com), was investigated. A Visco-Jet Micro mixer (VJM, www.theleeco.com) with an internal volume of 10 μL was also studied. All three have symmetric inlet ports, exchanging inlet flows has no effect on the mixing efficiency.

4.2.3 Fabrication of Optical Absorption Detector.

An LED based flow-through optical absorption detector (398 nm, Figure 4-4) was used. The detector was based on a flow cell (Dionex, ULT-UZ V03). A 398 nm LED (FWHM 13 nm, ETG-5UV-395-15, www.etgtech.com) was placed into a stainless steel tubing (8.00 mm × 5.06 mm I.D. × 6.10 O.D. mm) with one end touching the cell body to provide for heat dissipation as shown in Figure 4-4a. The LED, the stainless steel tubing, and the cell window were concentric so that most of the LED emission was incident on the window. The LED tip was 1.0 mm from the cell window. The assembly was fixed on the cell window by hot melt adhesive.

A 3x3 mm photodiode (Siemens BPW34) was placed into a straight TFE tubing (20.0 mm × 6.0 mm I.D. × 8.0 O.D. mm). The front surface of photodiode was perpendicular to the tube axis. The tube/photodiode was fixed on the opposite window of the cell by hot melt adhesive. The assembly on this side was then covered by aluminum foil to eliminate external light. The front surface of photodiode was very close to the cell window. Two PMMA plates held the detection cell together, as shown in Figure 4-4b.

A constant current source was used to power the 398 nm LED at 50 mA. Current-to-voltage conversion of photodiode was carried out with a current amplifier (model 427A, www.keithley.com). Data were recorded after current to voltage conversion with a 16-bit A/D card (USB-1608FS, www.mccdaq.com) at 1 Hz.

The LED emission spectrum was recorded by a fiber optic CCD spectrometer (Black comet, www.stellarnet.us). The UV-Vis spectrum of triiodide at different wavelengths was recorded by an Agilent 8453 UV-Vis diode array spectrophotometer.

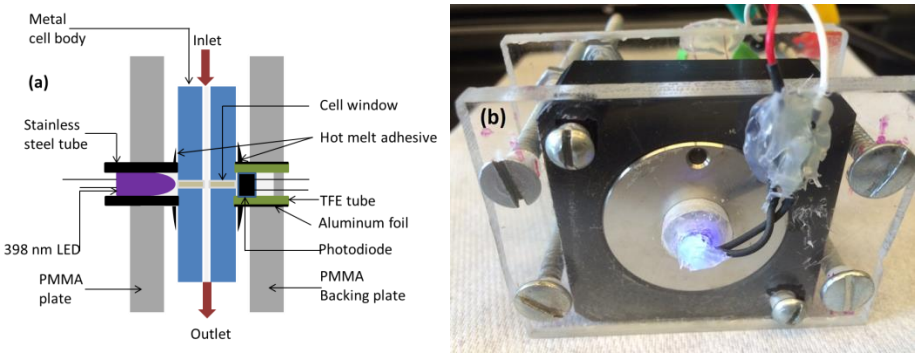

Figure 4-4 (a) Schematic diagram of a light emitting diode (LED) based flow-through optical absorption cell and (b) Photograph of the optical absorption cell.

4.2.4 Measuring Mixing Efficiency.

Mixing properties of all the six devices were investigated by two methods, the first being the Villermaux-Dushman reaction system (see below). Figure 4-1a illustrates the experimental setup and Figure 4-5 shows the chemical process. “Perfect” mixing

implies there is no inhomogeneity at any time, not attainable in reality in any process that involves mixing of two liquids. It is possible with homogeneous reagent generation. 100 mM H_3BO_3/100 mM $NaB(OH)_4$ buffer solution, containing 10.0 mM KI and 2.0 mM KIO_3, is delivered by pump 1. Different concentrations of H_2SO_4 are delivered by pump 2, the acid concentration and flow rates are so chosen that the final pH of a fully mixed solution will still be >7.0. Iodine (triiodide) from iodate and iodide is only produced (irreversibly) when mixing is imperfect and there is momentary local excess of acid. Poor mixing history is indicated by high optical absorption, measured in-line by the 398 nm LED based flow-through optical absorption detector.

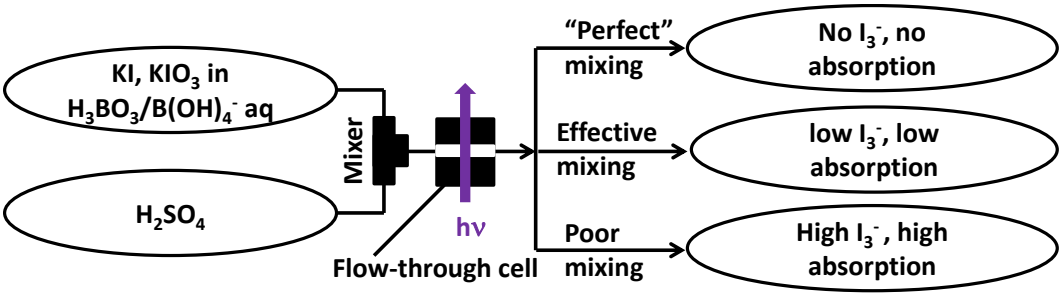

Figure 4-5 The Villermaux-Dushman reaction scheme for mixing measurement.

Whereas the above measurement largely provides an indication of the cumulative history of mixing inhomogeneity, in many cases the instantaneous inhomogeneity, as reflected by the noise registered by the detector, is of greater interest. This is commonly measured by mixing a dye with a diluent or mixing a pH-indicator dye in acid/base with a base/acid. Because a conductivity detector with very low intrinsic noise was available to us, we chose to measure the conductance noise after mixing water and an electrolyte (see Figure 4-1b). The noise necessarily includes that from momentary changes in the volume flow rates resulting from pump pulsations.

4.2.5 Dispersion measurement.

Minimum dispersion is desired in LC-PCR applications. The dispersion caused by the mixer was assessed from the difference in band volumes as measured by a small volume conductance cell (0.7 μL, Dionex 072041), when 10 μL 1 mM or 0.4 mM KCl was injected into a water carrier as shown in Figure 4-1b. It is important to note that for any two-inlet–one-outlet mixer, where the sample is injected into the principal flow, the measured band dispersion is a function of not only the principal flow but also the auxiliary (reagent flow). Without auxiliary flow, the fluid diffuses towards the unused inlet port and increases the apparent dispersion. The observed dispersion is thus expected to decrease as the auxiliary flow is increased. In addition, the sample is necessarily diluted by the auxiliary flow. If there was no dispersion, the volume half-width of the band will still increase with auxiliary flow but the time half width as observed by the detector will be unaffected because the velocity changes proportionately. The dispersion is calculated as $2F_p(W_{1/2}^2 - W'^2_{1/2})^{1/2}$, where F_p is the principal channel flow rate and $W_{1/2}$ and $W'_{1/2}$ are the respective peak half-widths in time units, observed with and without the mixer.[20] Note that an additional PEEK tubing (0.13 mm i.d. 180 mm long) had to be used for connection when VJM, HS-10, and HS-2 were measured (this was included in the no-mixer measurement).

The conductivity detector and the optical detector rise times were set at 0.5 and 0.2 s. The data were acquired with 16-bit resolution (USB-1608FS, www.mccdaq.com) at 1 Hz. Chromatographic data were acquired at 10 Hz.

4.3 Results and discussion

4.3.1 Characterization of Mixing.

Many methods have been used to test the performance of microscale mixers. When reactions and processes involved in mixing may be simple dilution or are fast or

reversible, baseline noise levels can be used to quantify the mixing performance.[136] In more complex reaction systems, when any of the involved reactions are irreversible (at least in the mixing and the subsequent observational timescale – some metal-ligand chromogenic reactions fall in this category), baseline noise measurement is not sufficient – an index of the cumulative history of the system inhomogeneity is needed. This is typically conducted using multicomponent competing parallel reactions that are sensitive to local excesses of one reagent or another and hence, mixing. Product yields or concentration distributions are used to quantify the mixing performance,[128,130,143,149] photometric measurement being most common.[143,146]

Of many reactions that have been used for the purpose, the Villermaux-Dushman reaction, involving mixing slightly alkaline borate-buffered solution of iodate and iodide with a solution of dilute H_2SO_4, is considered the benchmark.[128,130,149] Flow ratios and reagent concentrations are so chosen that if complete mixing occurred, the solution will still remain alkaline. So while some of the borate may be neutralized according to eq 1

$$B(OH)_4^- + H^+ \rightarrow B(OH)_3 + H_2O \quad \ldots(1)$$

In the presence of a local excess of acid, iodine is irreversibly formed:

$$5I^- + IO_3^- + 6H^+ \rightarrow 3I_2 + 3H_2O \quad \ldots(2)$$

and iodine is rapidly converted to triiodide (the species optically measured)

$$I_2 + I^- \rightarrow I_3^- \quad \ldots(3)$$

The neutralization of borate by H^+ is instantaneous (diffusion-controlled) while the iodine formation rate follows a fifth order process[150]

$$d[I_2]/dt = k[I^-]^2[IO_3^-][H^+]^2 \quad \ldots(4)$$

where the rate constant k is somewhat ionic strength dependent. Under most well mixed conditions, the total amount of iodine produced (and hence the consumption of I^- and IO_3^-) is relatively small and eq 4 thus reduces to a pseudo second order reaction:

$$d[I^2]/dt = k' [H^+]^2 \quad \ldots(5)$$

4.3.2 Mixing and Reynolds Number (N_{Re}).

Turbulent flow (N_{Re} >~2000) is known to provide effective mixing. Even at N_{Re} values considerably below this transitional regime, the extent of mixing may be related to N_{Re}. Computed N_{Re} values at the annulus (equaling $Qd/(\nu A)$, where Q is the total volumetric flow rate, d is the hydraulic diameter of the annulus, ν is the kinematic viscosity, and A is the hydraulic cross section) are shown in Figure 4-6 for the different mixers as a function of the auxiliary stream flow rate. N_{Re} values increase in the order BT~EMT < TM < VJM but all are far below the turbulence transitional regime. However, these small scale mixers cannot be properly considered by laminar flow models, as the length of the element in the direction of flow is not sufficient to fully develop laminar flow.[134]

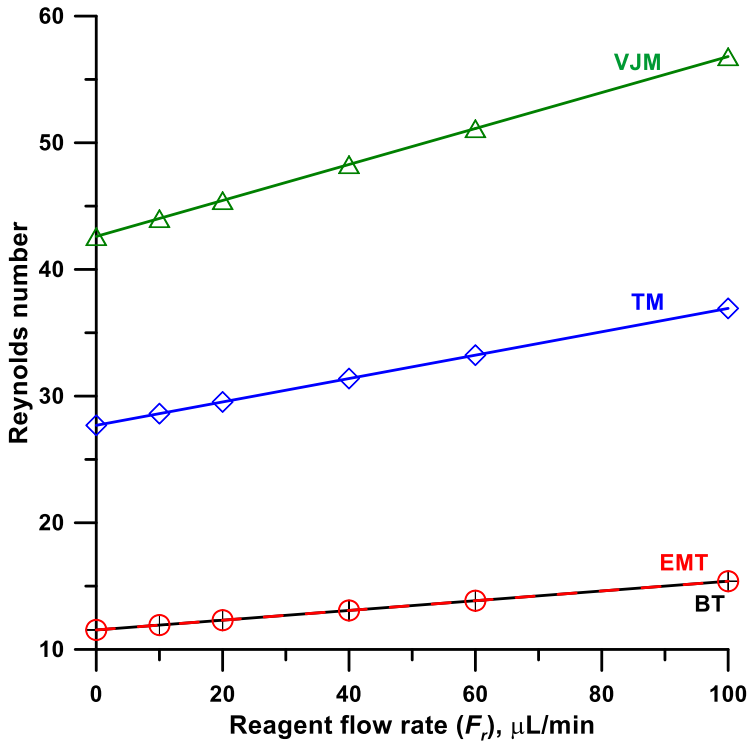

Figure 4-6 Reynolds numbers (N_{Re}) for BT, EMT, TM, and VJM.

Note that principal flow F_p maintained constant at 300 μL/min. For the homemade mixers, the calculations pertain to the annulus, for the membrane mixers, specifically it pertains to the terminal portion when the reagent flow F_r has fully exited the membrane. NRe is calculated as $Qd/(\nu A)$ where Q is the total flow rate $F_p + F_r$, d is the hydraulic diameter ($d_o - d_i$, d_o is the inner diameter of the PEEK tube and d_i is the outer diameter of the silica/Celgard® tube), ν is the kinematic viscosity of water (taken as 0.01 cm^2/s) and A is the hydraulic cross section $0.25\pi(d_o^2 - d_i^2)$. For the VJM, the flow passes through a series of orifices of diameter d= 0.13 mm and the area A also pertains to the same orifice.

4.3.3 Absorbance measurements.

The absorption spectrum for triiodide is shown in Figure 4-7. Although the emission peak of the LED was off the absorption maximum (353 nm), there was sufficient sensitivity for our purpose. The absorbance output signal $A_{398\ nm}$ was linearly related (r^2 =0.9980) to the triiodide concentration at [I_3^-] <0.60 mM (Figure 4-8).

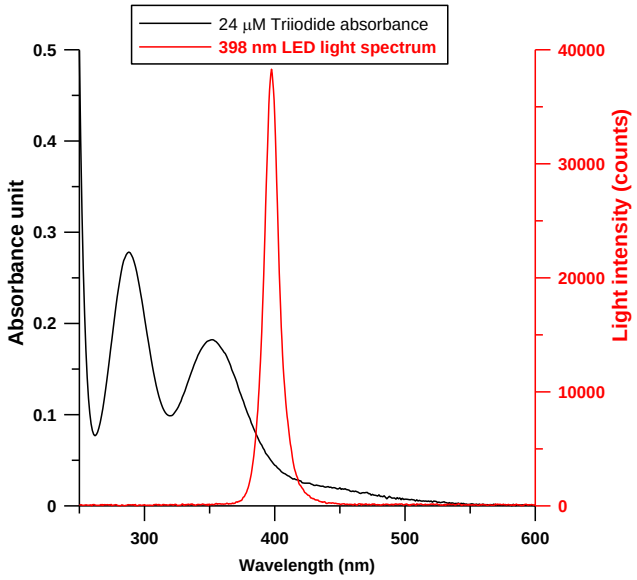

Figure 4-7 Black trace: the UV-Vis spectrum of 24 μM triiodide. Red trace: 398 nm LED (ETG-5UV-395-15, www.etgtech.com) emission spectrum.

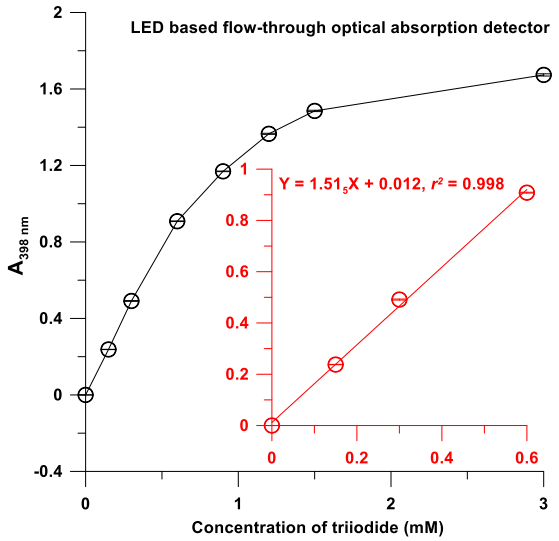

Figure 4-8 The relationship between the triiodide concentration and measured absorbance using the LED based absorbance detector.

4.3.4 Effect of Acid Concentration.

The relationship between the H_2SO_4 concentration used and the observed triiodide absorbance was studied for the VJM with identical volume flow rates for both streams. If eq 5 is valid, a plot of log A_{398} vs. log $[H^+]$ should have a slope of 2. Figure 4-9 shows such a plot ($[H^+]$ calculated for a final mixture where the principal stream would be water); the observed slope of 1.97 is in reasonable agreement with eq 5, given that no activity corrections were made. While the $[H^+]$ relevant to the actual reaction must be the local excess $[H^+]$ and not simply that of a diluted reagent, the only assumption we can make is that the two are related. As $[I_3^-]$ obviously increases with increasing $[H_2SO_4]$, we chose 49.0 mM H_2SO_4 as reagent for further experiments to magnify the difference between the mixers.

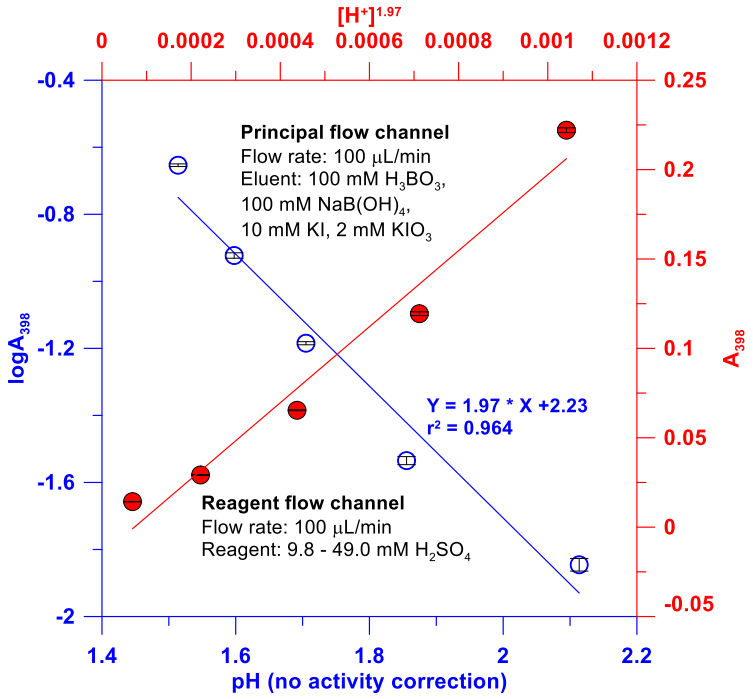

Figure 4-9 The relationship between the logarithm of the observed triiodide absorbance and the logarithm of the hydrogen ion concentration.

Error bars for each datum are shown as ±1 standard deviation. The Visco-jet mixer was used with equal flow rates. The hydrogen ion concentration is computed for a H_2SO_4 solution that will result if the reagent flow was diluted by a principal flow of water.

4.3.5 Mixing Flow Ratio and Interpretation of Mixing Efficiency.

Many, if not most, mixing studies are conducted with identical volume flow rates of both streams.[128,143] Mixing is generally optimum under these conditions. In most analytical applications, however, the intent is to form a product by adding a reagent to the analyte; the reagent flow rate is invariably set significantly lower than that of the analyte to reduce dilution. We presently studied principal: auxiliary (reagent) flow ratios from 1:1 to 10:1. Figure 4-10 shows $A_{398\ nm}$ plotted against the reagent flow rate. However, the triiodide yield depends not only on the mixing history, but also on the acid concentration

(Figure 4-9). As the reagent flow rate changes, at a constant acid concentration, the total amount of acid introduced also changes. A more appropriate way to compare the cumulative mixing history is to incorporate this $[H^+]$ dependence and plot $A_{398\ nm}/[H^+]^2$ as the dependent variable (Figure 4-11), $[H^+]$ again being computed for the final solution as if the principal flow was water. With the exception of HS-10 in the 10-40 μL/min reagent flow range, the mixing for all the mixers improved as the reagent flow rate approached the principal flow rate. Over the entire reagent flow rate range, BT exhibited the best cumulative mixing history. For BT, the principal flow channel has a much higher hydraulic cross section than the reagent channel, leading to a high reagent linear velocity and the reagent flow interacts directly with the central, highest velocity portion of the principal flow and penetrates into it. The interfacial area between two streams thus increases, resulting in good mixing. HS-2 provides the next best cumulative mixing while TM shows the poorest mixing history at low reagent flow rates (10.0 – 50.0 μL/min). In the TM design, an acidic layer is formed along the internal wall of the porous tube, promoting triiodide formation. This stagnancy breaks up at higher reagent flow rates and good mixing results. EMT and VJM show similar cumulative mixing history at all reagent flow rates. Curiously, HS-10 consistently exhibited greater cumulative inhomogeneity than HS-2. Individual mixing elements have larger dimensions in HS-10 compared to HS-2, poorer mixing per element results. It is tempting to add that the greater residence time in HS-10 leads to additional I_3^-; however, adding an additional 68 μL residence volume (0.76 mm i.d. × 150 mm PEEK tubing) after HS-2 produced a negligible amount of additional I_3^- (Figure 4-12) indicating that mixing was complete enough for the acid to have been already consumed.

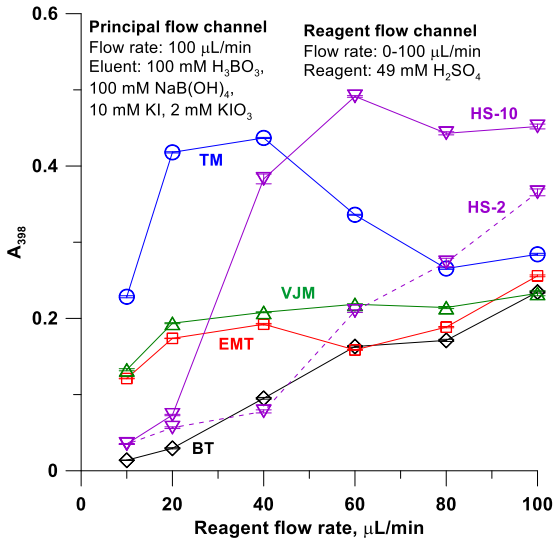

Figure 4-10 Triiodide yield under different reagent flow rates for different mixers.

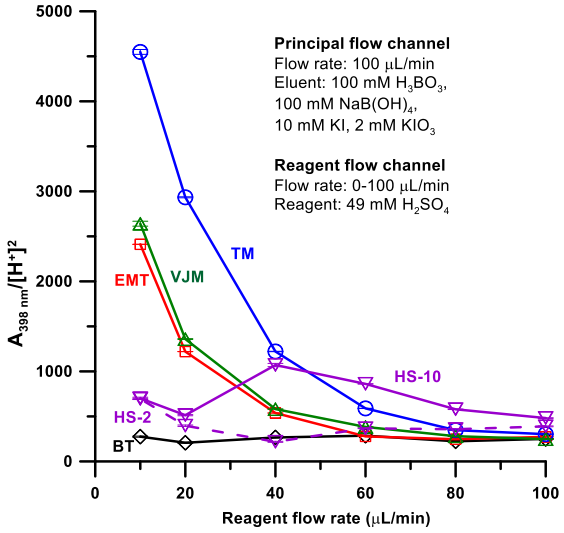

Figure 4-11 The triiodide yield, normalized to H^+ present, for the different mixers as a function of the reagent flow rate.

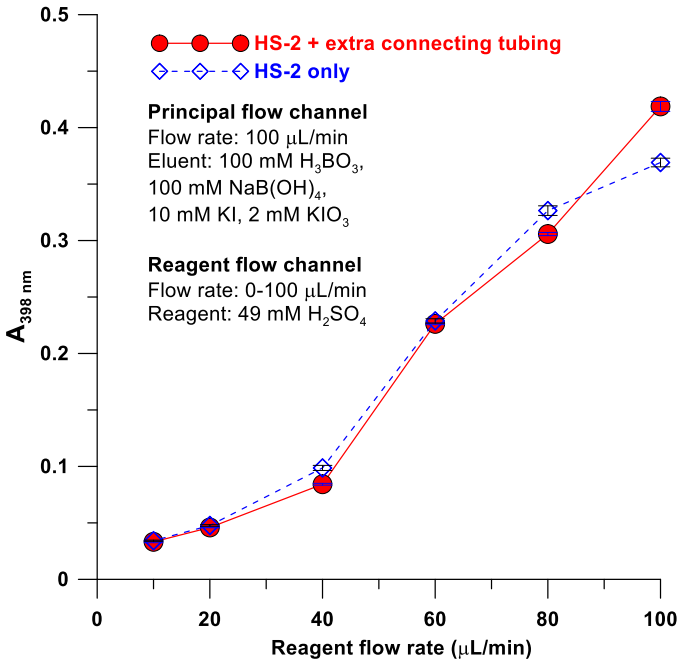

Figure 4-12 Triiodide production at different reagent flow rates for HS-2 with and without additional tubing after mixer.

4.3.6 Baseline Noise Measurements. Different Source Contributions.

For fast reactions without complications of parallel reactions, the parameter of interest is baseline noise. Different noise sources add in a root mean square (rms) fashion; the observed baseline noise (N_B) can be expressed as[151]

$$N_B = (N_M^2 + N_F^2 + N_O^2)^{1/2} \quad \ldots(6)$$

Where N_M is the mixing noise from imperfect mixing of two liquids, N_F is the noise from flow pulsations, and N_O is the noise from all other sources, including electronic noise. N_O is insignificant in the present system, (<0.2 nS/cm at 23 μS/cm background).[152] Illustrative data are provided for the VJM in Figure 4-13. Except as stated, numerical values of the noise cited in this paper represent the standard deviation of 5 minutes worth of baseline data (this approach somewhat overestimates the noise as drift is included in noise). Referring to Fig. 3-13, when 0.16 mM KCl (specific conductance 25 μS/cm) was pumped

by pump 2 (trace A) the measured noise was 0.4 nS/cm. The same solution when pumped with pump 1 at 300 μL/min produced slightly higher noise (trace B), 1.2 nS/min, much of this is caused by drift. Trace C represents the baseline noise observed upon mixing 0.16 mM KCl (pump 1 300 μL/min) with 0.16 mM KCl (pump 2, 100 μL/min) with the VJM; this was measured to be 2.3 nS/cm. This value is obviously significantly higher than the rms sum of A and B. The phenomenon is highly reproducible, The pump strokes are not synchronous and the pulsations from one apparently amplifies the pulsations from the other, resulting in a more than additive effect. We thus take N_F to be 2.3 nS/cm, as the two liquids being mixed are identical, N_M is zero. In trace D, deionized water is pumped by pump 1 at 300 μL/min and 0.64 mM KCl is pumped by pump 2 at 100 μL/min; the observed noise was 26.6 nS/cm. Based on eq 6, N_M would be 26.5 nS/cm; the mixing noise in this case thus accounts for 99.6% of the total noise.

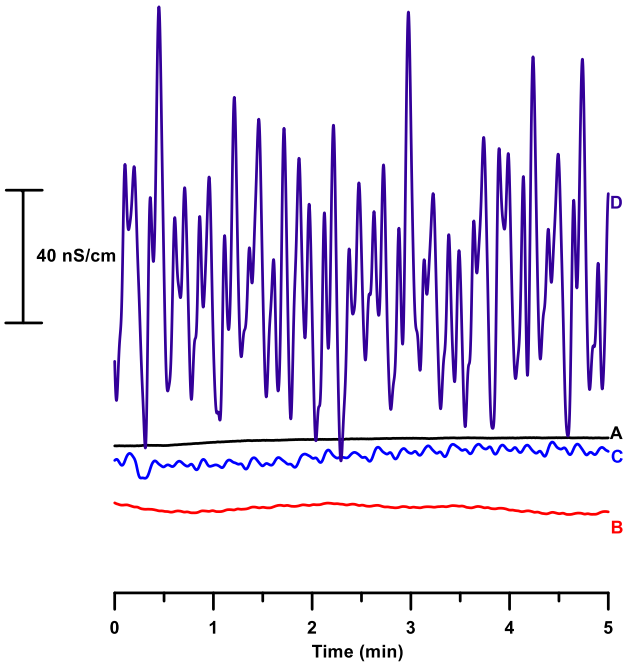

Figure 4-13 . Baseline noise for VJM with gradient pump and isocratic pump for eluent and reagent, respectively.

Curve A. noise for 0.16 mM KCl reagent at 100 μL/min; Curve B . noise for mixing 0.16 mM KCl reagent and 0.16 mM KCl eluent at 100 μL/min and 300 μL/min, respectively; Curve C . noise for 0.16 mM KCl eluent at 300 μL/min; Curve D. noise for mixing 0.64 mM KCl reagent and eluent (DI water) at 100 μL/min and 300 μL/min. The conductivity background of mixing flow of 0.16 mM KCl was maintained at 25 μS/cm.

4.3.7 Mixing Noise of Different Mixers at Different Reagent Flow Rates.

In general, the other mixers performed better than the VJM in this test. In the following, the principal flow (water) was maintained at 300 μL/min and KCl was pumped by pump 2 at 10-100 μL/min; the KCl concentration was varied to maintain a final effluent concentration of 1.0 mM KCl (147 μS/cm). The results appear in Figure 4-14; each run was carried out in triplicate and error bars of ± 1 sd are also shown. As sight variations in the background conductance cannot be avoided, the data are reported as a fraction of the background conductance.

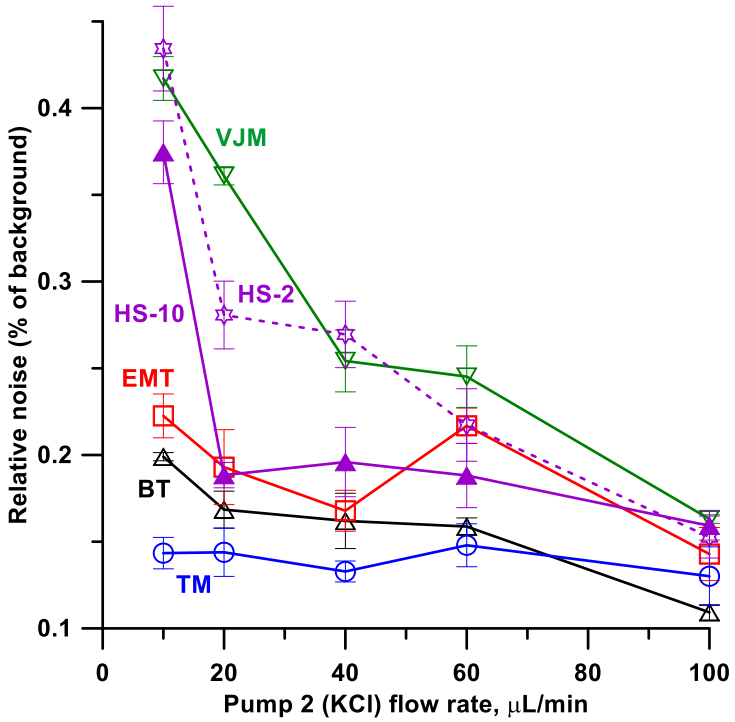

Figure 4-14 Noise level observed with different mixer devices.

With the possible exception of TM, for all other mixers, the baseline noise generally decreased with increasing reagent flow rate. Within experimental error, the noise with TM remained constant with the reagent flow rate. TM and BT exhibited the lowest baseline noise, TM providing the best noise characteristics at reagent flow rates up to 75.0 μL/min and BT outperforming it at higher flow rates. With the exception of one aberrant datum (at 60 μL/min reagent flow rate) for EMT, all three laboratory-made mixers with asymmetric inlet ports performed better than the commercial mixers, all with symmetric inlet ports.

Interestingly, although HS-2 showed better cumulative mixing history than HS-10, the substantially longer residence time in HS-10 resulted in the final mixture to be more homogeneous.

4.3.8 Internal Volume and Dispersion induced by Mixers.

In flow analysis and especially LC-PCR detection, it is important to minimize dispersion. While the internal volume of a mixer contributes to the dispersion, the flow geometry may be more important. The internal volumes (μL) of the mixers were measured via the residence time of a 10 μL 400 μM KCl plug (Figure 4-15, no auxiliary flow through the mixer (auxiliary inlet closed) at a principal flow rate of 300 μL/min). The volumes measured were: 8.3±0.6 (HS-2), 9.5±0.9 (VJM), 13.6±0.8 (TM), 16.7±1.0 (EMT), 17.1±0.6 (HS-10), and 20.3±0.9 μL (BT). Of the laboratory-made mixers, at 13.6 μL TM had the smallest volume but all three can be built with adjustable lengths. The manufacturer stated volumes for HS-2 and HS-10 are for the cartridge only; those for the whole assembly were significantly larger. The VJM volume precisely corresponded to the manufacturer stated value.

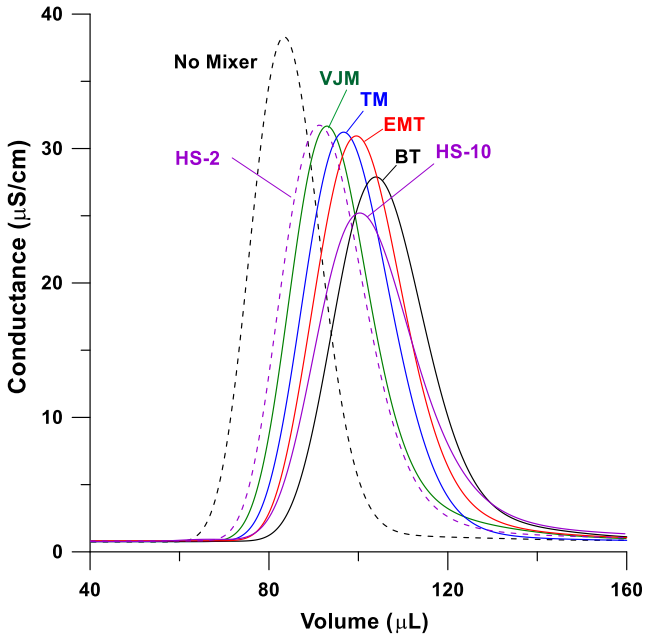

Figure 4-15 Internal volume and dispersion measurements of different mixer devices.

The dispersion data for the devices are shown in Figure 4-16a as a function of the auxiliary (reagent) flow rate. The VJM exhibits the lowest dispersion (with 100 μL/min auxiliary flow rate the dispersion is essentially zero) with TM a close second. HS-10 exhibits the highest dispersion. However, most reactions are not instantaneous and require a finite time. Often, a mixing coil or other reaction conduit that is knit in certain patterns or knotted, etc.[153] is put after the mixing point/tee to allow for the reaction to occur; this of course is not needed if the reaction is very fast. If an additional reaction conduit needs to be provided after the mixer, the dispersion induced by the mixer may be the lesser contributor. If the design permitted, the mixer itself can be made with greater residence volume to function both as the mixer and the reactor. Of course, the dispersion will increase as the residence volume is increased. The choice of the optimum mixer-reactor volume will clearly vary from one reaction to another and will be a combined function of the reaction kinetics, the dispersion induced by the mixer-reactor, and any decrease in noise brought about by the additional residence volume. While the absolute value of the dispersion induced by a mixer may be important for instantaneous reactions, often the more important characteristic in a mixer-reactor is the dispersion per unit residence volume, a dimensionless quantity, hereinafter termed Dimensionless Relative Dispersion. This is depicted in Figure 4-16b. By this measure, with the exception of the VJM at high reagent flow rates, all three laboratory made devices outperformed their commercial counterparts. The lowest volume mixer HS-2 had the worst relative dispersion and HS-10 the next; the large i.d. (0.50 mm) of the inlet ports of these devices doubtless contributed to this. The best overall relative dispersion was exhibited by TM, except for VJM at high flow rates.

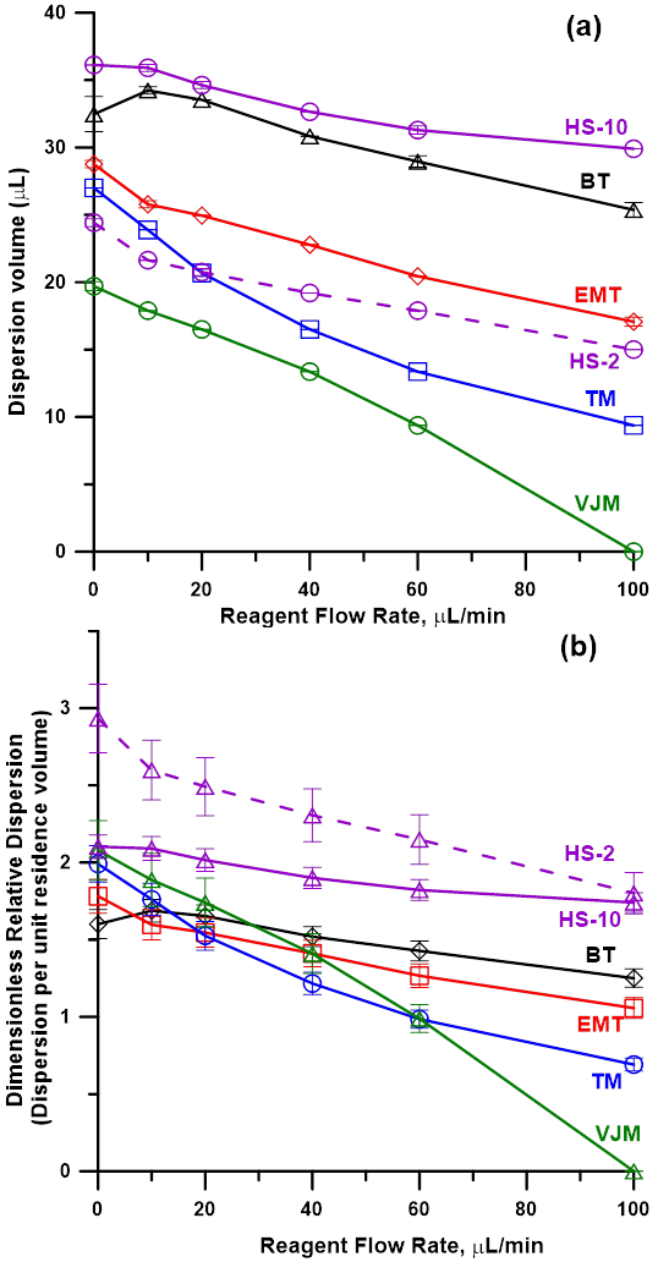

Figure 4-16 Dispersion of mixer devices with different auxiliary flow rates. (a) absolute value (b) Dispersion per unit residence volume.

As all the present laboratory-made mixers can be tailored to any length (residence volume), to function as a mixer-reactor and accommodate both the residence

volume and the mixing need, it was of interest to determine how the noise and the dispersion changes as a function of the device length/residence volume. Note that none of the conventional mixers can function as mixer-reactors. We studied the absolute and relative dispersion (black and red traces, respectively, Figure 4-17) induced by BT-330 devices for 5-25 cm device lengths. The noise in the effluent was studied for both BT-330 (5-50 cm) and BT-250 (10-100 cm) devices (for equal lengths, a BT-330 device has approximately twice the volume of a BT-250 device). Figure 4-17 shows that the dispersion asymptotically increases to some limiting value with length, while the relative dispersion similarly decreases to some limiting value. In both cases the behavior was well represented by quadratic equations. On the other hand, the noise changed relatively little as a function of device length: For BT-250, the noise was essentially constant at ~400 ppm of the baseline value up to a length of 80 cm and then decreased by 15% at 1 m. For BT-330, the decrease in noise with length was monotonic but from 5 to 50 cm the noise decreased by a mere 36%.

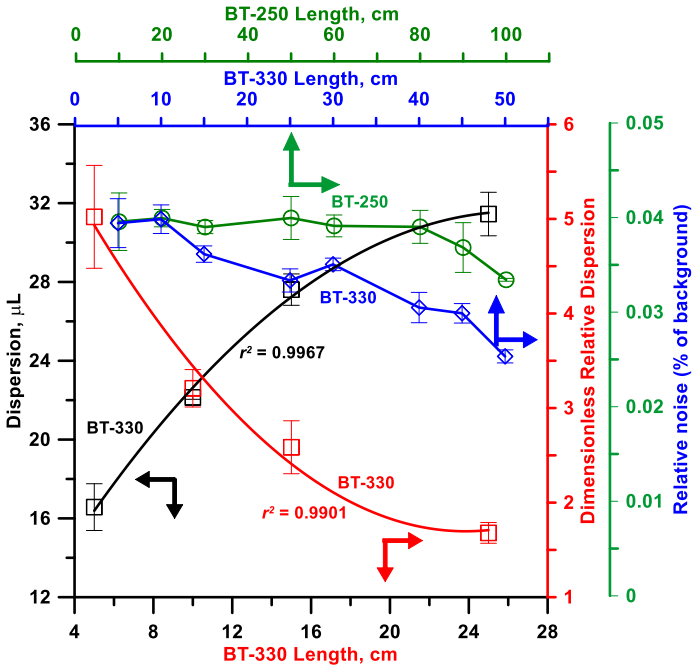

Figure 4-17 Dispersion, relative dispersion, and relative noise measurement. Note that All but the green trace pertains to BT-330. There were no auxiliary flow in these dispersion data. Triplicate measurements; ± 1 SD error bars are shown. Axes and title in one color indicates pertaining to that color trace only. \Axes and title in two colors indicate that the axis is relevant to traces of both colors. (1) Black trace: Dispersion of BT-330 as a function of length (2) red trace: Dimensionless relative dispersion for the same data. Large error bars result at small lengths because uncertainty in measuring the volumes increase as the volumes decrease. The lines shown are the best fits to a quadratic equation. (3) Blue trace: Baseline noise for BT-330 as a function of length. See Baseline noise measurement setup B, Figure 4-1b. (4) Green Trace: same as above for BT-250. All cases: F_p = 300 µL/min, auxiliary flow rate = 100 µL/min, CEG 0.80 mM LiOH (final mixed concentration 0.2 mM). The absolute noise level can be obtained by multiplying the relative noise by the background value of 47.5 µS/cm.

4.3.9 Application to Two-Dimensional Detection in Ion Chromatography.

The present practice of IC is largely limited to the detection of strong acids and moderately weak acids. Various efforts to detect weaker acids with greater sensitivity have been recently reviewed.[34] The authors specifically cite the decade long effort of our group towards such 2-D detection.[42,43,44,154] They note that despite successful approaches through many different PCRs, conductivity manipulations, and supported by extensive theoretical models and calculations, the practice has not been widespread due to the lack of commercial devices. The basic strategy takes advantage of the fact that a standard suppressed IC system produces a pure water background. After the conductivity detector (D1), a small constant amount of strong base (e.g., NaOH) is introduced to create a alkaline background. Introduction of 0.1 mM NaOH results in a background conductance comparable to that of a suppressed carbonate eluent. A second detector (D2) is now used to measure the conductance again. The background pH being 10, any eluting acid HA up to at least a pK_a of 9 is neutralized; effectively OH^- in the background is replaced by X^-. As the response is related to $\lambda OH^- - \lambda X^-$ and $\lambda OH^- >> \lambda X^-$, nearly universal equivalent response results regardless of the identity of X^-. For some general theoretical considerations not discussed in previous papers, see Appendix A and Figures A1 and A2. Consideration of first and second detector responses together provide valuable information as to analyte identity, pK_a, and occurrence of co-elution. The recently introduced ICS-5000 dual channel chromatograph used in this work provides a uniquely useful platform to carry out this type of 2D detection as illustrated below. The most common configuration of this 2-channel instrument is the one used in this work: one channel is intended for macroscale chromatography (2-4 mm i.d. columns) with a conventional gradient capable pump that is also provided with electrodialytic eluent gradient capability and an independent second channel that utilizes an isocratic capillary

scale pump, also capable of electrodialytic gradients. It thus becomes possible to carry out suppressed IC on the macrosystem and then introduce a small flow of electrogenerated strong base from the capillary scale generator through an efficient mixer such as those discussed herein.

Because of the very low dispersion provided by the VJM, we made a final comparison of it against a BT-330 mixer in the actual chromatographic setup. Chromatographic dispersion of injected samples was much higher compared to the flow Injection mode dispersion measurements and no difference in peak width between the VJM and the BT could be seen. Based on the noise results shown in Figures 3-14 and 3-18, we chose to use the BT mixer. The principal flow was 300 μL/min and final KOH concentration in mixed stream 0.1 mM in Figure 4-18. We studied electrogenerated KOH and LiOH as the base introduced, based on the results discussed in Appendix A and Figures A3, LiOH was chosen. An illustrative 2D chromatogram is shown in Figure 4-19. Best linear fits to calibration data for various ions on both detectors appear in Figure 4-20 and the limits of detection calculated on a S/N=3 basis appear in Table 4-1.

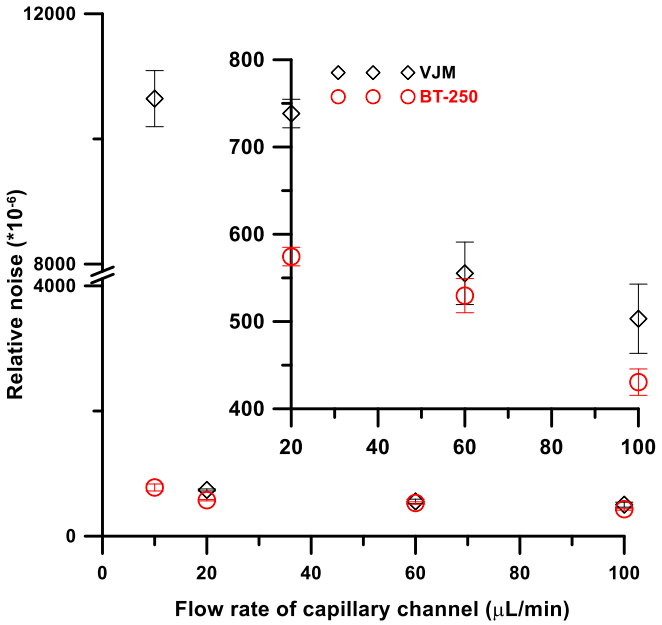

Figure 4-18 Comparison of the VJM with the BT-250 (25 cm) mixer.

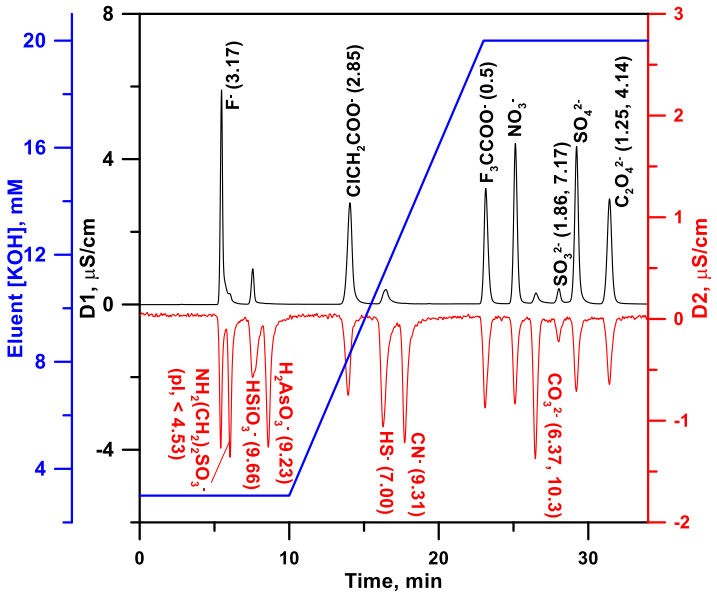

Figure 4-19 Illustrative application of 5 cm long BT-330 as a mixer. Two-dimensional ion chromatographic detection.

Background corrected chromatogram, 10 μL injection of 50 μM each sulfate and oxalate, 100 μM each fluoride, taurine, chloroacetate, trifluoroacetate and nitrate, 200 μM

each silicate, arsenite and sulfide, and 250 μM cyanide. Carbonate results from CO_2 intrusion into the sample. A weak acid like H_2CO_3 has a broader peak on D1 ($W_{1/2}$ 20.10±0.06 s) compared to D2 ($W_{1/2}$ 18.96±0.18 s) due to the nature of concentration dependence on ionization. The reader might wish to reflect on why in a conductometric detector a weak acid will produce a peak of greater half width compared to that of a strong acid peak, when the concentration profiles of both are identical. The sulfate-carbonate resolution actually improves therefore from D1 (4.87) to D2 (4.93).

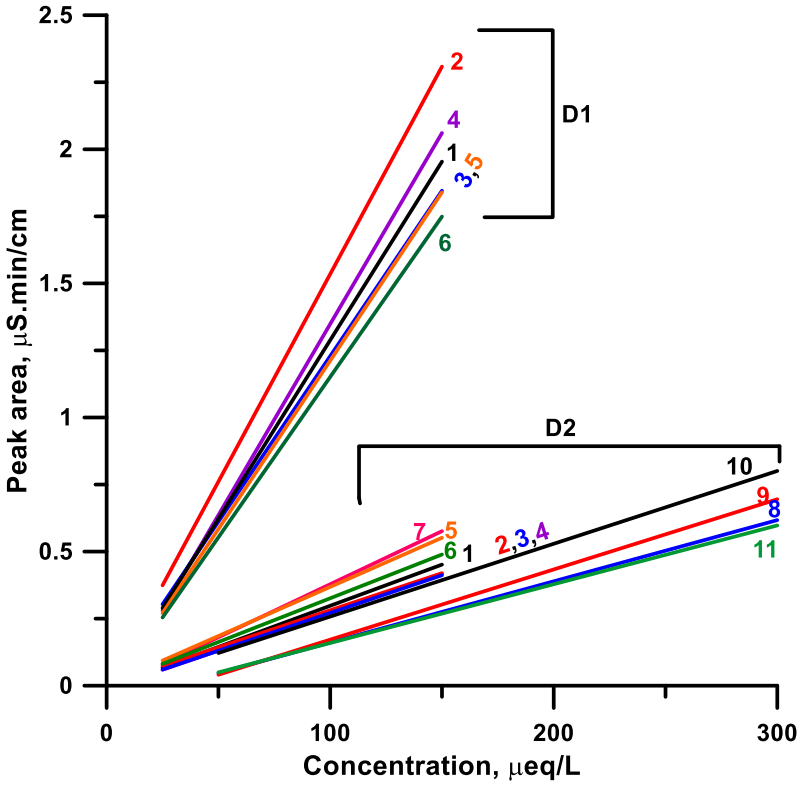

Figure 4-20 Calibration curves at D1 and D2 using AS11-HC column, Gradient program as in Figure 4-19.

(a) Peak area at D1. 1, fluoride: y = 0.0133x - 0.0436 (r^2 = 0.9991); 2, sulfate: y = 0.0155x - 0.0127 (r^2 = 0.9952); 3, oxalate: y = 0.0123x - 0.0049 (r^2 = 0.9952); 4, nitrate y = 0.0142x - 0.0762 (r^2 = 0.9986); 5, chloroacetate; y = 0.0126x - 0.0435 (r^2 = 0.9999); 6,

trifluoroacetate: y = 0.012x - 0.0447 (r^2 = 0.9998) (b) Peak area at D2. 1, fluoride: y = 0.0031x - 0.0091 (r^2 = 0.9980); 2, sulfate: y = 0.0055x - 0.0052 (r^2 = 0.9932); 3, oxalate: y = 0.0056x - 0.0103 (r^2 = 0.9986); 4, nitrate: y = 0.0029x - 0.0119 (r^2 = 0.9979); 5, chloroacetate: y = 0.0037x + 0.002 (r^2 = 0.9996); 6, trifluoroacetate: y = 0.0033x + 0.0003 (r^2 = 0.9997); 7, taurine: y = 0.0040x - 0.0174 (r^2 = 0.9966); 8, silicate: y = 0.0023x - 0.0672 (r^2 = 0.9633); 9, arsenite: y = 0.0026x - 0.0902 (r^2 = 0.9972); 10, sulfide: y = 0.0027x - 0.0138 (r^2 = 0.9928); 11, cyanide: y = 0.0022x - 0.0600 (r^2 = 0.9976).

Table 4-1 Calibration range, limit of detection (LOD) at D1, D2 and plate numbers for anions [a]

Analyte	Calibration Range, μM	LOD at D1, nM	LOD at D2, μM	Plate number at D1	Plate number at D2
Fluoride	25 – 150	23	2.1	3700 ± 200	2750 ± 150
Taurine	25 – 150		2.0		2978 ± 153
Silicate	50 – 300		5.0		2350 ± 100
Arsenite	50- 300		4.2		2850 ± 100
Chloroacetate	25 – 150	41	3.4	4300 ± 300	3800 ± 150
Sulfide	50 – 300	1400	5.2	3300 ± 300	3800 ± 100
Cyanide	50 – 300		5.2		9250 ± 400
Trifluoroacetate	25 – 150	22	2.3	33550 ± 400	26400 ± 1400
Nitrate	25 – 150	18	2.4	45100 ± 850	37450 ± 1300
Sulfate	12.5 – 75	8.2	1.2	78350 ± 900	53500 ± 1800
Oxalate	12.5 – 75	11	1.2	68000 ± 300	62500 ± 4100

[a] The uncertainties are calculated based on n =3 and represent ± SD. For weak acids that are visible at both detectors, e.g., sulfide, an increase in plate number from D1 to D2 is common. Sulfide behaves as a monoprotic acid. At D1 the acid form ionizes to a greater extent in the diluted region at the wings, effectively increasing the peak width. In contrast, at D2 HS^- is fully formed, the conductivity profile exactly follows the concentration profile. The plate numbers should be compared for a given ion between the two detectors; in going from one ion to another, computing plate numbers is inappropriate in a gradient run and has little meaning.

In summary, the two main test paradigms for testing performance of mixers do not necessarily lead to concordant results. While one provides a cumulative history of inhomogeneity, the other provides an instantaneous snapshot of the status of mixing, independent of previous history. While in synthetic and other similar efforts carried out in microfluidic formats, mixing history may be important, complications from competing or parallel reactions are rarely important in analytical reaction detection and only the final status of mixing matters. The backflow tee mixer provides excellent mixing in a small volume and small dispersion per unit volume. The geometry will allow microfabrication that we hope to report in the near future. In conjunction with the easily fabricated BT mixer, the ICS-5000 platform provides a facile means of performing two dimensional detection in ion chromatography.

4.4 Acknowledgements

This work was supported by NASA Grant NNX11AO66G and by Thermo Fisher Dionex. We thank C. Phillip Shelor for his assistance throughout this work. This chapter has been reprinted with permission from H. Liao, P.K. Dasgupta, K. Srinivasan, Y. Liu. Analytical Chemistry. 87 (1) 2015, pp 793-800. Copyright 2015 American Chemical Society

Chapter 5

Concurrent High Sensitivity Conductometric Detection of Volatile Weak Acids in a Suppressed Anion Chromatography System

5.1 Introduction

Suppressed conductometric ion chromatography (SCIC) has become the benchmark technique for anion analysis. It cannot, however, measure weak (and especially very weak) acids. Karu et al.[34] have recently reviewed extant strategies to determine such analytes by modified SCIC approaches. In their view, the most promising approach is to introduce a base at a constant concentration to the SCIC effluent and measure the conductivity again. Eluting acids (HA) react with OH^- as follows: $HA + OH^- \rightarrow H_2O + A^-$; the replacement of highly conducting OH^- by lower mobility A^- results in all acid analytes with pKa<10 showing up as negative peaks.[154] But mixing in a high conductivity base solution at a low flow rate to a principal flow steam requires a compromise between good mixing (to reduce baseline noise) and minimum band dispersion (that decreases peak height and deteriorates chromatographic resolution). The best case baseline noise with typical background conductivities (~25 μS/cm) is ~10 nS/cm.[155]

Among weak acid anions, sulfide and cyanide are of special interest. Both derive from the corresponding highly toxic volatile acids that play important roles in diverse areas ranging from biological cell signaling,[156] to corrosion in petrochemical plants,[157] to mine wastes,[158] to wastewater treatment.[159] Hydrogen sulfide is known to be involved in a number of specific physiological processes; there is much interest in slow in-vivo H_2S-releasing pharmaceuticals.[160] A large number of fire mortalities stem from HCN inhalation; developments in cyanide determination methods have been recently reviewed.[161] There are numerous colorimetric methods for both these analytes; recent

examples include nitroprusside-based determination of sulfide (limit of detection, LOD, 0.2 μM[162]) and cobinamide-based determination of cyanide (LOD 0.03 μM, 50 cm liquid core waveguide cell[163]).

While specific photometric approaches can be attractive with some sample types, interferences are possible and multiple analytes cannot be determined. Chromatographic separation and detection methods applicable to multiple analytes are therefore preferred. The dominant technique to measure sulfide and cyanide by IC has been pulsed amperometric detection (PAD): "sulfide or cyanide and pulsed amperometry" produces ~1000 citation hits. While PAD is sensitive, and more robust and reproducible compared to standard amperometry, it requires special sample preparation steps: The most cited article on the topic[164] emphasizes the necessity of "deep deoxygenation of the sample for at least 10 min" to achieve optimum results. For insufficiently alkaline samples, volatile analyte losses can occur with such procedures.

In the present paper, we provide a robust conductometric approach that uses the previously utilized[154] principle of reacting HA with OH^- and measuring the signal that results from the difference in mobilities of A^- and OH^-. But there are important differences: (a) no liquid mixing: volatile analyte acids transfer into the base stream through a nonpolar membrane; this reduces baseline noise by two orders of magnitude and makes the technique selective to only sulfide, cyanide and carbonate; (b) the base receiver stream has a flow rate much lower than the donor chromatographic effluent stream, leading to analyte enrichment. Compared to previous conductometric techniques,[154,155] these attributes improve LODs by > 100x.

5.2 Experimental section

Details are given in the Appendix B and Figure B-1. An ICS-5000 ion chromatography (IC) system (one analytical scale and one capillary scale

chromatograph), both configured for anion analysis (Figure 5-1, Figure B-1 gives further details). Chromatography was carried out on 2x50/2x250 mm AG11HC/AS11HC guard/analytical columns using an electrogenerated KOH gradient (0.3 mL/min). The receptor LiOH flow rate was in the range of 10-100 μL/min to permit analyte enrichment. Volatile analyte loss through the membrane suppressor used (2 mm ERS-500) was examined in comparison with a 2x50 mm packed column suppressor (400 mesh H^+-form Dowex 50wX8 resin). Water was pumped by the capillary pump (10 -100 μL/min) through the LiOH generator to produce ~0.1-0.2 mM LiOH. This stream flowed through the central lumen of the volatile analyte transfer device (VATD) to a second conductivity detector (D2) while the effluent from the suppressed conductivity detector (D1) flowed through the outer, annular channel of the VATD, with the two flows being in the same direction (cocurrent). Three membrane devices were used. The first was a commercially available capillary scale Carbon dioxide Removal device (cCRD). The holdup volumes in the inlet/outlet tees of this device, intended for a different application, is larger than the optimum for the present purpose. We therefore constructed and tested two other devices where these volumes are minimized; one with an effective membrane length (L_{eff}), smaller (5 cm, hereinafter VATD-5) than the cCRD (7.5 cm), the other being significantly greater (24 cm, hereinafter VATD-24). All three devices use the same type of membrane tube (courtesy ThermoFisher Dionex). The VATD design is similar to a previously described[155] tubular membrane mixer except for both inlet and outlet connections to the annulus. Detailed design and dimensions are in Figure 5-2.

Data collection (10 Hz) and analysis were performed using Chromeleon ver. 7.1; all above were from ThermoFisher Dionex. Standards were prepared with reagent grade chemicals.

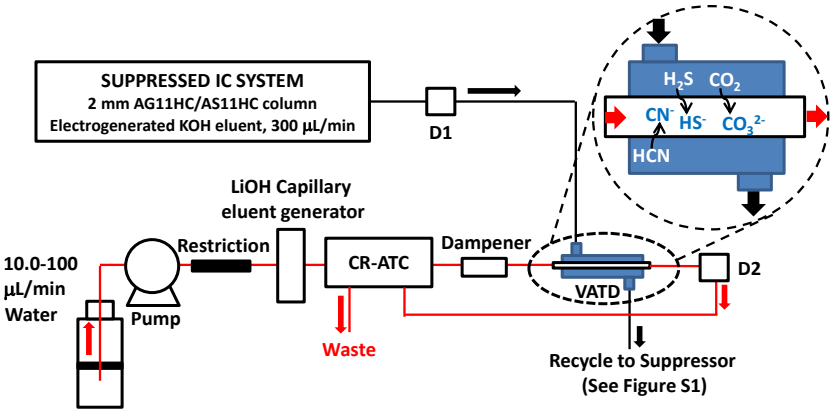

Figure 5-1 The experimental configuration.

The macroscale IC effluent flows through its detector D1 into the volatile analyte transfer device (VATD) to waste. Downstream of the capillary pump a restriction capillary (25 µm i.d.; 6.0-25.0 cm long depending on flow rate (100-10 µL/min)) is used to provide some backpressure for proper operation. To further reduce pump pulsations, a PEEK tubing (0.76x600 mm) is added after the capillary scale continuously regenerated impurity anion trap column (CR-ATC) that follows the LiOH generator.

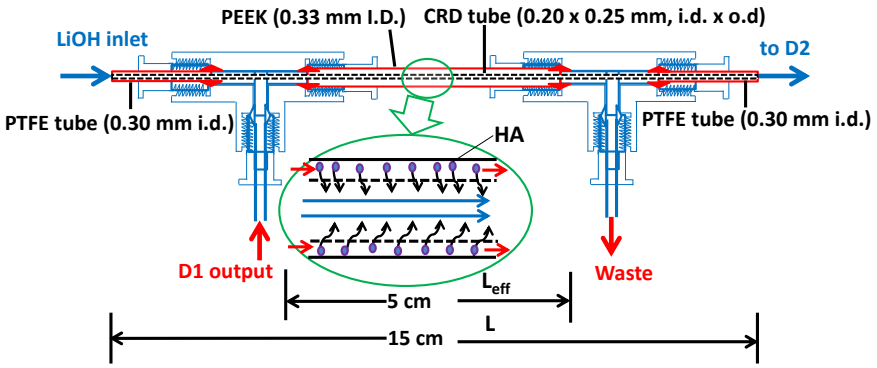

Figure 5-2 The design of the in-house fabricated 5 cm volatile acid transfer device (VATD-5).

Compared to the capillary CRD, the annular space is smaller. The drawing is not to scale. L_{eff}, over which both outer and central channel flow are present.

5.3 Results and discussion

5.3.1 High selectivity for cyanide and sulfide.

Figure 5-3 shows a gradient ion chromatogram containing 12 anions, including sulfide, cyanide and carbonate, anions derived from volatile weak acids. While sulfide and carbonate responds some in D1 because they ionize partially (pK1 ~6-7), the response is poor and highly nonlinear, characteristic of a very weak acid. Cyanide is derived from an even weaker acid (pK 9.3) and cannot essentially be seen in D1. All three respond selectively and sensitively in D2, which responds only to undissociated volatile acids. At concentrations used in Figure 5-3, formate, acetate, sulfite, etc. responds at the 5-10 nS/cm level, imperceptible in the ordinate scale of Figure 5-3. The pK_a is simply not high enough for significant amount of the unionized acid to exist at levels of analytical interest, in addition the Henry's law solubilities (see below) are high.

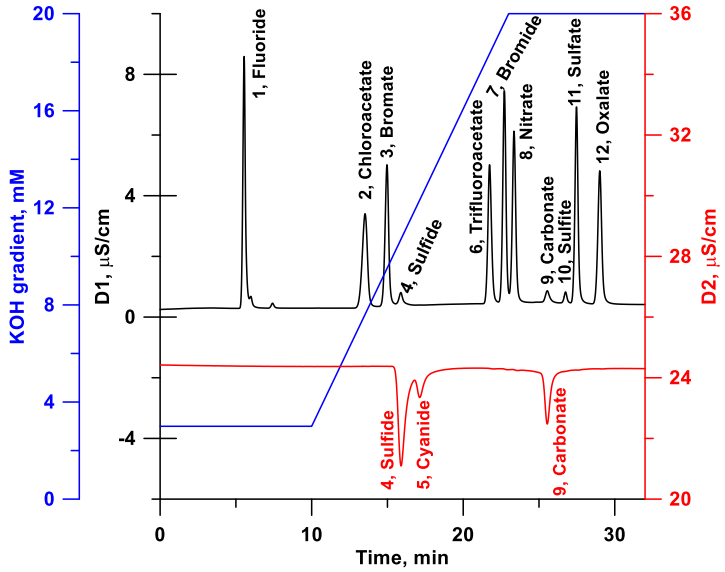

Figure 5-3 Illustrative application of VATD-5. Dual conductometric detection.

10 µL injection of 100 µeq/L for each ion; 0.1 mM LiOH flow. Carbonate results from CO_2 intrusion. Sulfite is an impurity in the sulfide standard used.

Strong acid analytes are fully ionized; D2 signal was neither expected nor observed. Overall the transport is proportional to $\alpha_0 C_x P/K_H$ where α_0 is the unionized fraction of the total concentration C_x, P is the permeability coefficient (product of solubility and the diffusivity of the analyte in the membrane), and K_H is the Henry's law constant for the gas. Since $pK_{a,HCN} >> pK_{a1},H_2S$, $\alpha_0,HCN > \alpha_0,H_2S$ but HCN produces a significantly lower response; there is a great difference in the respective K_H values ($K_{H,HCN} \sim 100\ K_{H,H2S}$).[165,166]

5.3.2 Volatile acids. Extent of loss in suppressors and transfer in the VATD.

In much the same way a volatile analyte goes through the VATD membrane to the receptor, it can be lost through the suppressor membrane in the IC system. This has been exploited for example in removing CO_2 from carbonated drinks by passage through a Nafion tube prior to IC analysis.[167] The exact loss of volatile weak acids in membrane suppressors have never been quantitated but is of obvious interest in the present application. We measured this by using both (a) a packed column suppressor, and (b) the membrane suppressor. To the suppressor effluent a 100 μL/min stream of LiOH was added to reach a final concentration of ~0.2 mM (Figure 5-4). The difference in the area signal (a-b) then gives a direct indication of the loss through the suppressor (the peak area is immune to broadening differences in the two suppressors). Figure 5-5 and Figure 5-6 shows the extent of the loss for H_2S/HCN. In the 50-2000 μM injected analyte concentration range, ~10-25% of the H_2S is lost through the membrane suppressor. The pattern of the H_2S loss is unexpected: greater loss is observed at lower concentrations. The loss through the membrane is augmented by a zero order loss in the suppressor from oxidation. This is discussed in more detail in the appendix B (Figure B-2). Over the same concentration range, HCN loss is relatively constant at 9.5-12%, with no discernible

dependence on the injected concentration. The difference between HCN and H_2S in the extent of the loss is likely due to the greater intrinsic solubility (K_H) of molecular HCN.

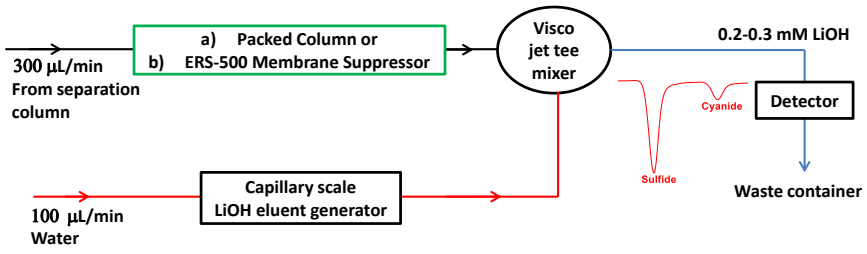

Figure 5-4 Experimental configuration for measurements of loss of volatile acid analytes in membrane suppressor.

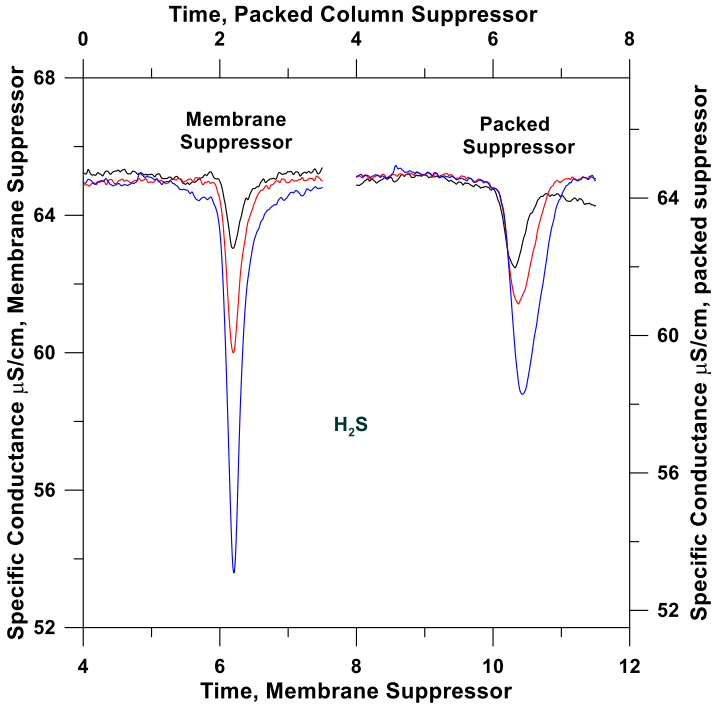

Figure 5-5 Measurements of loss of H_2S in membrane suppressor. Blue traces, 2.00 mM H_2S; red traces, 1.00 mM H_2S, black traces, 0.50 mM H_2S.

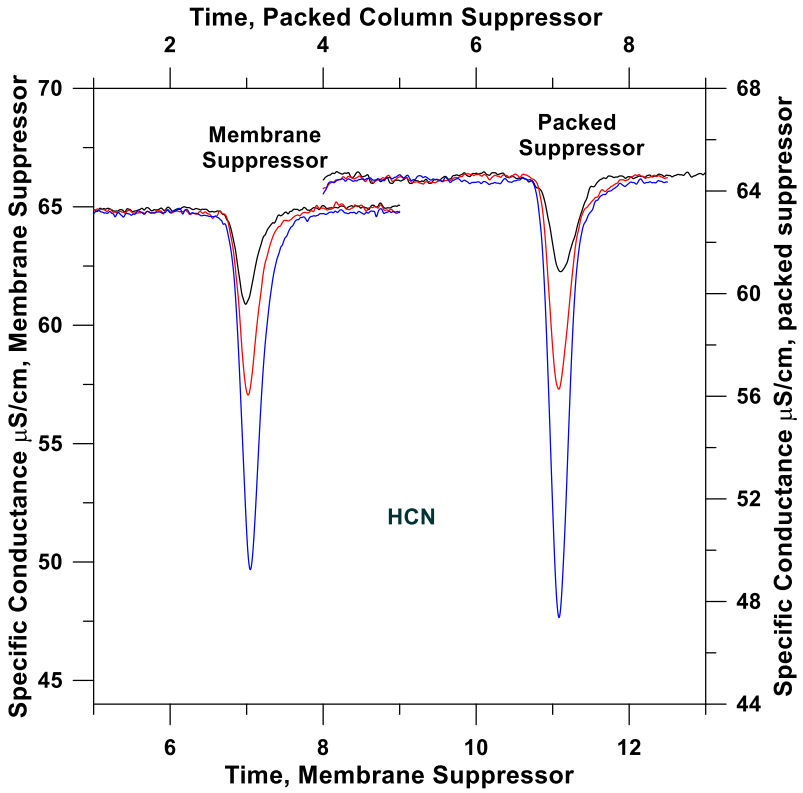

Figure 5-6 Measurements of loss of HCN in membrane suppressor.

Blue traces, 2.00 mM HCN; red traces, 1.00 mM HCN, black traces, 0.50 mM HCN.

Once the loss in the suppressor is accounted for, the amount transferred to the receptor in a VATD can be determined from theoretical considerations from known ionic mobilities as outlined in the appendix B. In the analyte concentration range investigated, ~18/58% of the H_2S is transferred in VATD-5/24. In contrast, 7/33% of HCN is transferred in VATD-5/24. The actual responses appear in Figure 5-7. There is clearly considerable room for improvement here, especially for HCN. In principle the extent of transfer should increase if the absolute pressure on the donor side is increased, e.g., by putting a restriction tubing at the VATD jacket outlet within limits of pressure tolerance of the suppressor; this was not presently investigated.

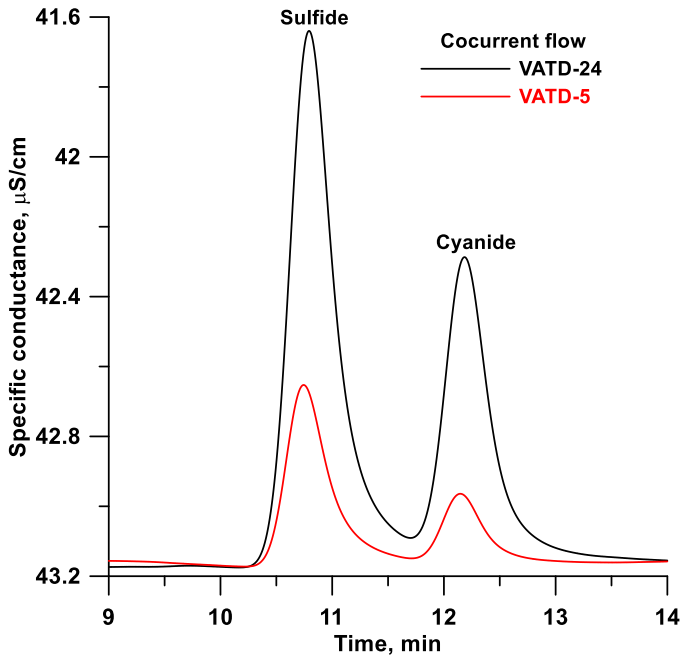

Figure 5-7 Chromatograms of 50 μM of sulfide and cyanide using both VATD-24 and VATD-5.

KOH eluent isocratic concentration, 5.0 mM; LiOH concentration, 0.2 mM; LiOH flow rate, 40 μL/min. The peak resolution is 1.96 vs 2.11 for VATD-24 vs. VATD-5.

5.3.3 Cocurrent vs. countercurrent flow in the transfer device. Band dispersion vs. mass transfer.

Typically the donor and receptor flows are countercurrent in membrane systems to maximize transport. For H_2S, without boundary layer stagnation, at the receptor (pH >10) undissociated H_2S concentration will be essentially zero. Thence its concentration gradient should solely be controlled by the donor concentration and its VATD residence time, the transfer extent should be flow-direction independent. For HCN (pKa 9.3), however, with 0.1/0.2 mM LiOH, some 17/9% of the permeate will remain unionized (and

any boundary layer stagnation will make this worse). In countercurrent flow a greater amount of fresh receiver is encountered; greater transfer is expected.

The results do indeed show that while the sulfide response does not change significantly between flow directions (peak area changes by ~5%, 0.767±0.008 vs. 0.731±0.006 area units), the cyanide response is discernibly higher (by ~15%, 0.453±0.007 vs. 0.391±0.024 area units) in countercurrent flow (Figure 5-8a).

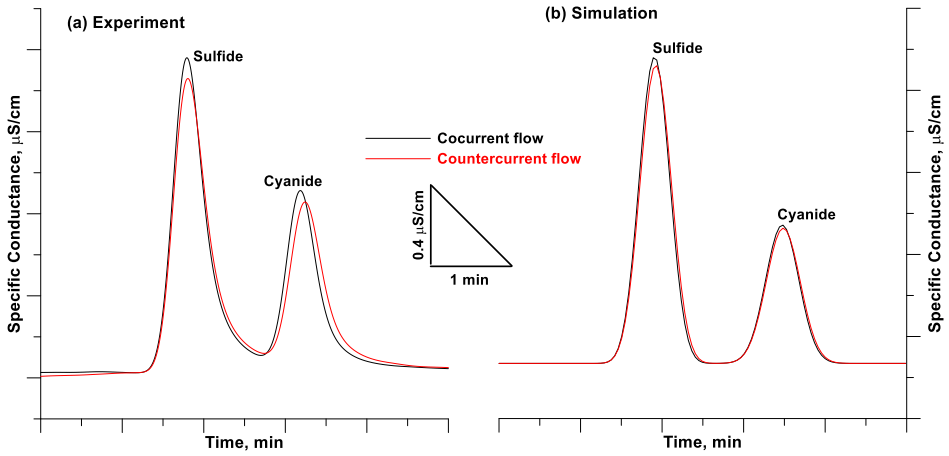

Figure 5-8 (a) Experimental (b) Simulated comparison between cocurrent flow and countercurrent flow in VATD-24.

Chromatograms of 50 µM sulfide and 50 µM cyanide. 5.0 mM KOH eluent @ 300 µL/min; VATD receptor 0.2 mM @ 40 µL/min.

It is intuitive that if the donor and receiver are moving in opposite directions, the permeated analyte band will spread across a greater volume. The sulfide-cyanide resolution in Figure 5-8a is 1.87 in countercurrent flow vs. 1.96 in cocurrent flow. While with cyanide, there is gain in mass transport with countercurrent flow, the peak height increase is marginal. The increase in transport is offset by added dispersion and thence

poorer resolution makes accurate quantitation at low levels increasingly difficult. Cocurrent flow was henceforth used.

5.3.4 Mass Transfer as a Function of Device Length.

Let the fraction collected by the VATD be denoted by f. Much like transmitted light, the transmitted fraction 1-f is expected to follow an exponential pattern and hence be expressible as

$$1- f = \exp (-aL) \quad \ldots(1)$$

where a is the extinction coefficient and L is the length. For L = 24 cm, f = 0.579 and 0.329, respectively for H_2S an HCN, the respective a values are computed to be 0.0360 and 0.0166 cm^{-1} for H_2S and HCN, respectively, a_{H2S}/a_{HCN} being 2.17. Predictions for f using L = 5 cm using these a values predict removal efficiencies of 0.165 and 0.080 in for H_2S and HCN in reasonable agreement with observed values of 0.185 and 0.074. Although empirical, if f is known for a certain membrane length, the results suggest that reasonable estimates can be obtained for other lengths. Given comparable permeabilities, the a values should be related to K_H; the relevant mass transfer equations suggest a_{H2S}/a_{HCN} should be related to log ($K_{H,HCN}/K_{H,H2S}$). The latter has a value of ~2 and the theoretical expectations are met. A first principles approach to estimating collection efficiencies is also possible and is discussed in the Appendix B and Figure B-3.

5.3.5 Effect of Receptor Flow Rates.

Dispersion will be minimum when both the donor and receiver are moving cocurrent isokinetically and the characteristic transmembrane transfer time is small relative to VATD residence time. For VATD-5/24, the annular/central volume ratio is 1.16:1; best dispersion and resolution is expected at this flow ratio. However, a larger donor:receptor flow ratio (DFR) greatly improves the signal and hence the LOD (Figure 5-9). The amount of analyte transferred is independent of receptor flow rate in the range

studied as indicated by the constancy of the peak area if the abscissa is expressed in volume units, also suggesting there is no lack of LiOH due to boundary layer stagnation. While peak resolution decreases some with decreasing receptor flow rate, a flow rate of 40 μL/min (DFR 7.5) still provides baseline resolution of sulfide and cyanide.

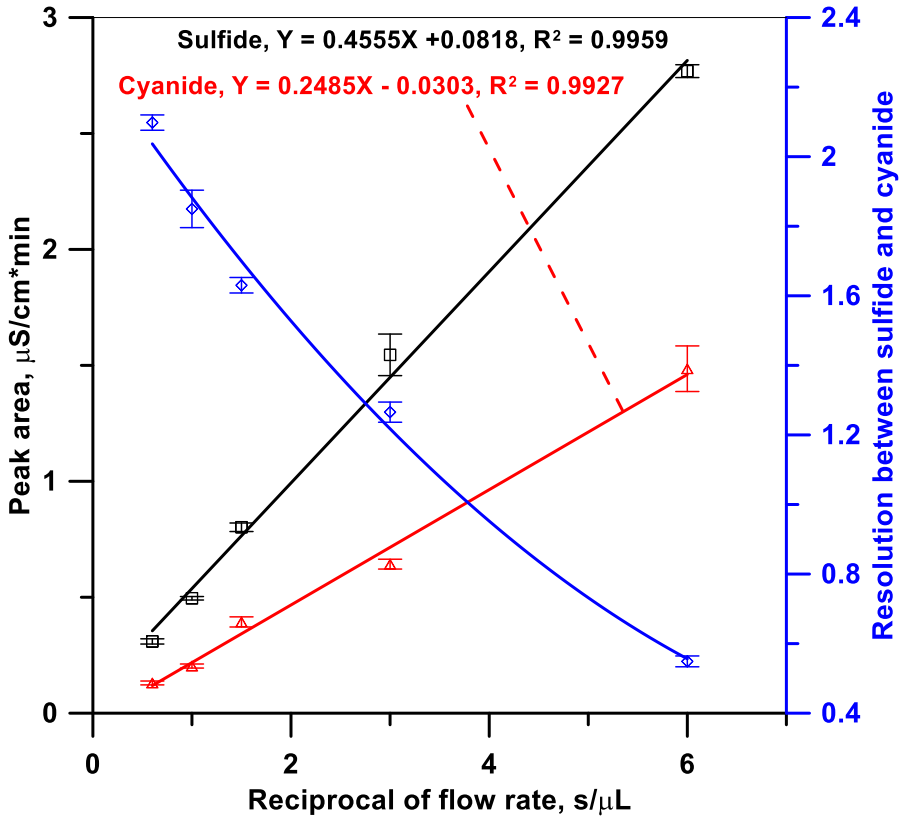

Figure 5-9 Chromatographic conditions, separation of 50 μM of sulfide and cyanide using VATD-24 device.

KOH eluent isocratic concentration, 5.0 mM; LiOH concentration, 0.2 mM; LiOH flow rate varied from 10 to 100 μL/min. (b) Relationship between peak area and peak resolution of chromatograms as a function of LiOH receptor flow (±1 SD error bars are shown, n=3).

5.3.6 Simulation of Cocurrent and Countercurrent Transport.

Spreadsheet software (e.g., MS Excel^{TM}) not only allows numerical simulation of the transport process and numerous other parametric effects, e,g., the length of the device, residence time, the effects of flow direction, etc. it can also provide pedagogically valuable quantitative understanding of such processes as well as predictive capabilities that allow for in-silico experiments.[168] Referring to Figure 5-10 as an illustrative example in cells A1:B22 we depict the HCN (approx. A1:A11) and H_2S (approx. B12:B22) bands exiting the suppressed detector, with 4 bit blue and red color gradation to indicate concentration magnitude. In reality both are of course present in the same flowing column (say B) but we distinguish between the separate chemical entities by putting them in separate columns. Similarly on the receiver side we designate column C for HCN and Column D for H_2S, although both are present in reality in the same column. A 20-row long membrane is present, indicated by the heavy line running between columns B and C, rows 22 through 41. The simulation begins by (a) transferring a fixed fraction (say 10% for H_2S and 5% for HCN) of the concentration difference in each row across the membrane and (b) then transferring contents of both columns B and C down one row and repeating the process. This process is repeated until the input bands are out of the system. The subsequent panels in Figure 5-10 depicts the progression of this process. Figure 5-11 shows the simulation vs. experimental data for the sulfide cyanide separation. Figures 5-8 compares simulation vs. experimental results for the cocurrent vs. countercurrent case.

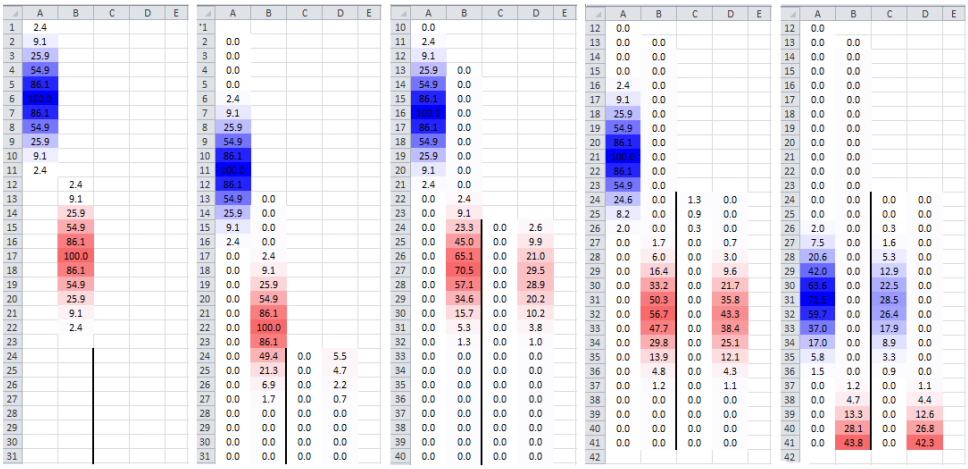

Figure 5-10 Screen output for Excel Simulation.

A, B: donor columns for HCN, H_2S; C, D: receiver columns for HCN, H_2S; heavy solid line represents membrane. The panels depict snapshots after 0, 5, 10, 15, 20, and 25 iterations.

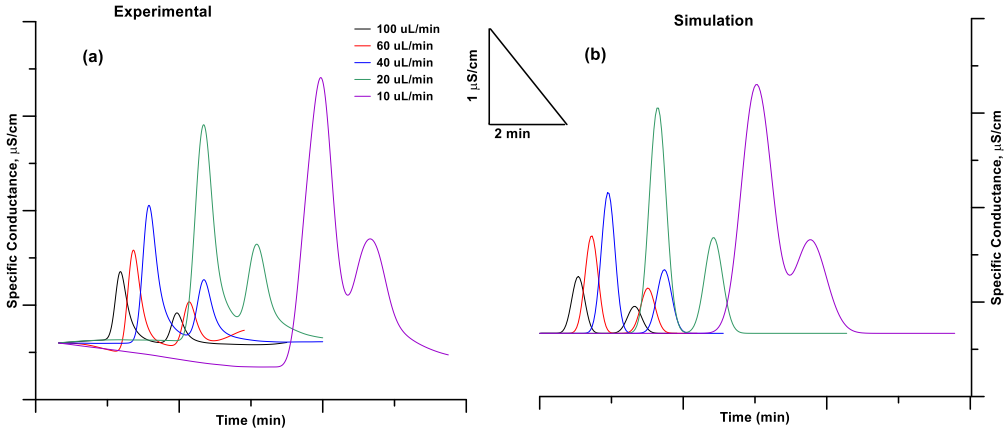

Figure 5-11 (a) Experimental (b) Simulated response of 50 µM each sulfide and cyanide in VATD-24.

The full simulation differs from the illustrative simulation above in that it uses conditions from the real system: (a) the input band width for H_2S is estimated from the small but finite first detector signal and that for HCN is estimated from the known retention time difference between sulfide and cyanide and assuming the same efficiency

as sulfide; (b) the simulation for the 24 cm membrane is assumed to span a 60-row length; this means that the donor and receptor (B and C) cell volumes are ~0.15 and ~0.13 μL, respectively; (c) the DFR being >1, during each iteration step the donor column moves a larger number of steps than the receptor: for donor:receptor flows of 300 and 40 μL/min, respectively the donor moves down 51 rows while the receptor moves down/up (cocurrent vs. countercurrent) 8 rows, the step duration representing 0.0251 min; (d) while sulfide is essentially completely ionized, for the [HCN] gradient, the computation takes into account that ~91% ionization will occur in 0.2 mM LiOH; (e) The fraction transferred values are adjusted so simulated transferred peak areas correspond to that observed; and (f) axial diffusive redistribution is applied to the receptor cells (a fixed fraction of the concentration difference is redistributed in the cell above and below) to simulate axial dispersion.

5.3.7 Performance of Different Devices.

The performances of VATD-5, the cCRD (inlet and outlet fittings were replaced with two 0.50 mm bore 10-32 threaded PEEK unions) and a 2 mm CRD were compared under chromatographic conditions. The results (Figure 5-12) indicate that the 2 mm CRD still exhibits too much dispersion to be attractive. The VATD-5 exhibits the least dispersion albeit the cCRD provides marginally higher signal for HCN.

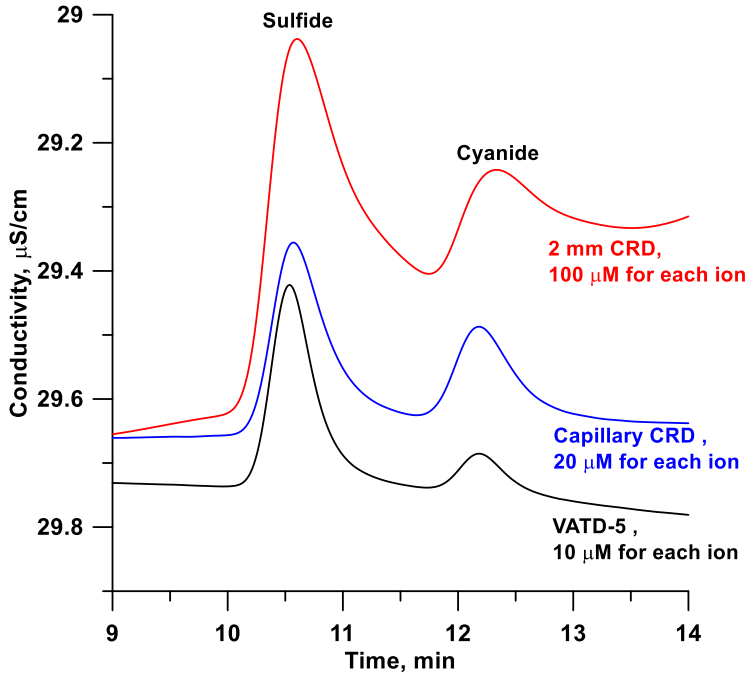

Figure 5-12 Comparison of VATD-5, 2 mm CRD, and cCRD under chromatographic conditions.

KOH eluent isocratic concentration, 5.0 mM; LiOH concentration, 0.1 mM; LiOH flow, 10 μL/min for VATD-5 and capillary CRD, and 100 μL/min for 2 mm CRD. The y axis is descending.

Both the VATD-5 and the cCRD were tested with a series of concentrations of sulfide and cyanide. The short term peak to peak noise level with 0.1 mM LiOH background was <0.1 nS/cm, comparable to the suppressed detector (D1) noise levels. Note that the base cation (Li^+) plays no role in the detection process but only contributes to the baseline conductance. For this reason, we use LiOH rather than KOH as the base, Li^+ has half the mobility of K^+. At 500 nM concentration, sulfide elicited a D2 response with an S/N >100 (Figure 5-13). However, at 100 nM (the LOD is estimated to be somewhat lower), the area response is much less than 1/5th of this. The principal reason

is the oxidative loss of sulfide in the system some of which seems to proceed on a zero order basis (see Appendix B and Figure B-2). At sub-μM levels, some oxidative loss may also be occurring during standard preparation. The LOD for cyanide is ~50 nM on the same device.

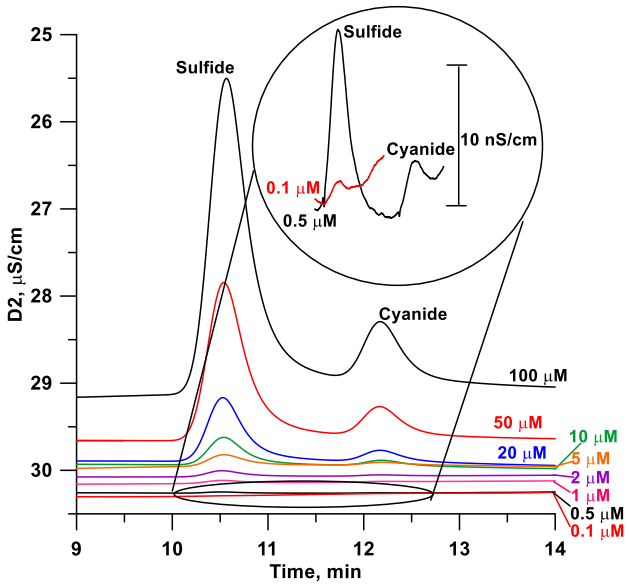

Figure 5-13 Chromatograms of a series of concentrations of sulfide and cyanide using VATD-5.

Calibration curves are shown in Figure 5-14. For both sulfide and cyanide, good linear relationships between concentration and D2 peak area were observed. The sensitivity of sulfide detection with VATD-5 is 1.5-2 orders of magnitude more sensitive due both to the enrichment in the VATD from the high donor/receptor flow ratio as well the difference in the degree of ionization in D1 vs. D2 (~11% and ~100%).

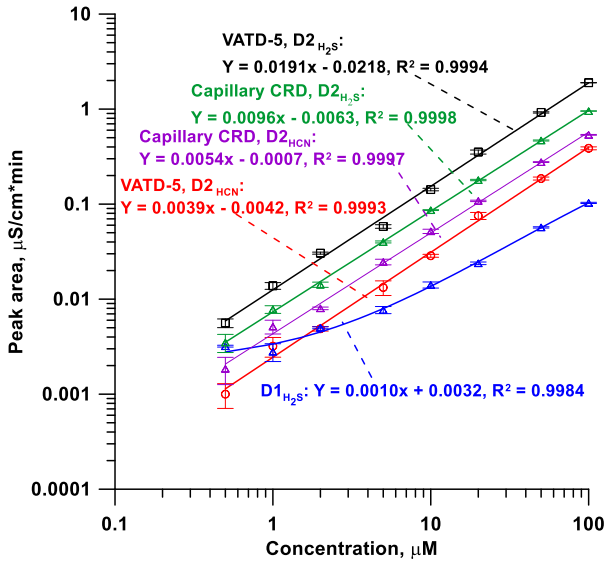

Figure 5-14 Calibration curves of sulfide and cyanide at both detectors using VATD-5 and Capillary CRD.

5.3.8 Potential applications.

The scope of the present approach may seem limited as of commonly encountered analytes only measurement of carbonate, cyanide and sulfide will benefit from this approach. However, the speciation and detection of metallocyanides is normally quite difficult. If these are separated with a saline eluent (Na_2SO_4), suppression will produce an acid environment for the liberation of HCN from acid dissociable cyanides and the more stable ones can also be similarly determined postcolumn after passage through a UV reactor that may also function as as the VATD: a UV-stable gas permeable tubing, e.g., -Teflon AF can be put inside a irradiated quartz tube.

5.4 Conclusions

The VATD is a robust low-noise device permitting highly sensitive, wide dynamic range conductometric detection of volatile weak acids like cyanide and sulfide, without the maintenance requirements of amperometric detection systems. The principle should

be extendable to volatile weak base analytes such as amines in a cation chromatography system with an acid receptor; this application area spans a greater range of analytes. Operation at an elevated temperature and increased backpressure on the VATD is expected to improve transfer efficiency and limits of detection for all analytes. Concentration through favorable donor/receptor flow rate ratios have generally not been practiced as a postcolumn detection enhancement; with the advent of electrodialytic ion isolators,[169] there are further avenues of general enhancement[169] of detection sensitivities.[169]

5.5 Acknowledgements

This work was supported by NASA Grant NNX11AO66G and by ThermoFisher Dionex. We thank an anonymous reviewer for suggesting potential applicability to metallocyanides. This chapter has been reprinted with permission from H. Liao, A. F. Kadjo, P. K. Dasgupta. Analytical chemistry. 87 (16) 2015, pp 8342-8346. Copyright 2015 American Chemical Society

I would like to thank Akinde Florence Kadjo for this chapter. She did the simulation of cocurrent and countercurrent transport part.

Chapter 6

Permeative Amine Introduction for Very Weak Acid Detection in Ion Chromatography

6.1 Introduction

Suppressed conductometric anion chromatography (SCAC) applications range from trace analysis in semiconductor manufacturing[1] to pharmaceutical analysis[2] to name a few. While SCAC excels in measuring strong acid anions, weak acid anions respond poorly or not at all. Even though acids with pKa <7 show some response, they do so in a nonlinear manner. Anions from very weak acids (pKa ≥ 7.0), e.g., silicate or cyanide are essentially not measurable.

A recent review by Karu et al.[34] addresses various efforts towards weak acid detection by modified SCAC; the most promising approach identified was strong base (e.g., NaOH) introduction after a conventional hydroxide eluent SCAC system, followed by a second conductivity detector (D2).[42,43,44] After NaOH introduction, a fraction *f* of the eluite acid HA is converted to NaX; *f*<1 and increases with decreasing pK_a (for example, *f* will be 0.5 for an acid with a pK_a of 10 if the pH after base introduction is 10). The D2 signal is thus negative and equals $fC(\lambda_{A^-} - \lambda_{OH^-})$ where *C* is the eluite concentration in eq/L, and λ_{A^-} and λ_{OH^-} are the limiting equivalent conductance of A^- and OH^-, respectively. The approach is particularly attractive for very weak acids ($10 > pK_a \geq 7$) that respond insignificantly in SCAC. The combination of the SCAC signal (D1) and that from D2 can also be used to identify coelution, estimate pK_a's and perform universal calibration.[42,43] The general approach has been extended so it can be used with standard commercially available equipment but very weak acid LODs remained at single digit μM levels.[155] Recently, it was demonstrated that volatile weak acid eluites, notably H_2S and HCN (also CO_2) can be transported into a base stream through a nonpolar membrane.[170] No liquid mixing is involved and noise improves by ≥100x, proportionately improving the LODs.

This does not of course work for nonvolatile inorganic acids which constitute the majority, e.g., borate, arsenite, and notably, silicate. In the present work, we use this lesson: we introduce a volatile base into the eluite stream. The permeative amine introduction device (PAID) consists of a jacketed narrow bore Teflon AF membrane tube, with an amine solution flowing on the outside and the SCAC effluent flowing through the lumen. Diethylamine (DEA) is chosen as the amine reagent, for its low pK_b (3.0) and high vapor pressure. The merits of very low level base introduction (~25 μM) are explored and exploited. The approach does not require electrical current sources or constant flow pumps; the permeative amine introduction device (PAID) is simple to build and use. We also look especially at the trace determination of silicate for which there are few applicable methods.

6.2 Experimental section

All equipment/components below that are not otherwise specified were from www.thermoscientific.com. An ICS-5000 ion chromatography (IC) with one analytical channel (2-4 mm ϕ columns) and one capillary channel (0.4 mm ϕ columns) was used (Figure 6-1). Chromatography was carried out at 35 °C on AG11+AS11 or AG24+AS24 columns (2 mm ϕ), a 2 mm ERS-500 membrane suppressor using a KOH eluent gradient at 0.30 mL/min and 10 μL or 1.0 mL sample volume. Importantly, in some applications the electrodialytic membrane suppressor was turned off for desired periods during the chromatography (vide infra, at the eluent concentration used, the static ion exchange capacity of the suppressor is such that it can maintain suppression for > 30 min even after turning off). The amine was introduced by the PAID (a Teflon AF® tube immersed in an aqueous DEA solution; see Figure 6-2 and construction details in the section 6.2.1), after the first conductivity detector (D1). After the PAID, the capillary scale conductivity detector from the capillary channel was used as the second detector (D2). Because D2

has limited flow capability, a PEEK tee was used to split the PAID effluent. The main portion (80%, 0.24 mL/min) passed through the regenerant channel of a membrane suppressor and then through the continuously regenerated anion trap column (CR-ATC), eventually to waste. The rest (0.06 mL/min) passed through D2 to waste. Data collection (10 Hz) and analysis were performed using Chromeleon v7.1. The post-suppressor eluent composition was characterized both by UV spectrometry with a photodiode array detector (1290 infinity, www.agilent.com) and mass spectrometry with a TSQ Quantum Discovery Max triple-quadrupole mass spectrometer equipped with enhanced mass resolution and heated electrospray ionization probes. The spent suppressor regenerant was characterized by UV spectrometry (Agilent model 8453).

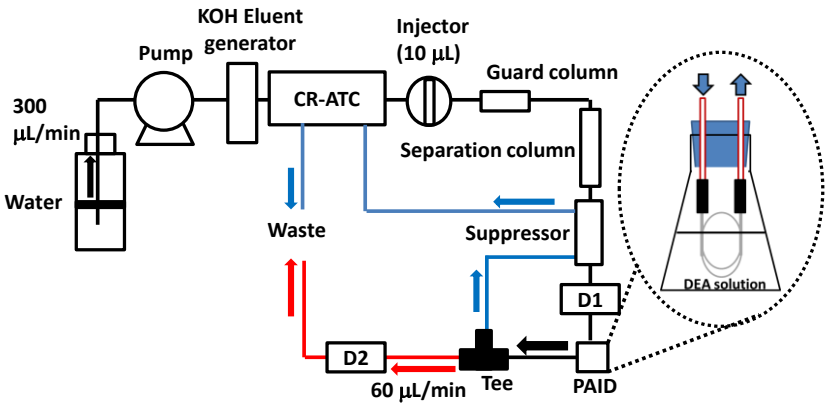

Figure 6-1 Experimental configuration shown schematically.

CR-ATC, continuously regenerated anion trap column; PAID, Permeative amine introduction device; D1, the first conductivity detector; D2, the second conductivity detector, which is in capillary scale; Tee, thread 10-32 and bore size 0.50 mm.

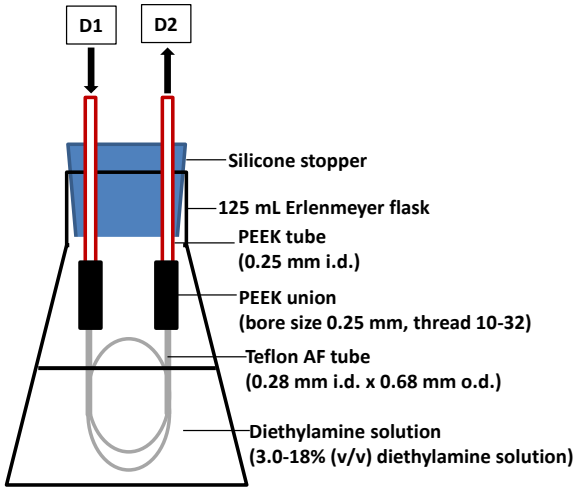

Figure 6-2 The design of a Permeative Amine Introduction Device (PAID).

The connecting inlet and outlet PEEK tubes are 18 and 10 cm long, respectively. In another format, The Teflon AF tube was coiled on a 4 mm support rod, thermoset by maintaining at 100 °C for 30 min and then the resulting coil used in the PAID.

6.2.1 Construction of PAID

A 60 cm length of Teflon AF tube (0.28 mm i.d. x 0.68 mm o.d., www.biogeneral.com) was used for gaseous amine penetration as shown in Figure 6-2. Each end was inserted into a polytetrafluoroethylene (PTFE) tube sleeve (25 mm x 0.71 mm i.d.) and sealed by standard compression fittings to a PEEK union (10-32 thread, 0.25 mm bore). The other end of the union was connected to a PEEK tubing (0.25 mm i.d.), which was inserted through a silicon stopper sealed tightly on a 125 mL Erlenmeyer flask. The flask contained 100 mL 3.0-18% (v/v) DEA solution. The suppressor and the PAID were both maintained in an enclosure at 15 °C.

6.2.2 Dispersion measurement

To measure the dispersion due to the PAID, the device was put before D1, with DEA on the outside. Dispersion was measured as the square root of the difference

between the square of the band volumes $((W^2-W'^2)^{1/2}$, where W and W' are the band volumes with and without the PAID being present, respectively.[20]

6.3 Results and discussion

6.3.1 Permeative Base Introduction and Choice of the Base.

Past efforts on base introduction for weak acid detection has involved strong base. An ionized species cannot be permeatively introduced; only a unionized molecule can. Diethylamine (DEA) is a compromise: with a pK_b of 3.0, a significant amount is unionized in aqueous solutions containing percent levels of DEA and it is not especially odorous or toxic. The infinite dilution equivalent conductance of DEAOH (240 $\mu S(cm*mM)^{-1}$) is only marginally lower than that of NaOH (248 $\mu S(cm*mM)^{-1}$). In the concentration range of interest for the present application (0-0.2 mM), NaOH is expected to have a linear concentration – specific conductance relationship; that for DEA ideally follows a quadratic relationship (Sp. Cond, $\mu S/cm = – 1.47 \times 10^{-4} C^2 + 0.234 C + 0.044$, r^2 = 1.0000) but over this limited range, a zero intercept linear fit is also acceptable (Sp. Cond, $\mu S/cm = 0.2103 C$, r^2 0.9982), Figure 6-3), the slope being 15% lower than that of NaOH due to incomplete ionization. The expected signals (peak heights) are readily calculated and are shown in Figure 6-4 for both a strong acid analyte HCl and a weak acid analyte HCN (pK_a 9.3) up to peak concentrations of 40 μM (accounting for typical chromatographic dilution, this would correspond to injected concentrations >10 ppm for most ions). Both NaOH and DEA provides linear response but the absolute response was predictably lower by ~20% for DEA than NaOH. Nevertheless, if this loss in sensitivity is made up by lack of dilution and better mixing through permeative introduction, this will be far more attractive than past approaches especially as neither pumps nor electrical means to introduce the base are required.

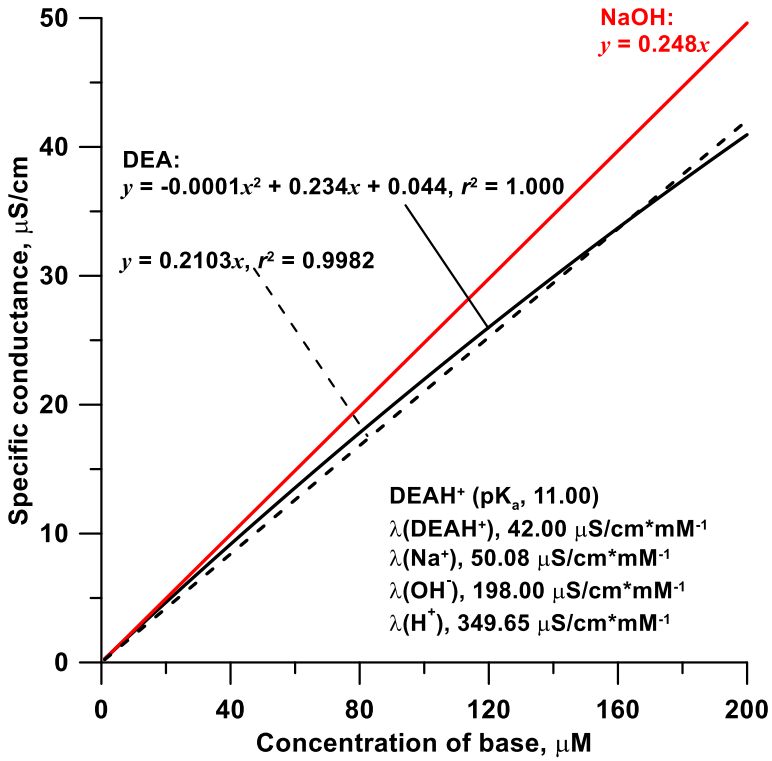

Figure 6-3 Theoretical specific conductance values for NaOH and DEAOH in the 0-200 μM range.

For DEA, the solid line indicates the actual data as well as the best quadratic fit, while the zero intercept best linear fit is shown by the dashed line.

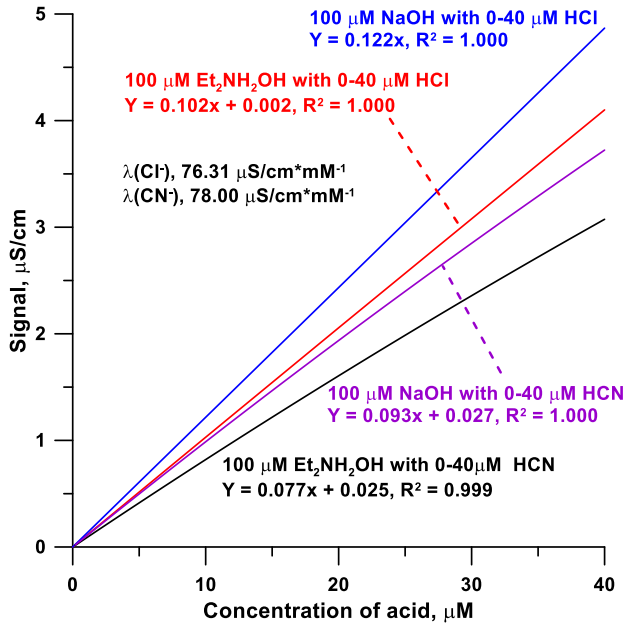

Figure 6-4 Calculated response of various concentrations of HCl and HCN (pK_a 9.31) using 0.1 mM NaOH or 0.1 mM DEA.

6.3.2 Relationship of Permeated DEA Concentration.

The amount of DEA permeated is expected to be proportional to the concentration of unionized DEA in the external solution. Within the range of interest, the DEA concentration in the external solution is relatively high and much of it is therefore unionized and the unionized concentration is thus linearly related to the total concentration. As a result, the permeated DEA concentration was found to be linearly proportional to the external concentration (Figure 6-5). Note that the amount of DEA permeated is so small compared to that externally present, the feed can be used for a very long period. For 125 mL external solution containing 18% DEA at 15 °C and an internal flow rate of 0.3 mL/min, the system will operate for >800 hours before there is a 1% relative decrease in the external concentration. This operational period can be extended even more by buffering the system to have a small amount of strong acid, such

that the external total DEA concentration has to be raised even further to maintain the same free [DEA] as before. However, as the operational period needed before refill/concentration adjustment was already very long, this was not explored.

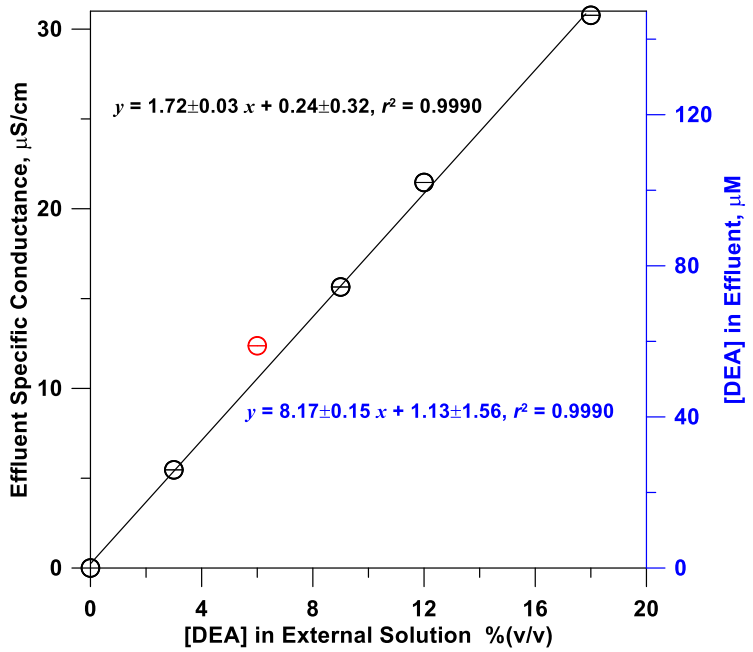

Figure 6-5 The DEA concentration and specific conductance of the effluent as a function of the concentration of the external DEA solution.

Water is flowing at 0.3 mL/min through a 60 cm long Teflon AF® tube (0.28 mm i.d., 0.68 mm o.d.) immersed in a DEA solution of indicated concentration. Note that the intercepts in both cases are statistically indistinguishable from zero. The symbol in red was not used in the best fit calculations.

6.3.3 Degradation products in electrodialytic suppression. Characterization of suppressor effluents.

The noise level at conductivity detector is very important, since it controls the limit of detection based on the signal-to-noise ratio. Degradation products formed during electrodialytic suppression have an important effect on baseline noise. We observed in

preliminary studies that the background noise levels at D1 were perceptibly lower with a chemically regenerated suppressor than with an electrically operated one. It was reported early that in electrodialytically suppressed anion chromatography, baseline noise levels increase with increasing suppressor current.[171] Although overall noise levels have since decreased by more than two orders of magnitude, qualitatively the same phenomenon is observed with modern day electrodialytic suppressors. The noise levels are greater in the electrodialytic mode and increase with increasing (excess) suppressor current. This is shown in Figure 6-6; however all data therein represent currents much higher than that needed for eluent suppression and the observed noise levels are therefore higher than what will be observed in practice. The exact cause for this noise has not been established. It can be due to electrolytic gas microbubbles or due to (redox?) degradation products from the membrane. The latter appears more likely due to several reasons: (a) There is no consistent relationship of the mean baseline conductivity with the excess suppressor current. In Figure 6-6 it generally increases with increasing suppressor current but a decrease with increasing suppressor current is also observed (Figure 6-7). Gas bubbles would be expected to consistently decrease the mean conductance; (b) Using fresh water or recycled suppressor effluent as the suppressor regenerant makes very little difference in the observed noise (Figure 6-6); increased dissolved gas in the input regenerant should have increased the noise substantially if gas bubbles were the principal source for noise; and (c) mass spectral examination of the suppressor effluent indicates that the total ion current increase with the suppressor current (Figure 6-8); further these components are likely acidic as in electrospray ionization, – HV produces much greater total ion current than +HV (Figure 6-9 and Figure 6-10). In Figure 6-9 the styrene sulfonate peak is readily identifiable and its presence as a graft monomer is readily explicable. However, it accounts for an insignificant portion of the total ion current,

much of which is centered around m/z 500-600. There is no analogous noise in the low wavelength UV absorbance trace that can be correlated to the conductance noise (Figure 6-11 shows the 208 nm absorbance trace). Also, the UV absorbance of the suppressor effluent is measurable only at very low wavelengths (<205 nm), the spectra are featureless with the absorbance rising monotonically at decreasing wavelengths (Figure 6-11), suggesting that the species responsible for the conductance noise may not be aromatic.

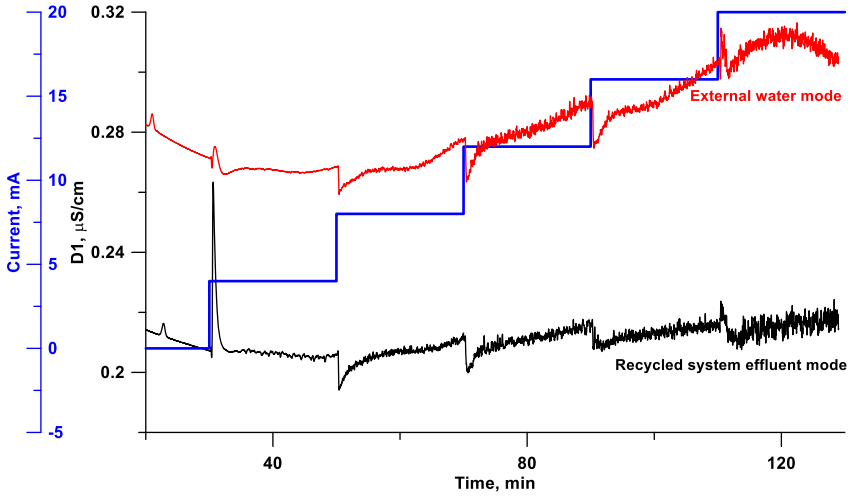

Figure 6-6 Effect of suppressor current on the baseline conductance of the first conductivity detector (D1).

The KOH eluent concentration was kept at 2.0 mM. The setup is the same as Figure 6-1. 18% (v/v) DEA solution is used in the PAID, resulting in a D2 background of 31 µS/cm. Eluent flow rate 0.30 mL/min; Flow rate through D2 was 20% of the PAID effluent (0.06 mL/min); 80% of the PAID effluent was recycled through the regenerant channel of the suppressor. The current was increased from 0.0 mA to 20 mA with 4 mA in each step. Note that even 1 mA is sufficient current to suppress this amount of eluent; the

noise is generally lower when the applied current goes towards eluent suppression; the excess current primarily contributes the noise.

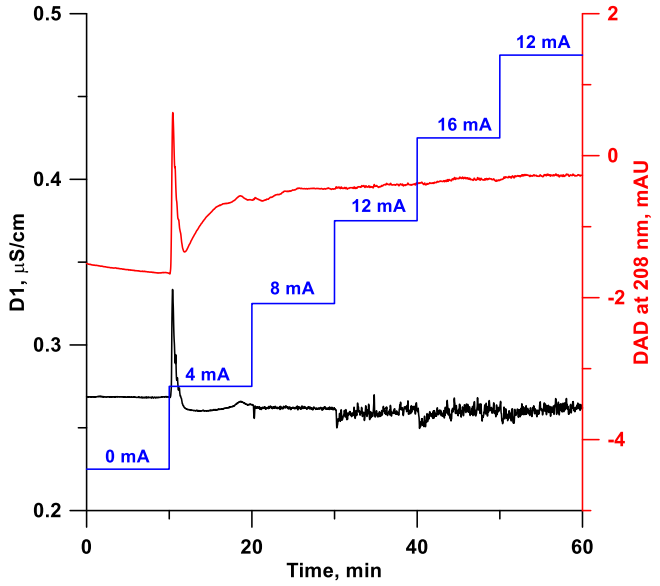

Figure 6-7 The effect of the suppressor current to the baseline noise at D1 (2.0 mM KOH at 0.30 mL/min.)

Black trace, baseline conductivity trace; Red trace, Agilent 1290 diode array absorbance trace at 208 nm. Note that the conductance noise is not reflected in the absorbance data, suggesting that the optically absorbing species is not directly related to the conducting species. In other experiments we have made observations that also suggest this, for example, during a particular current variation experiment, the mean background conductance may decrease while the absorbance increases.

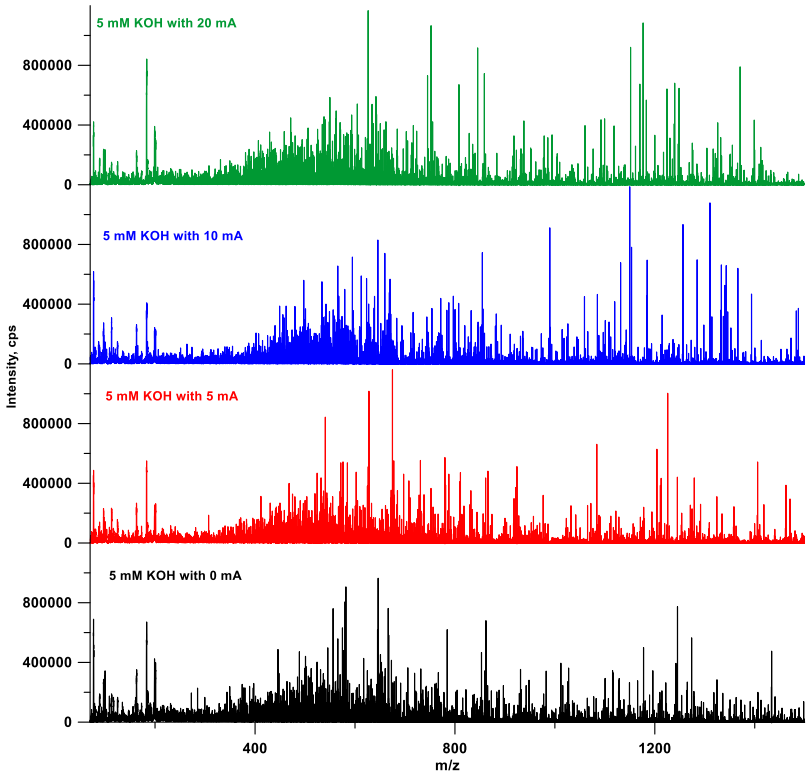

Figure 6-8 Negative mode electrospray full range mass spectra at different suppressor current levels.

Eluent is 5 mM KOH at 0.3 mL/min, Suppressor: 2 mm AERS500. 2.5 mA current is sufficient to suppress this amount of eluent. Note that 0 mA indicates that the power to the suppressor was briefly turned off, it continues to suppress for a substantial period from the static ion exchange capacity

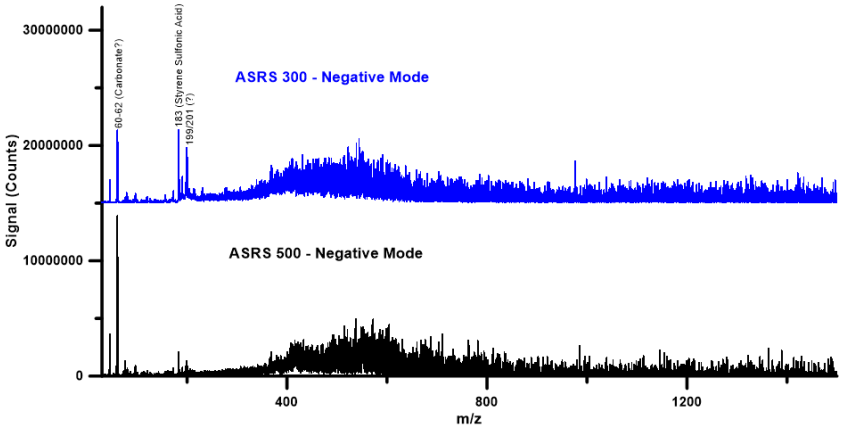

Figure 6-9 Negative Ion mode ESI-MS scans of two different suppressors.

The eluent was 30 mM KOH at 0.3 mL/min with a suppressor current of 50 mA. Spectra were recorded in both negative and positive modes (Figure 6-10) across the full mass range of the spectrometer (30-1500 m/z). The total background for negative ions was much greater than that for positive ions (Figure6-10) and was comparable between the two suppressors. The monomer ion styrene sulfonate is clearly visible at m/z 183 (confirmed by fragmentation spectra). Figure 6-9 uses the same scale as was used in the negative ion mode to show the vast difference in background noise. This is not unexpected as the suppressor removes any positively charged interferences from the eluent.

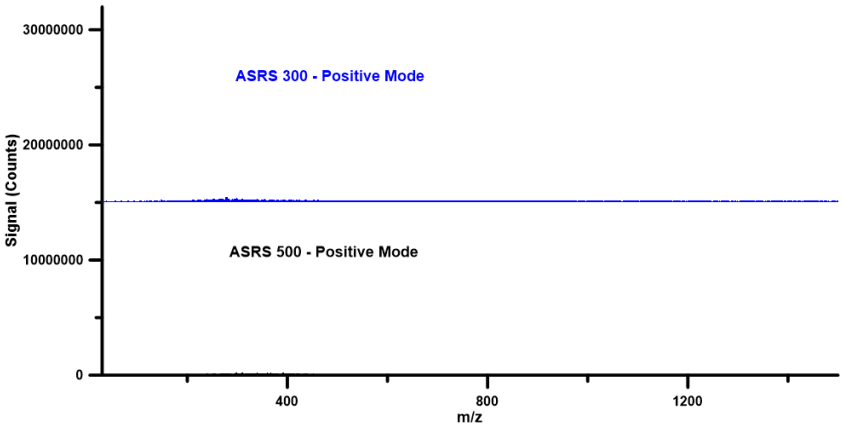

Figure 6-10 Positive Ion mode ESI-MS scans of the suppressors of two different suppressors, conditions same as in Figure 6-9.

The ordinate scaling is the same as in Figure 6-9 to illustrate the vast difference in background between positive and negative mode. The ASRS300 data are offset by 1,5000000 counts so both can be plotted on the same figure. To address whether any of the other components were affecting the background, the eluent generator and the carbonate removal device were systematically removed. Other than a change in the carbonate peak intensity, there were no significant changes. Removal of the suppressor dramatically decreased the total ion current in the negative electrospray mode, clearly establishing the role of the suppressor in creating the background. With the removal of the suppressor, appreciable background appeared in the positive electrospray mode, likely from column bleed.

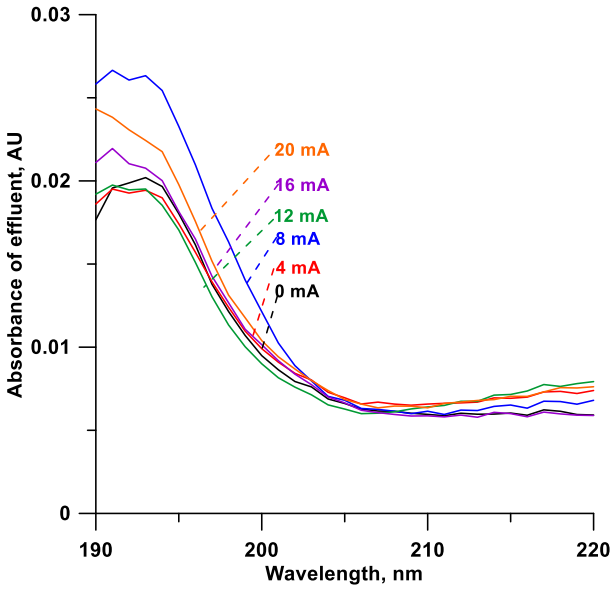

Figure 6-11 Absorption spectra of the suppressed detector effluent for a 2 mM electrogenerated KOH eluent at various suppressor currents.

The spectra is featureless and shows a general exponential rise at λ<205 nm. While there is probably a general increase in the low UV absorbing impurity with current, it is not particularly reproducible and the absorbance is very low.

All results above and those presented in the SI are consistent with excess suppressor current resulting in higher mass (polymeric/oligomeric) degradation products that are very weakly acidic, resulting in substantially greater noise at D2 after introduction. If processes at the electrode/membrane interface are responsible for the products that result in the observed noise, looking at the regenerant channel effluent from a suppressor may provide a better insight. Indeed, spectral examination of the regenerant effluent shows that the absorbance in the low UV does unquestionably increase with increasing suppressor current, the absolute values are ~100 times greater compared to those of the central channel effluent (Figure 6-13). Note that no significant absorption or spectral features were observed at λ>220 nm. It is also of interest to note in this context

that some degradation products accumulate even when a suppressor is not in use. When a suppressor is first used after prolonged storage, both UV and mass spectral studies indicate that the impurity background is much higher and a steady state value is reached only after prolonged washing/use. For most applications, the increase in noise will not be perceptible but in particular applications, reaching a steady state may require up to a week of continuous use.

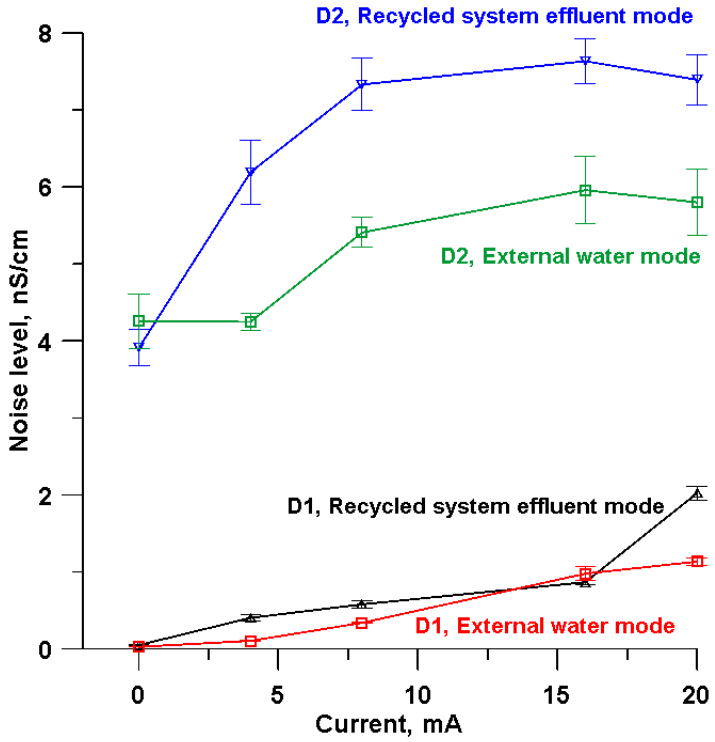

Figure 6-12 Effect of current of electrochemical membrane suppressor on the baseline noise at D1, D2.

The noise was computed over 2.5 min periods after subtracting baseline drift (predicted best linear fit of the data subtracted from the data). The current was increased from 0.0 mA to 20 mA with 4 mA in each step, while the KOH eluent was kept at 2.0 mM. The specific conductance background at D2 is ~31 μS/cm. In water recycled mode, the

main eluent stream after PAID device was used as regenerant stream. In external water mode, a fresh DI water stream was used as the regenerant stream.

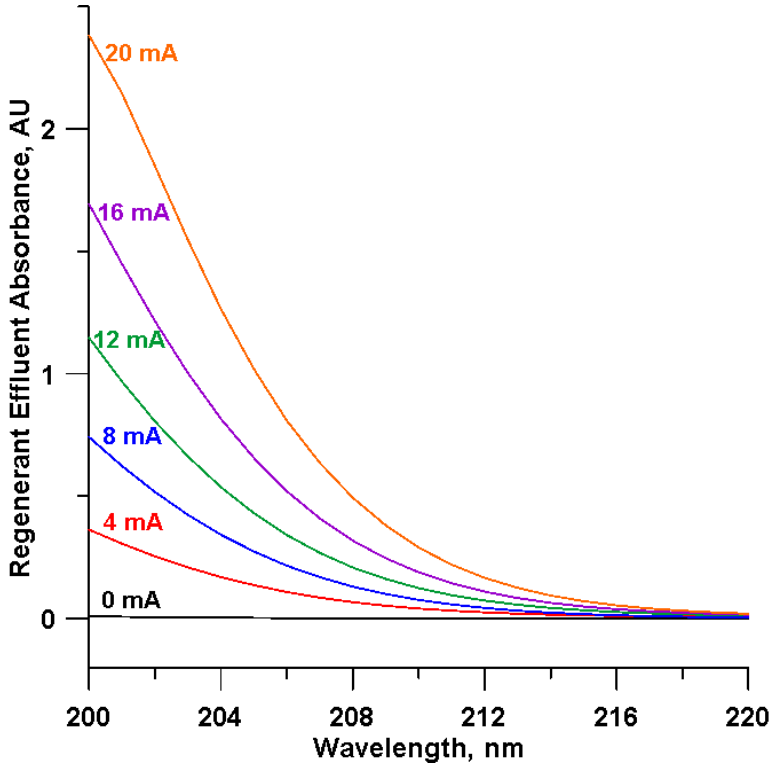

Figure 6-13 Low wavelength absorbance spectra of the regenerant channel effluent at various suppressor currents collected from an ESRS500 suppressor and measured offline after 5x dilution. Eluent was 2 mM KOH at 0.3 mL/min.

In the present setup, some noise can also originate from the possible back penetration/oxidation of DEA present in the liquid that is recycled through the regenerant channels. Figure 6-12 does show that the noise was discernibly smaller, especially for D2 if fresh water rather than the PAID effluent was the regenerant.

6.3.4 Using chemical or intermittent electrodialytic suppression vs. continuous electrodialytic suppression.

Electrodialytic membrane degradation associated noise can obviously be eliminated by using chemical suppression. Most (but not all) electrodialytic suppressors can also be chemically regenerated, especially if the eluent concentration to be suppressed is not particularly high. Intermittent electrodialytic operation basically results in chemical suppression during the time chromatography is conducted. If complete eluent suppression can be maintained, this represents the best of both worlds, at some expense to sample throughput. The present ESRS500 suppressor, has a large enough static (no power applied) ion exchange capacity to completely suppress 10 mM KOH at 0.3 mL/min for 30 min. Turning off power to the suppressor at sample injection and back on after complete separation offers the best baseline noise. It was also possible to turn suppression on or off in specific regions, although there is a shift in baseline and a brief peak/dip (see Figure S7), the equilibration is rapid and can be practiced if there are no analyte peaks of interest near the peak/dip. Electrolytic suppression also generates oxygen; we have observed serious loss of oxidation-susceptible sulfide with continuous electrodialytic suppression.[170] SCAC could not previously detect such weak acids at trace levels; to take advantage of the newfound ability prevention of such losses through appropriate suppression techniques is needed.

6.3.5 Internal volume, dispersion, and baseline noise.

The geometry and internal volume of a device govern band dispersion. Given the same geometry, a larger residence volume typically improves mixing and reduces noise at the expense of greater dispersion. Table 6-1 provides previously reported performance data in similar efforts, where the smallest dispersion and noise levels were 78±4 μL (25 μL injected sample) and 5±2 nS/cm. However, in all previous cases a mixing coil or

equivalent was used after base introduction and the dispersion induced by this additional device is not taken into account in the above. For the lowest noise case above, the total dispersion, including that produced by the mixing device, was 132±4 μL. The PAID induced dispersion was measured operationally with 10 μL of an 80 μM HNO_3 sample injected without column to be 48.8±0.2 μL. In the absence of electrodialytic suppression, there was no statistical difference in baseline noise whether fresh water or the PAID effluent was used for suppressor regeneration (see D2 data in Figure 6-12 for 0 mA current), effluent recycling was therefore used. The baseline noise for a background conductance of 30.8 μS/cm in the absence of suppressor current was 4.4 ± 0.6 nS/cm, and notably without the need for a further mixing coil used in many previous studies. Overall this performance is at least equal to or better than previous approaches (see Table 6-1).[43,44,154]

Table 6-1 Dispersion volume and baseline noise in current and Previous Studies.

Experimental conditions	**Dispersion volume**	**Noise level**	**Ref.**
25 μL injection, flow rate 1.0 mL/min; Electrodialytic base introduction	Band dispersion is for the base introduction device only; does not include that induced by the mixer. Band dispersion increases for all electrodialytic devices when it is actually operating (power is applied) 67 ± 4 μL power off; 94 ± 6 μL power on, device in actual operation.	20-25 nS/cm in a specific conductance background of ~25 μS/cm	[43]
25 μL injection, flow rate 1.0 mL/min; Electrodialytic base introduction using planar devices of various length and a tubular device.	All data below in power on condition and does not include dispersion induced by subsequent mixer. 8 cm planar, 89.2 ± 1.8 μL 4 cm Planar, 86.7 ± 3.3 μL 2 cm Planar, 78.1 ± 5.2 μL Tubular, 90.0 ± 3.4 μL Pump 2 had lower flow noise than pump 1.	8 cm planar, 17.2 nS/cm; Pump 1 4 cm Planar, 15.4 nS/cm, Pump 1 2 cm Planar, 34.3 nS/cm, Pump 1 2 cm Planar, 7.7 nS/cm, Pump 2 Tubular, 19.7 nS/cm, Pump 2 All in a specific conductance background of ~25 μS/cm	[44]
25 μL injection, flow rate 1.0 mL/min; Reports on both passive and electrodialytic base introduction	Planar, 96 ± 8 μL Tubular, 110 ± 4 μL Filament-filled annular helical (FFAH) design, passive introduction, 78 ± 4 μL Dispersion from subsequent mixer was measured as 55 μL. So, the total dispersion volume in the most favorable case was 132 ± 4 μL.	Planar sheet membrane design, 7 ± 2 nS/cm Straight tube in shell design, 7 ± 2 nS/cm FFAH, 5 ± 2 nS/cm All in a specific conductance background of ~28 μS/cm	[154]
10 μL injection, flow rate, 0.3 mL/min; Permeative base introduction	48.8 ± 0.2 μL as large diameter coil 30.3 ± 0.3 μL as a 4 mm diameter coil	4.4 ± 0.6 nS/cm for large diameter coil 3.6 ± 0.2 nS/cm for a 4 mm diameter coil. All in a specific conductance background of ~31 μS/cm	

However, a linear configuration (or a large coil radius as used here) has been reported to be most prone to poor mixing and large dispersion,[153] hence we coiled the Teflon AF tube in the PAID on a 3.7 mm support rod and thermoset the shape by putting it in boiling water for 30 min. Both the noise, and the dispersion decreased, respectively to 3.6 $\pm$ 0.2 nS/cm and 30.3 ± 0.3 μL, under the same test conditions. This improvement was discovered late in the work; other all other data reported in this paper was obtained without coiling.

6.3.6 Improving limits of detection through reduced background (Reduced added base concentration).

Most often baseline noise can be directly correlated with the absolute value of the background.[118] Reducing the introduced base concentration is thus expected to improve limits of detection (LODs) as the background conductance and hence the background noise will decrease. While a base concentration may also limit the upper measurement limit, this is of less importance when LOD improvement is the primary goal. Further, upper measurement limits may not have to be sacrificed with lower base concentrations, see below.

The typical dilution factor at the peak apex from sample injection to detection is ~10; so 10 μM base is enough to measure up to 100 μM monoprotic acid HX (amounting e.g., to 3.5 mg/L chloride to 10 mg/L perchlorate), a significant amount for trace analysis. For very weak acids, however, lowering the amount of the base introduced lowers the pH and may decrease the signal because of inadequate ionization. Theoretical simulations are straightforward; the results are shown in Figure 6-14. For a strong acid like HCl, with strong base introduction the signal remains constant and independent of base concentration (until, the amount of base present is inadequate to neutralize the HCl). With DEA, a weaker base, the signal actually decreases with increasing [DEA] because a

buffer is formed. However, as a first approximation if the noise is proportional to the background, the S/N ratio (SNR) increases linearly proportional to $[base]^{-1}$ resulting in no difference in SNR between NaOH and DEA introduction. The expected behavior for HCN is qualitatively similar; the 10 μM HCN signal remains almost the same down to 50 μM [base] but decreases steeply thereafter due to incomplete ionization. The overall gain in SNR with decreasing [base] is less steep than with HCl but here also SNR increases consistently with decreasing [base]. In going from 200 to 10 μM DEA, the SNR gain for 10 μM HCl and HCN are 21.7 and 6.8 times, respectively. Also importantly, no discernible difference in SNR is predicted for a weak acid like HCN between NaOH vs. DEA introduction.

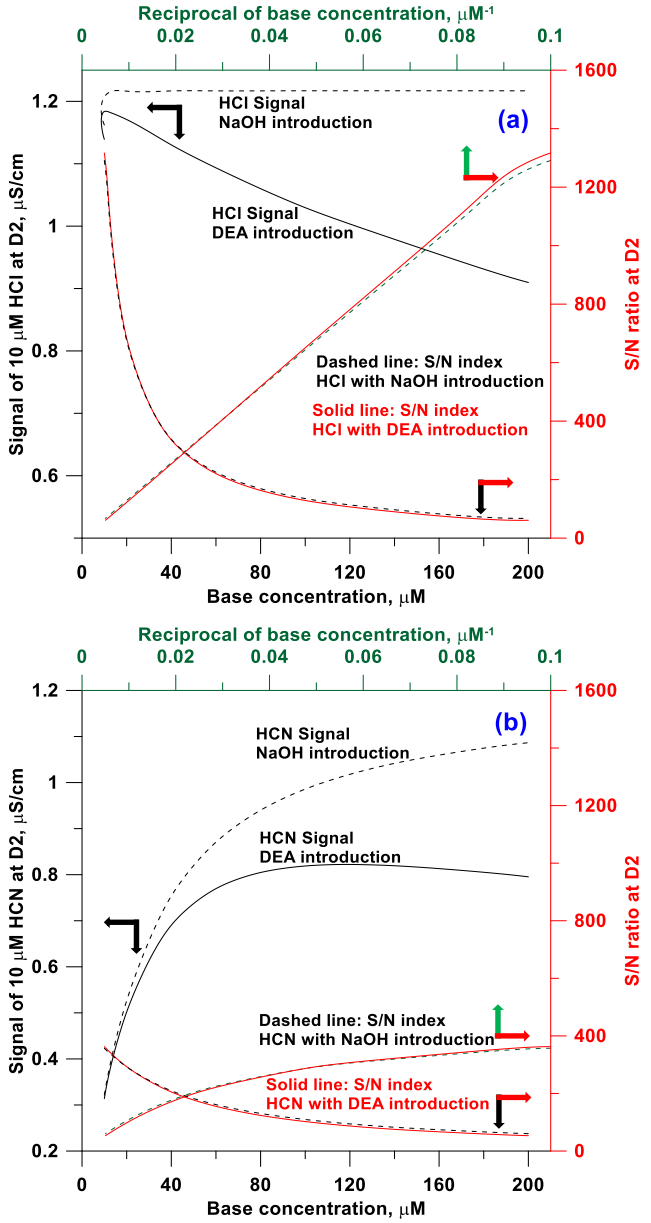

Figure 6-14 Theoretical simulations. Signal and S/N ratio of 10 μM HCl and HCN plotted for various concentrations of NaOH and DEA backgrounds (0.01-0.20 mM). The S/N ratio is plotted both against the base concentration (bottom axis) or its reciprocal (top axis). The noise level was assumed to be directly proportional to the corresponding background conductance.

Reality check is essential, however; there may be noise sources other than that related to the background, so the noise may stop decreasing linearly with the background conductance. Further, the computations ignore the unavoidable intrusion of CO_2. Figure 6-15 shows the dual detection chromatograms of a sample containing a variety of anions; the D2 trace is shown for two different [DEA] values. Predictably, zwitterionic taurine and very weak acid anions silicate/sulfide/cyanide produce negligible or nonexistent responses at D1 good responses at D2. The D2 responses for 27 μM vs. 150 μM [DEA] backgrounds follow the theoretically predicted behavior. Strong acid signals increases at lower [DEA] (see Figure 6-14a) but those for the very weak acids decrease with decreasing [DEA] (see Figure 6-14b). The 5.6 times decrease in [DEA] from 150 to 27 μM was almost exactly reflected in a 5.4 times decrease in noise from 4.4 to 0.83 nS/cm. As a result, despite a decrease in the response for taurine, silicate, and cyanide with a lower [DEA], the LODs still improve. Figure 6-16(a)-(d) depict very good linear calibration curves for all injected ions present in Figure 6-15 over a 2-200 μM range. Figure 6-17 summarizes the improvements in the LOD and the changes in sensitivity (calibration slope) for each ion as [DEA] is decreased from 150 to 27 μM; all the LODs decreased, sensitivity improved for all but 3. LODs are listed in Table 6-2, sub-μM LODs for the very weak acid analytes have never previously been attained with conductometric detection.

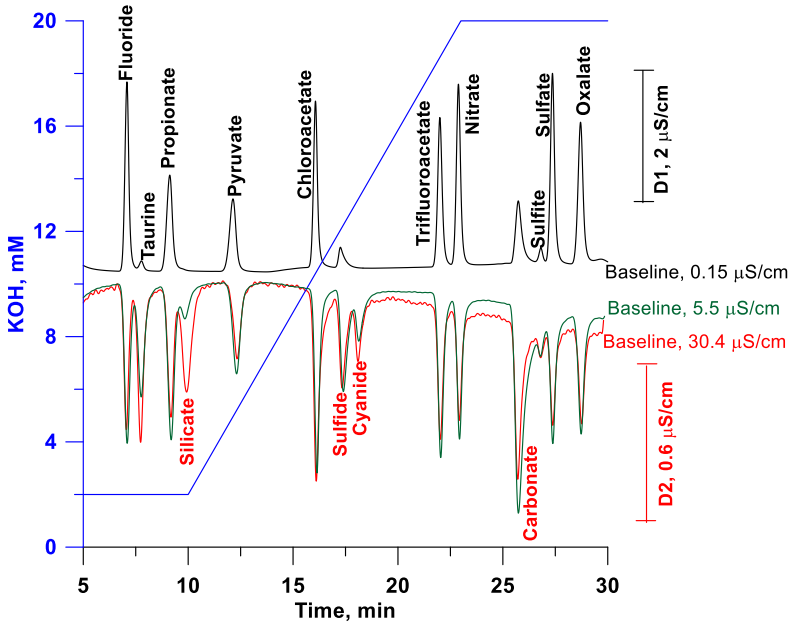

Figure 6-15 Illustrative application of dual conductometric detection with the PAID.

The suppressor was operated at 20 mA in the periods 0-4 and 30-36 min, and turned off during 4-30 min. 10 µL injection of 50 µeq/L for each ion. Carbonate results from CO_2 intrusion to sample and sulfite is an impurity in the sulfide standard. The top trace is the conventional suppressed detector response and the bottom two traces are the second detector responses at two different levels of [DEA], 27 (green) and 150 µM (red). 2 mm AS11 column, 0.3 mL/min. The gradient profile is shown with respect to the left ordinate.

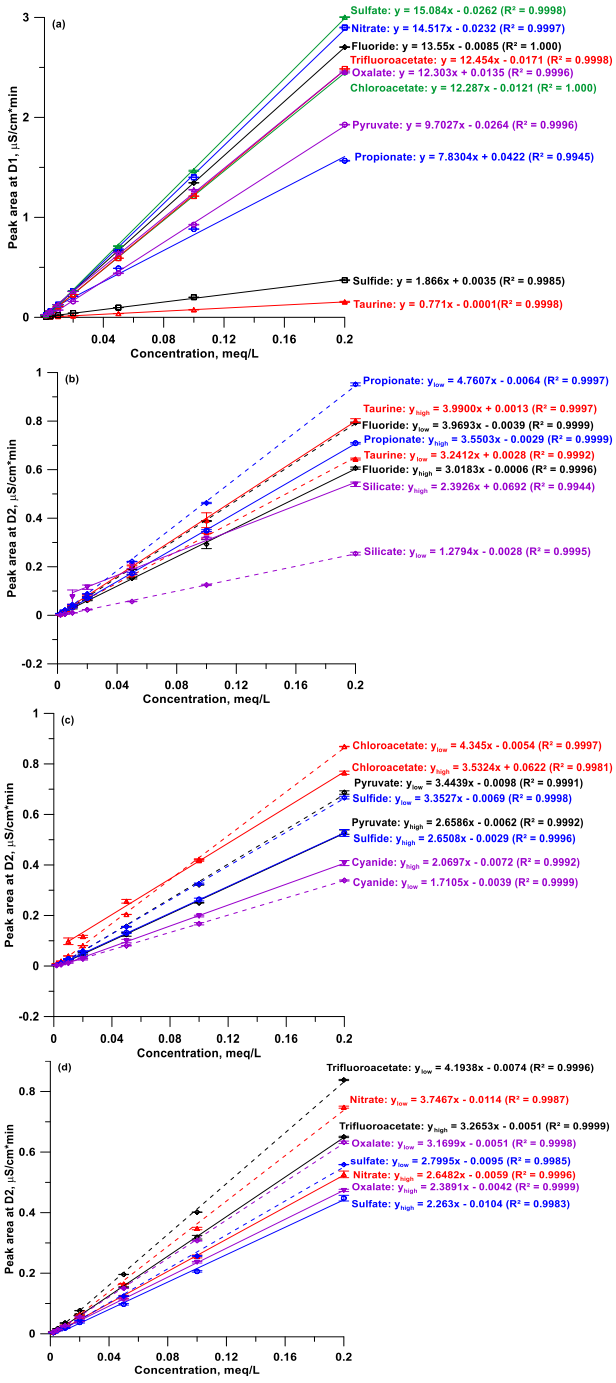

Figure 6-16 Calibration curves relevant to Figure 6-15. (a) Calibration curves at D1; (b), (c), (d) calibration curves at D2: solid traces for 150 µM DEA (30.8 µS/cm background)

and dashed traces for 27 μM DEA (background 5.5 μS/cm). Concentrations ranges from 2-200 μeq/L for each ion.

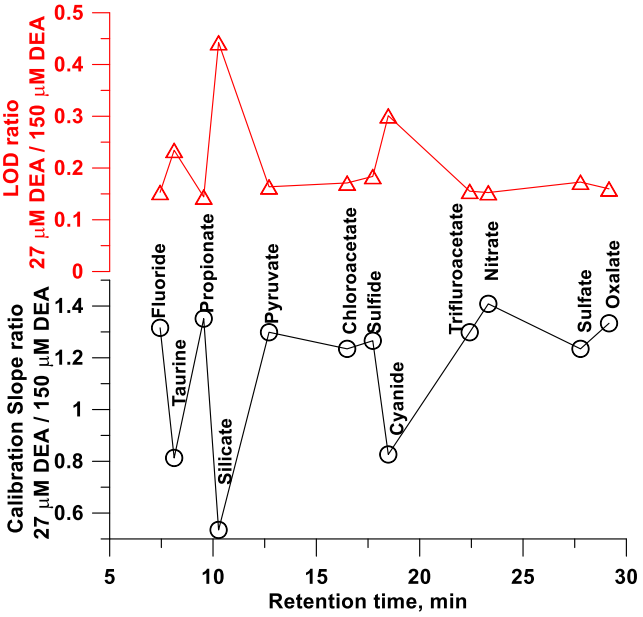

Figure 6-17 Calibration slope ratios, and LOD ratios of various anion at D2 between using 150 μM and 27 μM [DEA].

Limits of detection are listed in Table 6-2. The background conductance levels are 30.8 μS/cm and 5.5 μS/cm, respectively, with corresponding baseline noise levels of 4.4 and 0.83 nS/cm, respectively. A slope ratio of unity indicates sensitivity did not change while a value <1 indicates it was lower for a lower background [DEA] (taurine, silicate, cyanide). The LOD ratios fall within a range of 0.1-0.5, corresponding to a 10-2x improvement in the LOD in going from 150 to 27 μM [DEA].

Table 6-2 Limit of detection (LOD) at D1 and D2.[a]

Analytes	LOD at D1 (10 μL injeciton), nM	LOD at D1 (1.0 mL injection), nM	LOD at D2 using 150 μM DEA-OH (10 μL injeciton), μM	LOD at D2 using 27 μM DEA (10 μL injection), μM	LOD at D2 using 27 μM DEA(1.0 mL injection), nM
Fluoride	3.47	0.05	1.20	0.18	2.26
Taurine	72.27	0.94	1.14	0.27	2.61
Propionate[b]	5.56	NA	1.36	0.20	NA
Silicate	NA	NA	2.25	1.00	21.32
Pyruvate	9.35	0.12	2.30	0.38	4.51
Chloroacetate	3.80	0.04	1.04	0.18	1.68
Sulfide	29.83	0.32	1.91	0.35	2.79
Cyanide	NA	NA	2.66	0.80	13.06
Trifluoroacetate	4.40	0.05	1.30	0.20	2.10
Formate	NA	0.04	NA	NA	2.51
Chloride	NA	0.03	NA	NA	2.63
Nitrate	3.66	0.04	1.59	0.24	2.78
Sulfate	1.77	0.03	0.94	0.16	1.05
Oxalate	2.24	0.05	0.95	0.15	1.70

[a] The calibration ranges were from 10-200 μeq/L with 150 μM DEA introduction and 2-200 μeq/L with 27 μM DEA introduction. The calibration ranges were from 0.04-4.0 μeq/L for silicate and 0.02-2.0 μeq/L for all other ions with 1.0 mL sample injection.

[b] Propionate was not added for 1 mL sample injection, due to some coelution with silicate.

[c] LOD of silicate (as well as formate and chloride) with 1 mL sample size was calculated using AS24 column.

6.3.7 Quantitation at the second detector at high analyte concentrations.

At high analyte concentrations, the peak eluite acid concentration can exceed the introduced base concentration. While obviously such a sample can be diluted and reinjected, good quantitation is actually possible from the extant response. For a strong acid analyte, it is intuitive that in such cases, the response will be a W-shaped peak; the signal decreases initially and reaches a minimum when the entire base is neutralized and then starts rising again as excess acid is added. Depending on the extent of the acid excess, the center of the W-peak may exceed the original base line (beginning/ending points of the W). In flow-injection "titrations"[172] where an acid sample is similarly injected into a flowing base stream (or vice-versa), such W-peaks are well known. While conductometry has also been used,[173] more commonly the base or the acid can be doped with an indicator and the process followed optically. The original work[172] strived to produce an exponentially tailing peak so that the width of the peak at any specific height will be directly related to the logarithm of the injected sample concentration. Chromatographic peaks are Gaussian or nearly so and it is readily derived that the width (W_h) of a Gaussian peak of standard deviation s at any height h is given by:

$$\ln h_{max} = 0.125 (W_h^2/s^2) + \ln h) \quad \ldots(1)$$

The square of the peak width at any chosen height is therefore linearly related to the logarithm of the injected concentration. It is to be noted that this will remain true as long as the height h chosen for measuring the width is still in a region where the response is linearly related to the concentration. It does not matter whether past that point the detector response is nonlinear or is W-shaped. The full ramifications of this is beyond the scope of the present paper; presently we only note that extraordinary measures are taken to linearize the detector output over a large concentration range,[174] whereas the linearity of W_{h2} with ln C at low values of h is an inherent property even

when *h* and *C* are not linear over a large range. Experimental verification will be presented elsewhere.

6.3.8 An important PAID application. Determination of silicate.

Silicon is among the most abundant crustal elements; all natural water contains some dissolved silica. The silica content in natural water is typically in the range of 100-500 μM (2.8-14 mg/L Si).[175] The American Society for Testing and Materials specifies the maximum silica levels for Type 1, Type 2, and Type 3 Reagent Grade Water as 50 nM, 50 nM, and 8.3 μM, respectively.[176] Dissolved silica is problematic in many areas. In power plant boiler feed water it corrodes the heating equipment and turbines and reduces turbine efficiency.[177] Measurements at the lower nM levels are needed in the semiconductor industry as submicromolar levels can still affect surface reactions on silicon wafers[178] and low levels of dissolved silica are not detectable by conductivity or carbon measuring instruments. Silicate is also an essential aquatic macronutrient. Of many methods to measure silicate,[179] reactions with molybdenum salts in acidic media to form yellow silicomolybdic heteropolyacid or its reduction product heteropolyblue,[180,181] and their spectrophotometric measurement are the most common. This is satisfactory for some samples[182] but not when traces must be measured and/or the matrix is complex. The first application of ion exclusion chromatography (ICE) and/or inductively coupled plasma mass spectrometry (ICP-MS) to silicate/silicon determination[183] attained a limit of detection (LOD) of 80 nM; this remains the best reported LOD by ICP-MS. Interestingly, these authors report a lower silicon blank signal for a quartz torch rather than an alumina torch. In any case, this approach is capital intensive, require a skilled operator and still cannot meet the needs of the semiconductor industry. Li and Chen[184] reported ICE separation and conductometric detection of silicate with only water as eluent with an LOD of 20 nM. Unfortunately this paper is not credible. While the paper has been cited 33

times, no attempts have obviously been made to replicate the results. After failing to replicate the results, we realized that this approach can be shown ab initio to fall orders of magnitude short of the claimed LOD (see the next section 6.3.9).

The present method is sensitive enough to readily determine the gradual appearance of silicate in initially pure water kept in a glass vial even in acidic conditions, as shown in Figure 6-18. As may be anticipated, silicate continues to increase in concentration, essentially linearly, in a basic solution. Interestingly, the initial appearance of silicate in pure water is even more rapid (this observation is reproducible).

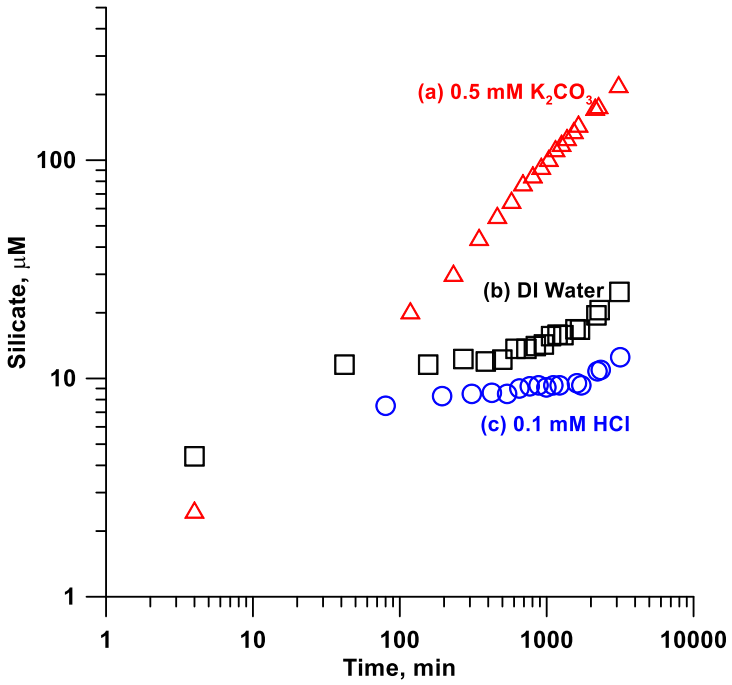

Figure 6-18 Temporal appearance of silicate in a borosilicate glass sample vial containing (a) mildly alkaline solution, (b) DI water and (c) a slightly acidic solution.

Only (a) contained an initially detectable concentration of silicate. Samples were transferred at desired times to polystyrene sample vials. Analytical conditions same as in Figure 6-15.

Albeit more sensitive than previously reported methods, the above silicate LOD (1.0 μM) is still inadequate for testing compliance in Type I reagent water. Large volume sample injection was therefore investigated to meet this goal. While good dual detection chromatograms were obtained with the AG11-AS11 columns used (Figure 6-19), we found that exposures of the sample/water to our laboratory environment results in contamination with traces of formate that co-elutes with silicate under these conditions. A more robust approach was realized with an AG24-AS24 column set which has an altogether different selectivity. Using the same KOH gradient, silicate was the first to elute and well separated from all other anions (Figure 6-20). The LOD of silicate thus achieved was 21 nM based on the S/N=3 criterion, sufficient to determine compliance to Type 1 reagent water specifications. A 1 mL injection volume also permits detection limits of 3 nM taurine, 3 nM sulfide, and 13 nM cyanide, respectively. We wish to note that the separation in Figure 6-20 was not optimized for the separation of silicate, which actually elutes with rather poor efficiency. Doubtless, in many samples the composition will permit an earlier elution with a steeper gradient as a much sharper peak, thus improving LOD further. The calibration curves of different analytes under the present elution conditions are shown in Figures 6-21(a)-(c).

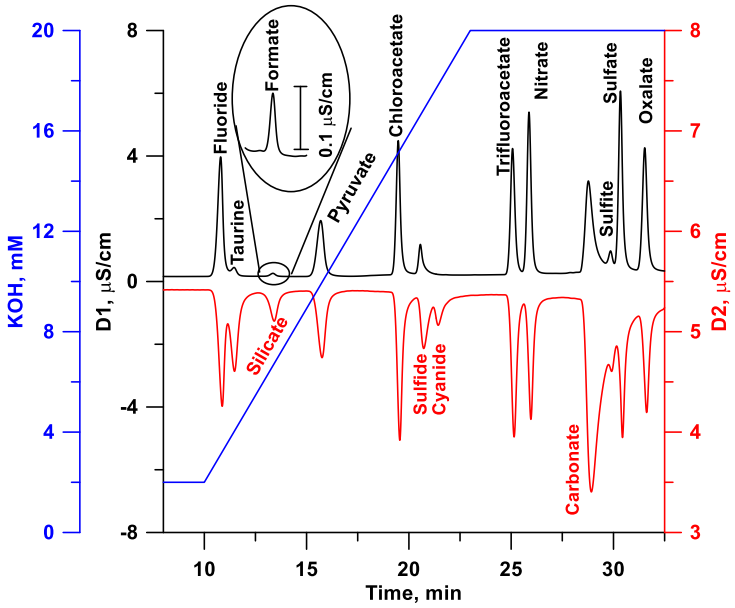

Figure 6-19 Dual conductometric detection using 1.0 mL sample injection. Sample injection time, 0.0 min; sample loading time, 32.5 min; current of suppressor, 0 mA from 6-32.5 min and 20 mA in the rest of time. 1.0 mL injection of 1.0 µeq/L for each ion. Carbonate results from CO_2 intrusion to sample. Sulfite is an impurity in the sulfide standard used. Formate impurity comes from both cyanide standard and formate intrusion in air to sample.

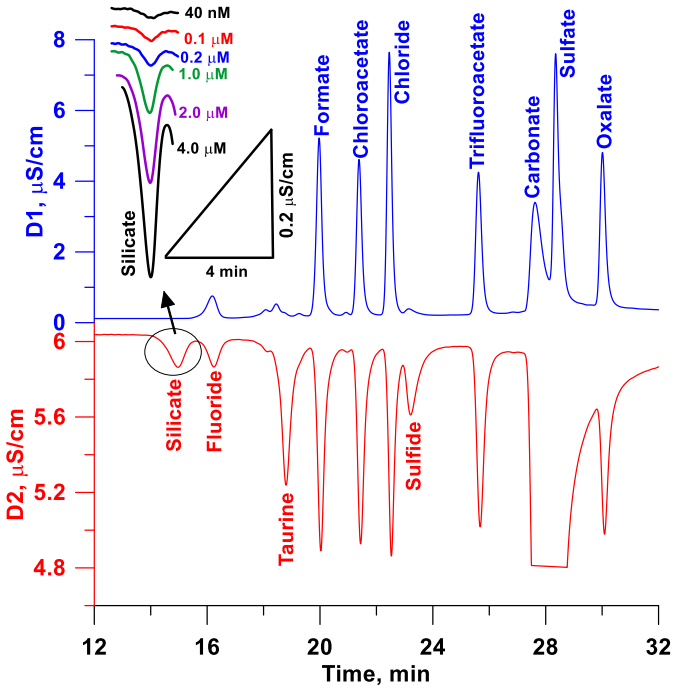

Figure 6-20 Dual conductometric ion chromatogram on AG24+AS24 columns using 1.0 mL sample injection.

Gradient profile same as Figure 6-15. Suppressor current 20 mA 0-6 and 32.5-40 min and off during 6-32.5 min. Sample concentrations (µeq/L): silicate (2.0), fluoride (0.25) and all other ions (1.0). Carbonate was not deliberately added. The separation under the given conditions on this column set was good for silicate but compromised other analytes. Pyruvate, cyanide and nitrate co-eluted with formate, sulfide, and sulfate, respectively, and were not present in this sample.

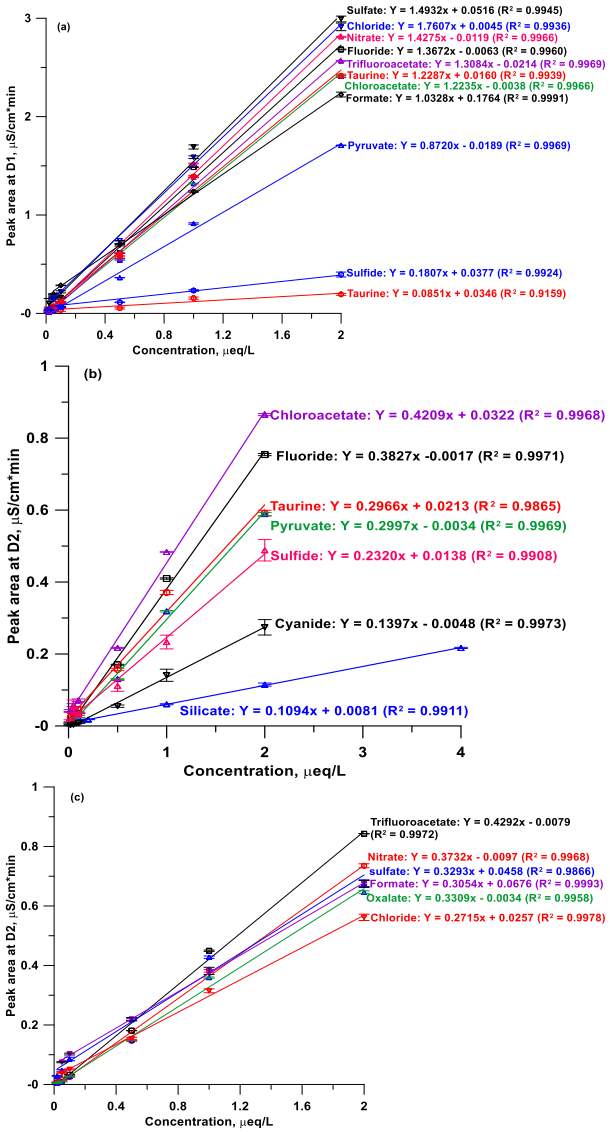

Figure 6-21 Calibration curves at D1 and D2. (a) Calibration curves at D1; (b), (c) calibration curves at D2. The calibration ranges are from 0.04-4.0 µeq/L for silicate and 0.02-2.0 µeq/L for all other ions. Quantifications of silicate, formate and chloride were achieved using AS24 column, all others on AS 11 column.

6.3.9 The impossibility of claims made in reference 184

6.3.9.1 Experimental conditions in Reference 184.

The authors used a Waters Model 432 Conductivity Detector and a sample Injection volume of 20 μL with a pure water eluent, the flow rate for the data discussed here was 1.0 mL/min.

6.3.9.2 Relevant Facts

The pK_a value of silicic acid is 9.7. Equivalent Conductance values of the silicate anion and the hydronium ion are, respectively, ~0.050 and and ~0.35 S/(cm•M) .The stated baseline noise for the detector is 5 nS/cm (http://www.waters.com/webassets/cms/library/docs/720000463en.pdf) While the pH of pure water is 6, in an environment that is not protected from atmospheric CO_2 (as used in this work), the eluent pH is likely to be closer to 6 (the pH of water in equilibrium with atmospheric CO_2 is 5.6).

6.3.9.3 Discussion Based on Figure 1 of Reference 184

Figure 1 in reference 25 depicts a silicic acid peak that results from the injection of 20 μL of 100 μM of a silicate solution. The peak has a half width of 0.5 min and hence a triangulated volume of 1 mL. The peak concentration is twice the average concentration and hence the peak concentration is (20 μL/1000 μL)*100 μM*2 = 4 μM.

If very conservatively we assume that the eluent pH is 6.7, for an analyte of pK_a 9.7, only 1/1000th will be ionized. 4 nM additional ions (hydronium and silicate) will maximally be produced that amounts to a conductance of (0.35+0.05)S/(cm•M) X 4 x 10^{-9} M = 1.6 nS/cm. This value is >3x below the noise level of the detector and it should not be possible to detect even 100 μM, much less the claimed LOD of 20 nM

In all probability, the signal height of 100 μM injected silicate is likely going to even less that what has been calculated above because autoprotolysis of water

contributes to the background conductance at these levels and any addition of H^+ from any external source will result in decreased ionization of the background and the net signal is likely to decrease.

6.4 Conclusions

The PAID is a robust low-dispersion low-noise device that brings remarkable simplicity and ease of use to dual conductometric detection to improve detectability of weakly ionized analytes. The ability to measure low levels of silicate is an attribute that can be particularly useful. Although not described here, it is obvious that acids can be introduced just as easily for the detection of very weak bases, e.g., various amines.

6.5 Acknowledgements

This work was supported partially by NASA (NNX15AM76G), NSF (CHE-1506572), ThermoFisher/Dionex and the Hamish Small Chair Endowment at the University of Texas at Arlington. We thank C. Phillip Shelor for carrying out the initial work with mass spectrometric characterization of suppressor effluents and Dr. Ilia Koev, (www.Biogeneral.com) for the gift of the Teflon AF tubing.

This chapter has been submitted to Analytical Chemistry. Future Copyright 2015 American Chemical Society.

Chapter 7

Summary and future work

7.1 Summary

The main research described in this dissertation is about how to achieve sensitive conductometric detection of very weak acids in IC. It also describes the use of IC for the determination of anion composition in different fruit samples. It also explored and explained the unusual ion-exchange behavior of myo-inositol phosphates, a very important class of sugar phosphates involved in neurosignaling.

The determination of principal organic acids in fruit juices, especially grape juice (for general characterization and for determination of maturity for harvesting), by SCAC has been previously proposed.[99,100,101] The SCAC technique has grown remarkably in this field since it is possible to generate an essentially complete anion profile, especially the essential part of organic acids. The presented research has employed SCAC for the determination of composition of different açaí, açaí-pomegranate juice, and grape juice samples. The highly characteristic anion profile and in particular the absence of tartrate can be readily used to identify authentic açaí products that do not contain other fruit juices. With the açaí products as the focus, we hope to have clearly established the power of this SCAC technique.

The work described in chapter 3 explored the unusual ion-exchange behavior of myo-inositol phosphates. The separation of myo-inositol mono-, di-, tri-, tetra-, pentakis-, and hexakisphosphate ($InsP_1$, $InsP_2$, $InsP_3$, $InsP_4$, $InsP_5$, and $InsP_6$) was carried out in a SCAC system based on hydroxide eluent. The retention of $InsP_3$ −$InsP_6$ was determined to be controlled by steric factors while elution was influenced by eluent cation complexation. These highly phosphorylated $InsP_s$ have a much greater affinity for alkali metals ($Li^+ > Na^+ > K^+$) than quaternary ammonium ions. Cation interaction is often

ignored in anion-exchange chromatography but may play an important role in improving separations of highly charged analyte anions.

Previous studies of two-dimensional conductometric detection in IC that utilized base introduction after a conventional SCAC were further developed in chapter 4. One of the major factors inhibiting the application of such a two-dimensional detection system has been the lack of commercially available MENG device. The recent introduction of ICS-5000 IC system that contains two independently operable ion chromatographs makes it easy to implement such a scheme with minor modifications. After suppressed conductometric detection of a hydroxide eluent, the eluent goes through a mixer device where electrogenerated LiOH from the second channel is introduced into the eluent stream. Sensitive determination of weak acids in a second dimension was carried out in such a scheme. In order to achieve good mixing efficiency and small dispersion, different mixer designs were investigated. Three mixer designs, a back-flow tee mixer (BT), an end-blocked membrane tee mixer (EMT), and a tubular membrane mixer (TM), were fabricated and compared to three commercially available mixers, Visco-Jet Micro mixer (VJM) and HS binary tee mixer with 2 and 10 µL volume (HS-2 and HS-10) mixing cartridges. Based on its mixing efficiency and small dispersion, the BT design was found to be the best for practicing base introduction hereinabove or postcolumn reaction generally.

In chapter 5, we provide a robust conductometric approach that uses the same principle of reacting HA with OH^- and measuring the signal that results from the difference values in limiting equivalent conductance of A^- and OH^-. A volatile analyte transfer device (VATD) was fabricated for volatile analyte mass transfer and enrichment. The VATD is a robust low-noise device permitting highly sensitive, wide dynamic range conductometric detection of volatile weak acids like cyanide and sulfide. The principle

should be extendable to volatile weak base analytes such as amines in a cation chromatography system.

A permeative amine introduction device (PAID) for very weak acid detection is described in chapter 6. The PAID is placed after a conventional KOH eluent SCAC system. The PAID converts the suppressed eluites from the acid form to the corresponding ammonium salt ($NR_2H + HA \rightarrow NR_3H^+ + A^-$) and allows very weak acids HX (pKa ≥ 7.0) to be measured by D2 following the PAID. The PAID is a robust easy-to-build low-dispersion low-noise device. It can be operated with no pump and no electrical current supply. Although not described here, it is obvious that acids can be introduced by a similar design, for the determination of very weak bases, e.g., various amines.

7.2 Future work

7.2.1 Two dimensional conductometric detection (TDCD) with an integrated device

Post-suppressor introduction of hydroxide can lead to dilution and/or band dispersion. In order to compare the two detector outputs, one must correct for dispersion, not a simple task. Any dilution effect also decreases the sensitivity. To eliminate dilution and minimize band dispersion, I envision an integrated device that combines an electrochemical suppressor, the first conductivity detector cell, the micro-electrodialytic hydroxide generator, and the second detector cell into a signal device. This simpler system with fewer components will reduce dispersion and improve resolution. The main obstacle is the current mismatch between the four electrical components. The typical 2 mm suppressor operates in the range of ≤100 mA DC, while both conductivity detectors require AC potentials with μA levels of current and the hydroxide generator will requires a constant DC current at tens of μA levels. The conductivity detectors can be isolated from the rest of the system by operating at unique frequencies that can be tuned into. The solution will become highly resistive after the suppressor. If the connection between this

point and the hydroxide generator is made through a narrow conduit, sufficient electrical isolation will result. The commercial availability of such an integrated device will greatly facilitate the application of dual conductometric detection.

7.2.2 Conductometric detection of very weak acids in ion-exclusion chromatography

As discovered in section 6.3.8, formate co-elutes with silicate on the AG11-AS11 columns. In addition, weak acids like silicate and borate are of interest in seawater but it is difficult to separate these from the overwhelming large chloride peak by conventional anion exchange chromatography. In contrast, ion-exclusion chromatography (ICE) can do this well, since strong acid elute much faster than weak acids in the ion-exclusion mode. Inductively coupled plasma mass spectrometry (ICP-MS) has been coupled ICE for silica determination; a limit of detection (LOD) of 80 nM was attained.[183] However, quartz torches in ICP-MS fundamentally limit the LOD for silicon. I propose ICE for very weak acids with water as eluent. Different ion-exclusion columns will be tested to achieve good separation of different very weak acids. A permeative amine introduction device (PAID), will then convert the weak acids from the acid form to the corresponding ammonium salt ($NR_2H + HA \rightarrow NR_3H^+ + A^-$). As a result, very weak acids HX ($pK_a \geq 7.0$) will be well measured by a conductivity detector following the PAID.

7.2.3 TDCD in cation chromatography

While TDCD in anion chromatography has been explored in a number of papers.[42,43,44,155,170] Similar weak base cation analysis systems have never before been studied. Amines, including aliphatic amines ($pK_b > 3$) and anilines ($pK_b > 8$), have been used extensively in agriculture, food and pharmaceutical industries. The determination of amines by suppressed IC has been attempted,[185] but they respond poorly and nonlinearly. Anilines with $pK_b > 8$ are hardly detected by SCD. It should be straightforward to extend this approach to weakly and very weakly basic cation analysis.

Unlike in the case of base introduction where a strong base that readily permeates through Teflon AF or other nonpolar membranes are not available, because of much greater vapor pressure, numerous strong acids (including HCl) and many moderately strong acids will readily permeate, making the task actually simpler.

7.2.3.1 TDCD in cation chromatography with ICS-5000 IC system

The ICS-5000 IC system can provide a facile method of performing two-dimensional detection of aliphatic amines and anilines in cation chromatography. The proposed experiment will have configuration similar to that in in Figure 4-1b (See Chapter 4.2). Methanesulfonic acid (MSA) will be used as the eluent and an electrodialytic cation suppressor will be used for suppression. MSA to be introduced for the second dimension detection will be generated by a capillary MSA generator and introduced by the back-flow tee mixer. The suppressed eluites in base form B will be converted into the corresponding ionized salt ($B + CH_3SO_3^- + H^+ \rightarrow CH_3SO_3^- + BH^+$). The resulting negative signal from the large difference in mobility between H^+ and BH^+ (this difference is even larger, typically about twice, than the corresponding difference between OH^- and a typical anion X^-) will allow weak and very weak bases ($pKb \geq 7$) to be sensitively measured at the second detector. The commercial ICS-5000 IC system can be used in this dual conductometric detection to improve detectability of aliphatic amines and anilines, with minor modifications.

7.2.3.2 Permeative acid introduction device for weak base detection in cation chromatography

As mentioned in chapter 6.4, the PAID, in this case meaning permeative *Acid* Introduction Device, can be used as a volatile acid introduction device. The design will be the same as the PAID in Figure 6-2, but with an acid external solution. A high concentration of HCl solution can be an ideal acid source. Although ionized species, both

H^+ and Cl^-, cannot be permeatively introduced, a unionized molecule HCl can. Unlike diethylamine, HCl will be fully ionized in the suppressed eluent stream. The PAID is placed after a MSA eluent based suppressed conductometric cation chromatography system. The PAID converts the suppressed eluites from the base form B to the corresponding chloride salt ($B + H^+ + Cl^- \rightarrow BH^+ + Cl^-$) and allows weak and very weak bases to be measured by a second detector. In short, PAID can be used for the sensitivity determination of weak and very weak bases like aliphatic amines and anilines, respectively.

Appendix A

Supporting Information for Chapter 4

A.1 Theoretical Considerations on Two-dimensional Detection

Consider when an eluite HX appears in the first detector (D1), the D1 signal G_{1sm} μS/cm is given by

$$G_1 = 1000C'(\lambda_{H+} + \lambda_{X-}) \quad \ldots(A1a)$$

Where λH^+ and λX^- are the equivalent conductance of H^+ and X^- (we assume a typical value of λX^-, 60 S*cm^2/eq) and C' is given by

$$C' = 0.5(-K_a + (K_a^2+4K_aC)^{1/2}) \quad \ldots(A1b)$$

K_a being the dissociation constant of acid HX. For strong acids, K_a is very large and eq A1a reduces to

$$G_1 = 1000C(\lambda_{H+} + \lambda_{X-}) \quad \ldots(A1c)$$

The second detector background G_{2bgnd}, is dependent on the base concentration coming from the capillary channel, and the flow rates of both channels:

$$G_{2bgnd} = 1000C_{CE}(F_c/(F_p+F_c))(\lambda_{M+} + \lambda_{OH-}) \quad \ldots(A2)$$

Where C_{CE} and F_c is the base concentration and flow rate of the capillary channel, and F_p is the principal or eluent flow rate, λ_{M+} and λ_{OH-} are the equivalent conductances of M^+ and OH^-, the constituent ions of generated MOH.

If we assume that that the final MOH concentration is 1 mM and the chromatographic process results in 10X dilution of an analyte by the time it reaches the detector, for strong acids to weak acids with pK_a <8, neutralization of eluite HX by the background MOH will be complete for injected analyte concentrations <0.5 mM). The D2 signal G_2, can be given by

$$G_2 = 1000C(\lambda OH^- - \lambda X^-) \quad \ldots(A3)$$

G_2 is thus directly proportional to [HX] injected up to this pK_a. The ratio R of the two detector signals is given by

$R = G_1/G_2 = C'(\lambda H^+ + \lambda X^-)/ C(\lambda OH^- - \lambda X^-)$ …(A4)

Incorporating eq A1b into eq A4 gives

$R = 0.5(-K_a + (K_a^2+4K_aC)^{1/2})((\lambda H^+ + \lambda X^-)/(\lambda OH^- - \lambda X^-))/C$ …(5)

For any given acid HX, the ratio of $(\lambda H^+ + \lambda A^-)/(\lambda OH^- - \lambda A^-)$ is constant. For a given pK_a, we can calculate the analyte concentration where $G_1 = G_2$, this can be considered the turnover point at which the second dimension detection becomes more attractive. In Figure A1 we show the results for such calculations for the transition range of pK_a values from pK_a 5.0, to 6.0 to 7.0, the turnover point equals concentrations of 68.5 μM, 5.1 μM, and 0.8 μM, respectively. The noise being higher in the second dimension, the actual turnover point concentrations will be somewhat higher when S/N is considered but still the advantage for very weak acids is obvious. In addition, the response in the second dimension is linear with concentration as indicated by eq A3, the same cannot be said for G_1 vs C for weak acids.

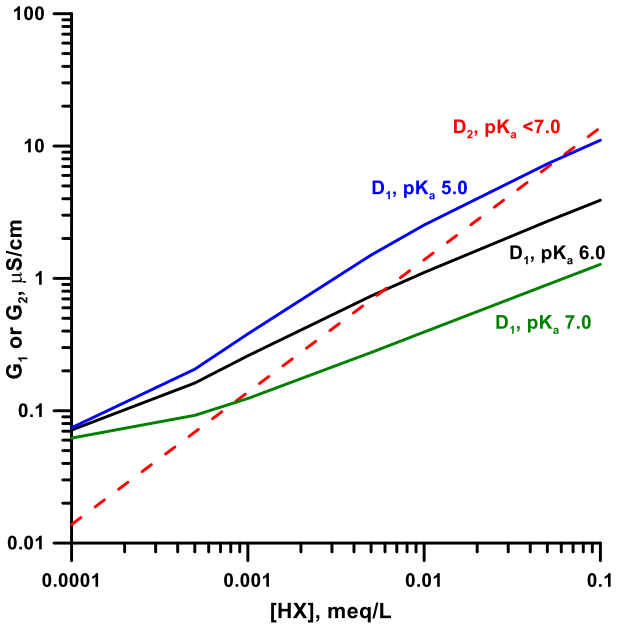

Figure A-1 Theoretical simulation of D1 and D2 signals as a function of concentration of eluite HX at the detector.

A slightly different perspective is to look at the two detector signals at a fixed analyte concentration as a function of pK_a. This is depicted in Figure A2. For a strong acid, G1 ~ 3G2; but G2 hardly changes up to a pKa of 8 and at this pKa, $G_2 \sim 35G_1$. With analytes of pK_a >8.0, the pH provided by the introduction of 100 µM OH^- is not enough to achieve full ionization. With an analyte of pK_a of 10.0, G_2 is 38% of G_2 for analytes with pK_a < 7.0, but it is >400 G_1. For all practical purposes analytes of pK_a >7 are not detectable by D1.

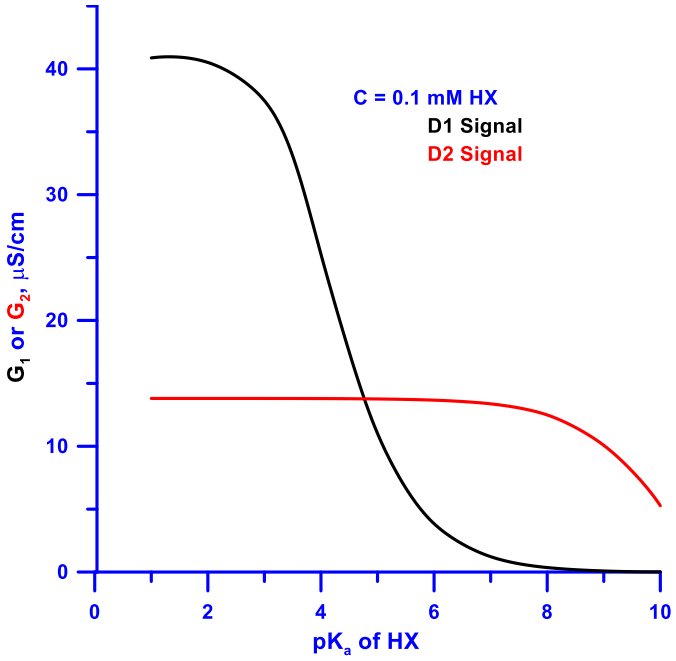

Figure A-2. Simulation of G_1 and G_2 at a constant C of 0.1 mM HX as a function of pK_a of HX.

A.2 Comparison of LiOH vs. KOH Introduced as Base

The performances of a LiOH capillary eluent generator (CEG) and a KOH CEG were investigated. Because the generated concentrations are very low, Donnan forbidden leakage over which the applied current has no effect, affects the generated concentrations at these low levels. As this leakage is approximately related to the square of feed electrolyte concentration (Dasgupta, P. K.; Bligh, R. Q.; Lee, J.; D'Agostino V. Anal. Chem. 1985, 57, 253-257. doi:10.1021/ac00279a058), we also tested a specially made KOH CEG in which the cartridge contained 1/4th the standard KOH concentration. 4.0 mM KOH eluent flow rate was 300 µL/min and capillary flow rate was 100 µL/min. CEG primary concentration was varied from 0.4 – 8.0 mM KOH or LiOH. Figure A3 shows the relative noise levels as a function of the introduced concentration for both the standard LiOH and KOH CEGs and the lower feed concentration KOH CEG. The

headroom (the maximum concentration of analyte that the background can neutralize) is dependent on the background concentration of the base while the noise is related to the background conductance of the base. As the equivalent conductance of LiOH (237.3) is significantly less than that of KOH (272.1), the noise at equivalent concentration was also less for LiOH. The difference of between the KOH and diluted KOH cartridge was statistically insignificant.

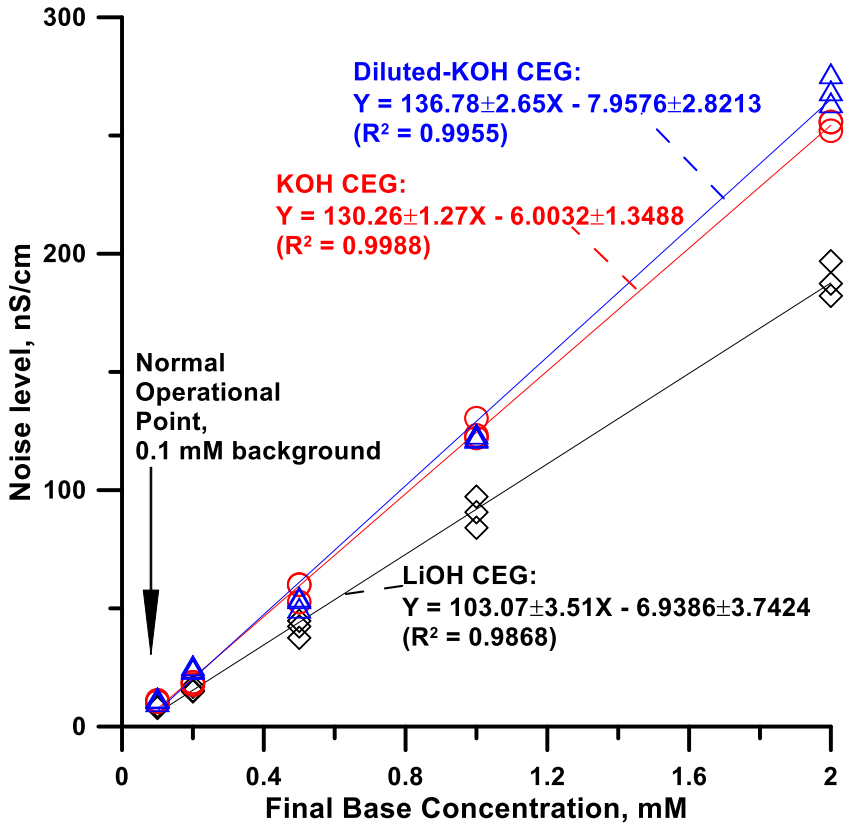

Figure A-3 Noise level under different concentration of KOH or LiOH CEG.

Appendix B

Supporting Information for Chapter 5

B.1 Experimental configuration

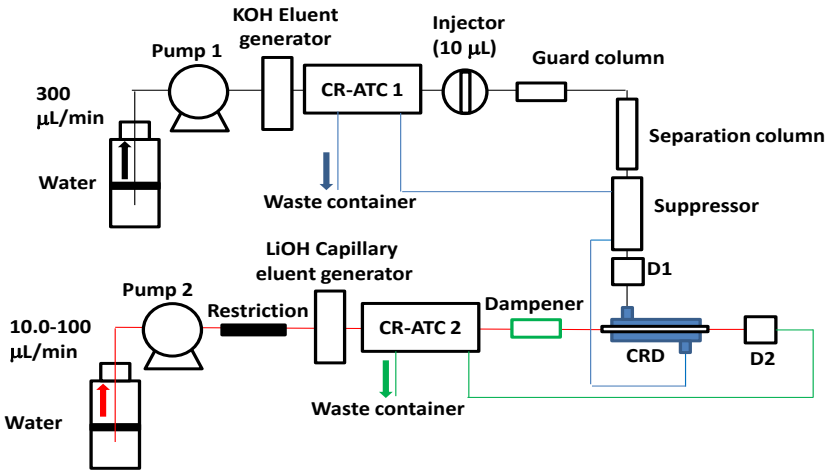

Figure B-1 Detailed experimental configuration.

A restriction capillary (25 µm i.d.; 6.0-25.0 cm long depending on flow rate (100-10 µL/min)) is used before the capillary LiOH generator to provide some backpressure to Pump 2 for proper operation. To reduce pump pulsations, a PEEK tubing (0.76x600 mm) is added after the capillary scale continuously regenerated anion trap column (CR-ATC2). The similar macroscale device is labeled CR-ATC1.

B.2. Comparison between electrical and chemical suppression of sulfide loss

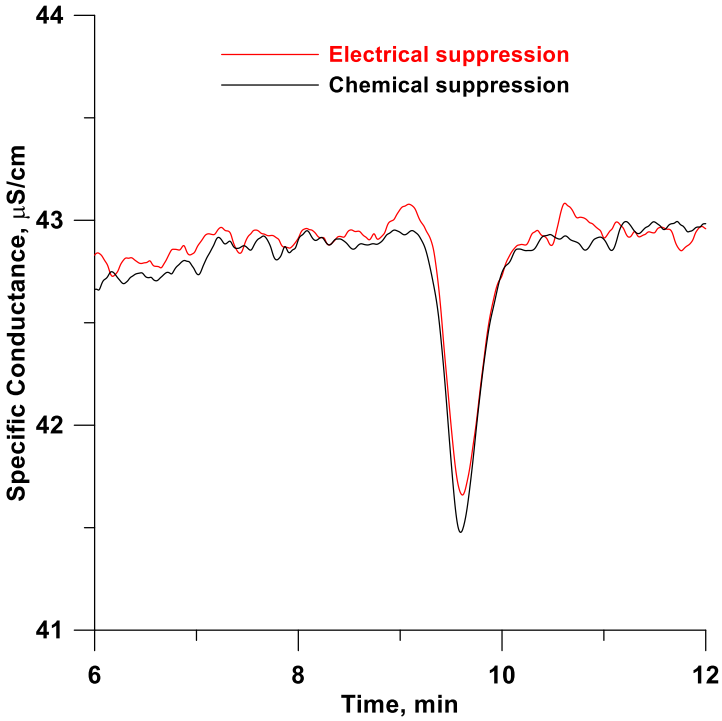

Figure B-2 Loss of sulfide due to redox reaction in electrodialytic membrane suppressor.

Chromatographic response to 0.50 mM sulfide using VATD-5 device. KOH eluent isocratic concentration, 5.0 mM; receptor 0.2 mM LiOH @ 10 μL/min. The black and red traces were obtained with power to the suppressor turned on and off.

The electrodialytic membrane suppressor was utilized for the experiment in Figure B-2. The static suppression capacity of this suppressor is ~50 μeq. After turning off power (chemical suppression), full suppression can be maintained for >15 min, longer than the duration of a single chromatographic run (12 min). It is clear that application of potential causes loss of sulfide, presumably due to oxidation. Interestingly, this oxidation requires both applied potential and dissolved oxygen, no difference between chemical and electrical suppression cases were seen if the water used for the preparation of the electrodialytic eluent was freshly deoxygenated and then protected with a hydrochlorofluocarbon blanket (1,1 Difluoroethane, electronics duster can).

B.3 First Principles Approach to Estimating Transfer Efficiencies

Numerical solutions to equations involving heat transfer in an annulus where only the inner surface is a sink are available[186] and have been applied in analogous annular membrane gas collection devices.[187] An Excel-based calculator is also available.[188] The fractional transfer efficiency *f* can be computed as a function of the dimensionless axial parameter $\bar{x}$ where

$$\bar{x} = \pi DL(d_o + d_i)/(Q(d_o - d_i)) \quad \ldots(B1)$$

with D, L, Q, d_o, and d_i being respectively the diffusion coefficient of the analyte, active length of the device, donor flow rate, outer and inner diameters of the annulus, respectively. These calculations provide an upper limit to the transport as the implicit assumption is that the inner surface is a perfect sink. Using d_o, d_i, and Q being 0.033 cm, 0.025 cm, and 0.005 cm^3/s, respectively, and 2 x 10^{-5} cm^2/s for D (value for dissolved O_2 at room temperature, a comparably sized molecule), one calculates a theoretical maximum removal efficiency of 65% and 99% for L = 5, and 24 cm, respectively (See Figure B3). The transmembrane transfer rate can be the limiting process that results in the perfect sink criterion not being met. The intrinsic time constant for the transfer process does not appear to be a limiting factor (<1 s, the difference in the rise time of a signal upon injection of a solution of KCN in the outer channel of the VATD and that of an

Length (cm)	R inner (cm)	R outer (cm)	Vol Flow (cm	Flow Units	Flow Rate	D (cm^2/s)	BC (A, B, C)	BC (1,2,3)
24	0.0125	0.0165	0.005	cm^3/s	0.005	2.00E-05	B	2

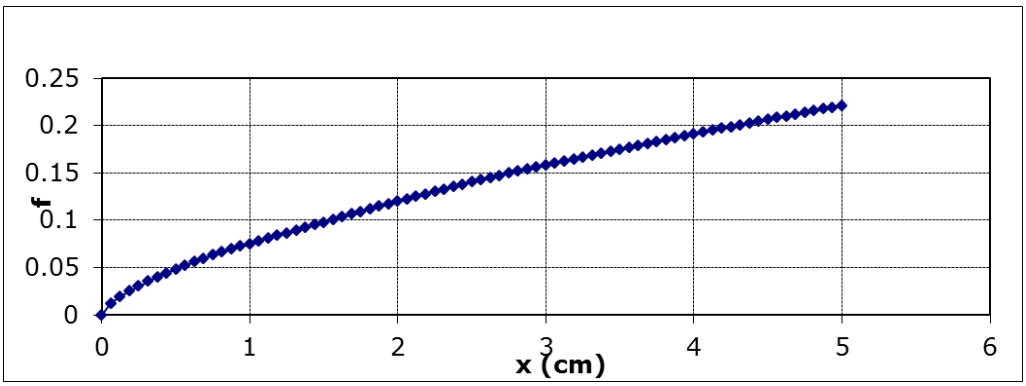

Full Length			Full Length			Full Length	
x (cm)	f		x (cm)	f		x (cm)	f
0	0.000		8.1	0.813		16.2	0.961
0.3	0.110		8.4	0.824		16.5	0.963
0.6	0.177		8.7	0.834		16.8	0.965
0.9	0.231		9	0.843		17.1	0.967
1.2	0.278		9.3	0.852		17.4	0.969
1.5	0.321		9.6	0.861		17.7	0.971
1.8	0.361		9.9	0.868		18	0.972
2.1	0.399		10.2	0.876		18.3	0.974
2.4	0.432		10.5	0.883		18.6	0.975
2.7	0.463		10.8	0.890		18.9	0.977
3	0.492		11.1	0.896		19.2	0.978
3.3	0.520		11.4	0.902		19.5	0.979
3.6	0.547		11.7	0.907		19.8	0.980
3.9	0.573		12	0.912		20.1	0.981
4.2	0.597		12.3	0.917		20.4	0.982
4.5	0.620		12.6	0.922		20.7	0.983
4.8	0.642		12.9	0.926		21	0.984
5.1	0.663		13.2	0.931		21.3	0.985
5.4	0.682		13.5	0.934		21.6	0.986
5.7	0.700		13.8	0.938		21.9	0.987
6	0.718		14.1	0.942		22.2	0.987
6.3	0.734		14.4	0.945		22.5	0.988
6.6	0.749		14.7	0.948		22.8	0.989
6.9	0.763		15	0.951		23.1	0.989
7.2	0.777		15.3	0.954		23.4	0.990
7.5	0.790		15.6	0.956		23.7	0.991
7.8	0.802		15.9	0.959		24	0.991

Figure B-3 Excel Calculator output for d_o = 0.033 cm, d_i = 0.025 cm, Q = 0.005 cm^3/s and D = 2 x 10^{-5} cm^2/s.

electrolyte injected into the lumen of the VATD with a water carrier could not be statistically distinguished). This is particularly true as the total transit time of the eluite band through the VATD is large (100-120 s). But an insufficient concentration gradient across the membrane can limit the transport. We propose that this can be partially simulated by assuming the collection surface is smaller than the actual value. Values of di of 8.6×10^{-3} and 2.8×10^{-3} cm, for example reasonably match the observed transfer efficiencies for H_2S and HCN for L = 24 and 5 cm, respectively, predicting 56 and 18.5, and 32 and 9% collection efficiencies.

B.4 Mass transfer efficiency calculation

B.4.1 Mass transfer efficiency of sulfide

For 50 μM sulfide with 10 μL injection volume, the theoretical peak area will be equal to

S_{H2S} = 0.05 mM x 10 μL x (198-65) μS/cm* mM-1 = 66.5 μS/cm* μL

For VATD-5, the actual peak area is

S_{VATD-5} = 0.234 μS/cm*min x 40 μL/min = 9.36 μS/cm* μL

For VATD-24, the actual the peak area is

$S_{VATD-24}$ = 0.731 μS/cm*min x 40 μL/min = 29.24 μS/cm* μL

H2S is fully ionized in 0.2 mM LiOH flow with pH 10.3. The mass loss of 50 μM sulfide caused by the membrane suppressor was seen to be about 24%.

The mass transfer efficiency of VATD-5 will be: = 9.36/(66.5*(1-0.24)) x 100% = 18.5%.

The mass transfer efficiency of VATD-24 will be: = 29.24 x 100%/(66.5*(1-0.24)) = 57.9%

B.4.2 Mass transfer efficiency of cyanide

The HCN (pKa 9.3) is 90% ionized in 0.2 mM LiOH (pH 10.3). For 50 μM cyanide with 10 μL injection volume, the theoretical peak area is:

SHCN = 0.05 mM x 10 μL x (198-78)*90% μS/cm* mM-1 = 54.0 μS/cm* μL

For VATD-5, the actual peak area is

S_{VATD-5} = 0.088 μS/cm*min x 40 μL/min = 3.52 μS/cm* μL

For VATD-24, the real peak area is

$S_{VATD-24}$ = 0.391 μS/cm*min x 40 μL/min = 15.64 μS/cm* μL

The mass loss of cyanide caused by the membrane suppressor was about ~12%.

The mass transfer efficiency of VATD-5 will be: = 3.52 x 100%/(54.0*(1-0.12)) = 7.4%.

The mass transfer efficiency of VATD-24 will be: = 15.64 x 100%/(54.0*(1-.12)) = 32.9%.

B.5 Excel simulation of acid gas transfer in the VATD illustrated with HCN

Imagine that Figure B-4 below depicts the concentration profile of HCN at the VATD inlet:

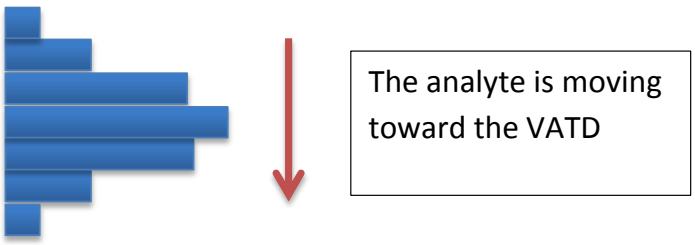

Figure B-4 Input concentration of HCN at the VATD inlet.

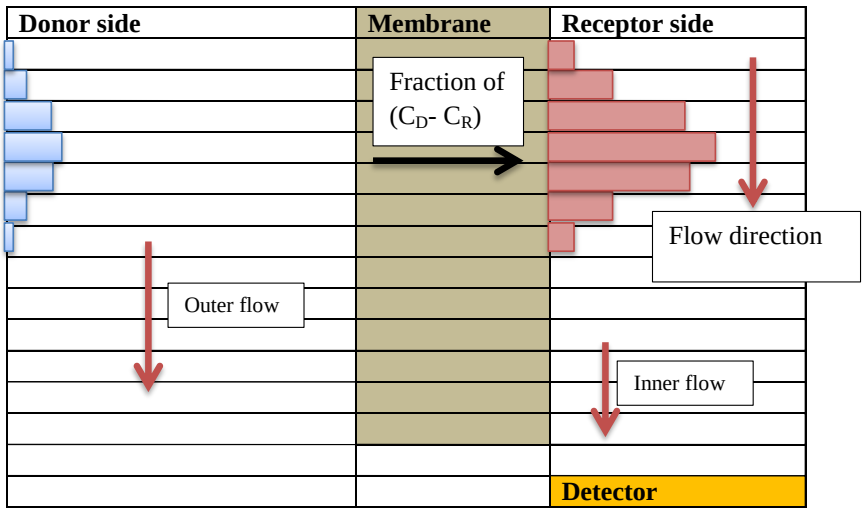

Figure B-5 Schematic Depiction of the transfer process simulated.

Upon reaching the membrane, some fixed fraction of the HCN on the donor side, proportional to the concentration gradient across the membrane, goes from the donor side to the receptor side. Once HCN reaches the receptor side, reaction with hydroxide forms CN^- (the exact fraction still remaining undissociated depends on the assumed pK_a of HCN and the LiOH concentration). The CN^- then moves toward the detector but at a flow rate different from that of the donor side, usually lower.

In the simulation, we start out with input concentration profiles of HCN and H_2S before they reach the membrane. The concentration profiles (segregated in plates of 0.146 μL) are assumed to be perfectly Gaussian, the lower bounds are 0.001 % of the peak height. The total number of moles ($500*10^{-12}$ moles) is equal to the assumed initial 10 μL of the 50 μM standards injected into the system. For the VATD-24, the calculated outer volume and inner volume of the membrane are respectively 8.75 μL and 7.53 μL.

For simulation purposes, we assumed the membrane to be composed of 60 plates (1 plate =0.145 μL on the donor side and 1 plate =0.125 μL on the receptor side) and one iteration is equal to a time step of 0.0251 min. These values can be freely

changed to accommodate the user need. The experimental flow rates are translated in our simulation flow rate as in the table below.

Table B-1 Experimental flow rates and simulation flow rates

Side	Experimental Flow Rates (μL/min)	Simulation Flow Rates (plates / iterations)
Donor	300	51*
Receptor	100	20*
Receptor	60	12*
Receptor	40	8*
Receptor	20	4*
Receptor	10	2*

* These values were calculated based on 1 iteration= 0.0251 min; 1 plate =0.145 μL for donor side; 1 plate =0.125 μL for receptor side.

B.6 Summary of Simulation actions in the Excel sheet

In the following, we will detail the steps of the simulation along with the explanation of the Macros.

The first Macro that simulates the transfer is activated by pressing “Ctrl+q” while the second Macro resets all of the previous actions; this is activated by pressing “Ctrl+m”.

Column E and F contain the concentration profile of HCN and H_2S before their movement toward the membrane. The Macro starts by assigning letters to the cells values in column B in order to make the programing simpler.

```
m = Cells(12, 2).Value '# iterations'
n = Cells(13, 2).Value '# of plates'
o = Cells(14, 2).Value 'outer flow rate'
p = Cells(15, 2).Value 'inner flow rate'
```

This allows the user to freely change variable such as the number of iterations, number of plates, number of iterations/plate on the donor side and number of iteration/plate on the receptor side; all of these values are located in column B.

The concentration profiles are moved down the donor side of the membrane located in column I and K respectively for HCN and H_2S. Below is the Macro action responsible for the movement.

```
For b = 1 To o
    Cells(3 + o - b, 9).Value = Cells(i + 1 + b + c, 5).Value
    Cells(3 + o - b, 11).Value = Cells(i + 1 + b + c, 6).Value
Next b
c = c + o - 1
```

Which means that if the outer (or donor) flow rate is of 3 plates/ iteration; Cell E3-value, Cell E4-value and Cell E5-value will respectively move into Cell I5, Cell I4, Cell I3. The component “c” is added so that on the next iteration (next i value), the next cells are moved. Same is done for the values moving from the F to the K column.

The concentration profiles in column E and F are only taking in account the total concentration of the species. So once the total species get into column I and K, they dissociate according to the K_a-dependent dissociation equilibria: the values of HCN, CN^-, HS- and H_2S are written into columns L, M, N, and O, respectively. Columns P through S contains the concentration of the corresponding species on the receptor side. Columns T and U contain the amount to be transferred at each plate based on the concentration gradient across the membrane. For example the amount to be transferred at plate3 for HCN is L3-P3 times the user-set transfer coefficient in cell B8 (the user-set transfer coefficient of H_2S appears in cell B9. In column V through Y, the readjusted concentration of the analytes (since the plate volumes are not equal on both sides) are computed.

Once the analytes cross the membrane, the change in pH from the presence of LiOH causes dissociation. For H_2S, we assume no undissociated H_2S remains, the pK_a1

is 4 orders of magnitude smaller than the prevailing pH. For HCN, ~91% of the total cyanide ionizes in 0.2 mM LiOH.

The next set of columns are used for capturing the effects of motion. For example, Column AN to AQ are first cleared, then the values in column AJ and AQ are copied into column AN and AP but shifted down. The amount of rows shifted is dependent on the flow rate used. The shifted values are then copied back into column H and J.

```
Range("AN3:AQ1002").Value = 0
Range("AZ3:BC1002").Value = 0
Range(Cells(3 + p, 52), Cells(1002 + p, 52)).Value = Range(Cells(3, 44), Cells(1002, 44)).Value
Range(Cells(3 + p, 53), Cells(1002 + p, 53)).Value = Range(Cells(3, 46), Cells(1002, 46)).Value
Range(Cells(3 + p, 54), Cells(1002 + p, 54)).Value = Range(Cells(3, 48), Cells(1002, 48)).Value
Range(Cells(3 + p, 55), Cells(1002 + p, 55)).Value = Range(Cells(3, 50), Cells(1002, 50)).Value
Range(Cells(3 + o, 40), Cells(1002 + o, 40)).Value = Range(Cells(3, 36), Cells(1002, 36)).Value
Range(Cells(3 + o, 42), Cells(1002 + o, 42)).Value = Range(Cells(3, 38), Cells(1002, 38)).Value
Range("H3:K1002").Value = Range("AN3:AQ1002").Value
Range("P3:S1002").Value = Range("AZ3:BC1002").Value
```

Note that in the macro, columns can also be referred to either in the number or in the letter format.

Lastly, once the analytes exit the VATD they enter the detector. It is possible to assume that there is no delay or dispersion in this step. A more realistic scenario invokes a finite volume represented by a number of discrete volume elements and that longitudinal diffusive broadening can occur during this passage. The Excel file in the SI has an extra “p” variable to incorporate the experimental connecting tubing volume of 51 μL that was divided into 406 discrete volume elements. To simulate diffusive broadening, a user-defined fixed fraction (cell B10 for HCN, B11 for H_2S) of the concentration difference between two consecutive volume elements are transferred into the preceding and following volume elements). We will take the example of CN^- concentration in cell AC4. The concentration in AC4 will diffuse into its neighboring cells AC3 and AC5, based on the concentration gradient across the cells. The diffusive transfer coefficient in cell B10 and B11 was taken to be equal to 0.2, then the amount that will be subtracted from

AC4; AU4 (located in column AU) will be 0.2*(AC4-AC5) +0.2*(AC4-AC3). The result may be either positive of negative. Then the final CN^- concentration in cell AT4 = AC4- AU4. The same is done for all of the other species.

Finally, for each iteration, the value in the cell representing the detector is stored in column BH and BI for HCN and H_2S respectively. The values in column BH and BI correspond to the detector signal.

```
    Cells(i, 60).Value = Cells(3 + n, 53).Value
    Cells(i, 61).Value = Cells(3 + n, 55).Value

Next i
End Sub
```

The basis is the same for counter current flow.

Appendix C

Publication Information of Chapters

The chapter 2 has been reprinted with permission from H. Liao, C.P. Shelor, Y. Chen, A.U.O. Sabaa-Srur, R.E. Smith, P.K. Dasgupta. Journal of Agricultural and Food Chemistry. 61 (25) 2013, pp 5928-5935. Copyright 2013 American Chemical Society

The chapter 3 has been reprinted with permission from C. P. Shelor, H. Liao, A. F. Kadjo, P. K. Dasgupta. Analytical chemistry. 87 (9) 2015, pp 4851-4855. Copyright 2015 American Chemical Society

The chapter 4 has been reprinted with permission from H. Liao, P.K. Dasgupta, K. Srinivasan, Y. Liu. Analytical Chemistry. 87 (1) 2015, pp 793-800. Copyright 2015 American Chemical Society

The chapter 5 has been reprinted with permission from H. Liao, A. F. Kadjo, P. K. Dasgupta. Analytical chemistry. 87 (16) 2015, pp 8342-8346. Copyright 2015 American Chemical Society

The chapter 6 has been reprinted with permission from H. Liao, P. K. Dasgupta. Analytical Chemistry. Xxx. Future copyright 2015 American Chemical Society. (Still in reviewing process)

Besides, the contents of Chapter 1.4 about research presented in this dissertation were copied from the abstracts of above five articles.

References

[1] Vanatta, L. E. TrAC Trends. Anal. Chem. 2001, 20, 336-345.

[2] Michalski, R. Mini-Rev. Med. Chem. 2014, 14, 862-872.

[3] Haddad, P. R.; Jackson, P. E. Ion Chromatography: Principles and applications; Elsevier: NewYork, 1990.

[4] Fritz, J. S.; Gjerde, D. T. Ion Chromatography; Wiley-VCH: Weinheim, 4th ed., 2009.

[5] Clarke, A. P.; Jandik, P.; Rocklin, R. D.; Liu, Y.; Avdalovic, N. Anal. Chem. 1999, 71, 2774-2781.

[6] Yu, H.; Ding, Y.; Mou, S.; Jandik, P. Cheng, J. J. Chromatogr. A 2002, 966, 89-97.

[7] Ding, Y.; Yu, H.; Mou, S. J. Chromatogr. A 2002, 982, 237-244.

[8] Small, H.; Stevens, T. S.; Bauman, W. C. Anal. Chem. 1975, 47, 1801-1809.

[9] Gjerde, D. T.; Fritz, J. S.; Schmuckler, G.; J. Chromatogr. A 1979, 186, 509-519.

[10] Rocklin, R. D.; Johnson, E. L. Anal. Chem. 1983, 55, 4-7.

[11] Han, K.; Koch, W. F. Anal. Chem. 1987, 59, 1016-1020.

[12] Willians, R. J. Anal. Chem. 1983, 55, 851-854.

[13] Small, H.; Miller Jr., T. E.; Anal. Chem. 1982, 54, 462-469.

[14] Dasgupta, P. K. J. Chromatogr. Sci. 1989, 27, 422-448.

[15] Spackman, D. H.; Stein, W. H.; Moore, S. Anal. Chem. 1958, 30, 1190-1206.

[16] Christian, G. D.; Dasgupta, P. K.; Schug, K. Analytical chemistry; Wiley, 7th ed., 2014.

[17] Haddad, P. R.; Jackson, P. E.; Shaw, M. J. J. Chromatogr. A 2003, 1000, 725-742.

[18] Stevens, T. S.; Davis, J. C.; Small, H. Anal. Chem. 1981, 53, 1488-1492.

[19] Stevens, T. S.; Jewett, G. L.; Bredeweg, R. A. Anal. Chem. 1982, 54, 1206-1208.

[20] Dasgupta, P. K. Anal. Chem. 1984, 56, 103-105.

[21] Dasgupta, P. K. Anal. Chem. 1984, 56, 769-772.

[22] Dasgupra, P. K.; Bligh, R. Q.; Mercurio, M. A. 1985, 57, 484-489.

[23] Stillian, S. LC 1985, 3, 802-812.

[24] Pohl, C.; Slingsby, R. W.; Stillian, J. R.; Gajek, R. Modified Membrane Suppressor and Method For Use, US Patent 4,999,098; 1991.

[25] Tian, Z. W.; Hu, R. Z.; Lin, H. S.; Wu, J. T. J. Chromatogr. 1988, 439, 159-163.

[26] Strong, D. L.; Dasgupta, P. K. Anal. Chem. 1989, 61, 939-945.

[27] Rabin, S.; Stillian, J.; Barreto, V.; Friedman, K.; Toofan, M. J. Chromatogr. 1993, 640, 97-109.

[28] Srinivasan, K.; Pohl, CA.; Method and Apparatus for Gas-Assisted Suppressed Chromatography, US Patent 6,425,284; 2002.

[29] Advances in Chemical Suppression. http://www.dionex.com/en-us/webdocs/61381-Bro-SuppressorHistory-22Dec08-LPN1855-01.pdf (accessed Sep 20, 2015).

[30] Small, H.; Liu, Y.; Riviello, J.; Avdalovic, N.; Srinivasan, K. Continuous Electrolytically Regenerated Packed Bed Suppressor for Ion Chromatograph, US Patent 6,325,976; 2001.

[31] Thermo Scientific Dionex ERS 500 suppressor Manual. http://www.dionex.com/en-us/webdocs/114530-BR-ERS-500-Suppressor-BR70662_E.pdf (accessed Sep 20, 2015).

[32] Suppression in ion chromatography Manual. http://www.metrohm.com/en/company/news/news-suppression-in-ic (accessed Sep 20, 2015).

[33] Small, H.; Riviello, J. Anal. Chem. 1998, 70, 2205-2212.

[34] Karu, N.; Dicinoski, G.; Haddad, P. R. TrAC, Trends Anal. Chem. 2012, 40, 119–132.

[35] Tanaka, K.; Fritz, J. S. Anal. Chem. 1987, 59, 708-712.

[36] Berglund, I.; Dasgupta, P. K. Anal. Chem. 1991, 63, 2175-2183.

[37] Berglund, I.; Dasgupta, P. K. Anal. Chem. 1992, 64, 3007-3012.

[38] Caliamanis, A.; McCormick, M. J.; Carpenter, P. D. Anal. Chem. 1997, 69, 3272-3276.

[39] Caliamanis, A.; McCormick, M. J.; Carpenter, P. D. Anal. Chem. 1999, 71, 741-746.

[40] Zhu, Y.; Wang, S.; Liu, W. P. LC-GC N. Am. 2000, 18, 200-204.

[41] Huang, Y.; Mou, S.; Liu, K. J. Chromatogr. A 1999, 832, 141-148.

[42] Berglund, I.; Dasgupta, P. K.; Lopez, J. L.; Nara, O. Anal. Chem. 1993, 65, 1192-1198.

[43] Sjogren, A.; Dasgupta, P. K.; Anal. Chem. 1995, 67, 2110-2118.

[44] Sjogren, A.; Dasgupta, P. K.; Anal. Chim. Acta 1999, 384, 135-141.

[45] Schauss, A. G. Biosocial Publications: Tacoma, WA, 2006.

[46] Seeram, N. P.; Aviram, M.; Zhang, Y.; Henning, S. M.; Feng, L.; Dreher, M.; Heber, D. J. Agric. Food Chem. 2008, 56, 1415 −1422.

[47] Rodrigues, R. B.; Lichtenthaler, R.; Zimmermann, B. F.; Papagiannopoulos, M.; Fabricius, H.; Marx, F.; Maia, J. G.; Almeida, O. J. Agric.Food Chem. 2006, 54, 4162 −4167.

[48] Hassimotto, N. M.; Genovese, M. I.; Lajolo, F. J. Agric. Food Chem. 2005, 53, 2928 −2935.

[49] Matheus, M. E.; de Oliveira Fernandes, S. B.; Silveira, C. S.; Rodrigues, V. P.; de Sousa Menezes, F.; Fernandes, P. D. J. Ethnopharmacol. 2006, 107, 291 −296.

[50] Schauss, A. G.; Wu, X.; Prior, R. L.; Ou, B.; Patel, D.; Huang, D.; Kababick, J. P. J. Agric. Food Chem. 2006, 54, 8604 −8610.

[51] Noratto, G. D.; Angel-Morales, G.; Talcott, S. T.; MertensTalcott, S. U. J. Agric. Food Chem. 2011, 59, 7999 −8012.

[52] Del Pozo-Insfran, D.; Percival, S. S.; Talcott, S. T. J. Agric. Food Chem. 2006, 54, 1222 −1229.

[53] Smith, R. E.; Eaker, J.; Tran, K.; Goerger, M.; Wycoff, W.; SabaaSrur, A. U. O.; Menezes, E. M. S. Nat. Prod. J. 2012, 2, 95 −98.

[54] Zhang, Y.; Krueger, D.; Durst, R.; Lee, R.; Wang, D.; Seeram, N.; Heber, D. J. Agric. Food Chem. 2009, 57, 2550 −2557.

[55] Smith, J. http://www.aprovenproduct.com/acailand.php (accessed May 6, 2012).

[56] Hamilton Media LLC. http://www.scribd.com/doc/51511856/The-Acai-Berry-Scam (accessed Dec 25, 2012).

[57] Madden, J. E.; Shaw, M. J.; Dicinoski, G. W.; Avdalovic, N.; Haddad, P. R. Anal. Chem. 2002, 74, 6023 −6030.

[58] Mato, I.; Suarez-Luque, S.; Huidobro, J. F. Food Res. Int. 2005, 38, 1175 −1188.

[59] Widodo, S. E.; Shiraishi, M.; Shiraishi, S. J.Fac. Agric. Kyushu Univ. 1995, 40, 39 −44.

[60] Shiraishi, S. C.; Kawakami, K.; Widodo, S. E.; Shiraishi, M.; Kitazaki, M. J. Fac. Agric. Kyushu Univ. 1996, 41, 29 −33.

[61] Barden, T. J.; Croft, M. Y.; Murby, E. J.; Wells, R. J. J. Chromatogr., A 1997, 785, 251 −261.

[62] Jurado-Sanchez, B.; Ballesteros, E.; Gallego, M. Talanta 2011, 84, 924 −930.

[63] Irudayaraj, J.; Tewari, J. Appl. Spectrosc. 2003, 57, 1599 −1604.

[64] Bureau, S.; Ruiz, D.; Reich, M.; Gouble, B.; Bertrand, D.;Audergon, J. M.; Renard, C. M. G. C. Food Chem. 2009, 115, 1133 −1140.

[65] Loredana, L.; Diehl, H.; Socaciu, C. Bull. Univ. Agric. Sci. Vet. Med. 2006, 62, 288 −292.

[66] Santalad, A.; Teerapornchaisit, P.; Burakham, R.; Srijaranai, S. LWT−Food Sci. Technol. 2007, 40, 1741 −1746.

[67] Nutku, M. S.; Erim, F. B. J. Microcol. Sep. 1999, 11, 541 −543.

[68] Tezcan, F.; Gultekin-Ozguven, M.; Diken, T.; Ozcelik, B.; Erim, F. B. Food Chem. 2009, 115,873 −877.

[69] Camara, M. M.; Diez, C.; Torija, M. E.; Cano, M. P. Z. Lebensm. Unters. Forsch. 1994, 198, 52 −56.

[70] Grosheny, B.; Isengard, H. D.; Philipp, O. Dtsch. Lebensm. Rundsch. 1995, 91, 137 −140.

[71] Huopalahti, R.; Jarvenpa a, E.; Katina, K. A J. Liq. Chromatogr. Relat. Technol. 2000, 23, 2695 −2701

[72] Koyuncu, F. Chem. Nat. Compd. 2004, 40, 367 −369.

[73] Raffo, A.; Paoletti, F.; Antonelli, M. Eur. Food Res. Technol. 2004, 219, 360 −368.

[74] Gao, H. Y.; Liao, X. J.; Wang, S. G.; Hu, X. S. Chin. J. Anal. Chem. 2004, 32, 1645 −1648.

[75] Marconi, O.; Floridi, S.; Montanari, L. J. Food Qual. 2007, 30, 253 −266.

[76] Cunha, S. C.; Fernandes, J. O.; Ferreira, I. M. Eur. Food Res. Technol. 2002, 214, 67 −71.

[77] Nour, V.; Trandafir, I.; Ionica, M. E. Fruits 2011, 66, 353 −362.

[78] Chinnici, F.; Spinabelli, U.; Riponi, C.; Amati, A. J. Food Compos. Anal. 2005, 18, 121 −130.

[79] Ergoenuel, P. G.; Nergiz, C. Czech J. Food Sci. 2010, 28, 202 −205.

[80] Lin, J. T.; Liu, S. C.; Shen, Y. C.; Yang, D. J. Food Anal. Methods 2011, 4, 531 −539.

[81] Eyeghe-Bickong, H. A.; Alexandersson, E. O.; Gouws, L. M.; Young, P. R.; Vivier, M. A. J. Chromatogr., B 2012, 885, 43 −49.

[82] Muñoz-Robredo, P.; Robledo, P.; Manríquez, D.; Molina, R.; Defilippi, B. G. Chil. J. Agric. Res. 2011, 71, 452 −458.

[83] Shui, G. H.; Leong, L. P. J. Chromatogr., A 2002, 977, 89 −96.

[84] Veberic, R.; Jakopic, J.; Stampar, F.; Schmitzer, V. Food Chem. 2009, 114, 511 −515.

[85] Hernandez, Y.; Lobo, M. G.; Gonzalez, M. Food Chem. 2009, 114, 734−741.

[86] Silva, B. M.; Andrade, P. B.; Ferreres, F.; Domingues, A. L.;Seabra, R. M.; Ferreira, M. A. J. Agric. Food Chem. 2002, 50, 4615 −4618.

[87] Suarez, M. H.; Rodriguez, E. R.; Romero, C. D. Eur.Food Res. Technol. 2008, 226, 423 −435.

[88] Arslan, D.; Ozcan, M. M. Sci. Hortic. 2011, 130, 633 −641.

[89] Zhang, A.; Fang, Y. L.; Meng, J. F.; Wang, H.; Chen, S. X.; Zhang, Z. W. J. Food Compos. Anal. 2011, 24, 449 −455.

[90] Oatway, L.; Vasanthan, T.; Helm, J. H. Food Rev. Int. 2001, 17, 419 −431.

[91] Schlemmer, U.; Frolich, W.; Prieto, R. M.; Grases, F. Mol. Nutr. Food Res. 2009, 53, S330 −S375.

[92] Kell, D. B. Arch. Toxicol. 2010, 84, 825 −889.

[93] Horwitz, W., Ed. Association of Official Analytical Chemists: Arlington, VA, 2000; pp 57 −58.

[94] Smith, R. E.; Macquarrie, R. A. Anal. Biochem. 1988, 170, 308 −315.

[95] Skoglund, E.; Carlsson, N.-G.; Sandberg, A.-S. J. Agric. Food Chem. 1997, 45, 4668 −4673.

[96] Carlsson, N.-G.; Bergman, E.-L.; Skoglund, E.; Hasselblad, K.; Sandberg, A.-S. J. Agric. Food Chem. 2001, 49, 1695 −1701.

[97] Chen, Q. C.; Li, B. W. J. Chromatogr., A 2003, 1018, 41 −52.

[98] Blaabjerg, K.; Hansen-Moller, J.; Poulsen, H. D. J. Chromatogr., B 2010, 878, 347 −354.

[99] Saccani, G.; Gherardi, S.; Trifiro, A.; Soresi Bordini, C.; Calza, M.; Freddi, C. J. Chromatogr., A 1995, 706, 395 −403.

[100] Kupina, S. A.; Pohl, C. A.; Gannotti, J. L. Am. J. Enol. Vitic. 1991, 42, 1 −5.

[101] Masson, P. J. Chromatogr., A 2000, 881, 387 −394.

[102] Yang, B.; Takeuchi, T.; Dasgupta, P. K.; Umemura, T.; Ueki, Y.; Tsunoda, K.-I. Anal. Chem. 2007, 79, 769 −772.

[103] De Stefano, C.; Milea, D.; Sammartano, S. J. Chem. Eng. Data 2003, 48, 114–119.

[104] Crea, F.; Crea, P.; De Stefano, C.; Milea, D.; Sammartano, S. J. Mol. Liq. 2008, 138, 76–83.

[105] De Stefano, C.; Milea, D.; Pettignano, A.; Sammartano, S. Anal. Bioanal. Chem. 2003, 376, 1030–1040.

[106] Crea, F.; De Stefano, C.; Milea, D.; Sammartano, S. Coord. Chem. Rev. 2008, 252, 1108–1120.

[107] Liao, H.; Shelor, C. P.; Chen, Y.; Sabaa-Srur, A. U. O.; Smith, R. E.; Dasgupta, P. K. J. Agric. Food Chem. 2013, 61, 5928–5935.

[108] Evans, W. J.; McCourtney, E. J.; Shrager, R. I. J. Am. Oil Chem. Soc. 1982, 59, 189–191.

[109] Talamond, P.; Gallon, G.; Treche, S. J. Chromatogr. A 1998, 805, 143–147.

[110] Talamond, P.; Doulbeau, S.; Rochette, I.; Guyot, J. P.; Treche, S. J. Chromatogr. A 2000, 871, 7–12.

[111] Skoglund, E.; Carlsson, N. G.; Sandberg, A. S. J. Agric. Food Chem. 1998, 46, 1877–1882.

[112] Phillippy, B. Q.; Bland, J. M. Anal. Biochem. 1988, 175, 162–166.

[113] Binder, H.; Weber, P. C.; Siess, W. Anal. Biochem. 1985, 148, 220–227.
[114] Mathews, W. R.; Guido, D. M.; Huff, R. M. Anal. Biochem. 1988, 168, 63–70.

[115] Rounds, M. A.; Nielsen, S. S. J. Chromatogr. A 1993, 653, 148–152.

[116] Shelor, C. P.; Liao, H.; Kadjo, A.; Dasgupta, P. K. Ion Chromatographic Retention Behavior of a Sugar Polyphosphate. Presented at the Pittsburgh Conference, Philadelphia, PA, March 17–21, 2013; Abstract 1710-8.

[117] Cosgrove, D. J. Biochem. J. 1963, 89, 172–175.

[118] Small, H.Ion Chromatography; Plenum Press: New York, 1989.

[119] Mo, Y.Investigations in Capillary Liquid Chromatography. M.S. Thesis, Texas Tech University, 1997.

[120] Walsh, S.; Diamond, D. Talanta 1995, 42, 561–572.

[121] Dasgupta, P. K. J. Chromatogr. A 2008, 1213, 50–55.

[122] Caceci, M. S. Anal. Chem. 1989, 61, 2324–2327.

[123] Lamb, J. D.; Smith, R. G. J. Chromatogr. A 1991, 546, 73–88.

[124] Thermo Fisher Dionex. Ionpac Cryptand A1 Anion Exchange Column. http://www.dionex.com/en-us/webdocs/4222-DS_IonPac_Cryptand%20A1_V30_released102706-R2.pdf.

[125] Moore, S.; Stein, W. H.Methods Enzymol. 1958, 6, 819–831.

[126] Macchi, F. D.; Shen, F. J.; Keck, R. G.; Harris, R. J. In Amino Acid Analysis Protocols; Cooper, C., Ed.; Humana: New York, 2000; pp 9–30.

[127] Weinberger, R.; Fremia, A. In Selective Sample Handling and Detection in High-Performance Liquid Chromatography; Frei, R. W.; Zech, K., Eds.; Elsevier: New York, 1988; pp 395–436.

[128] Panić, S.; Loebbecke, S.; Tuercke, T.; Antes, J.; Bošković, D. Chem. Eng. J. 2004, 101, 409–419.

[129] Majumdar, Z. K.; Sutin, J. D. B.; Clegg, R. M. Rev. Sci. Instrum. 2005, 76, 125103–1–125103–11.

[130] Falk, L.; Commenge, J. M. Chem. Eng. Sci. 2010, 65, 405–411.

[131] Hessel, V.; Löwe, H.; Schönfeld, F. Chem. Eng. Sci. 2005, 60, 2479–2501.

[132] Lee, C. Y.; Chang, C. L.; Wang, Y. N.; Fu, L. M. Int. J. Mol. Sci. 2011, 12, 3263–3287.

[133] Beisler, A. T.; Sahlin, E.; Schaefer, K. E.; Weber, S. G. Anal. Chem. 2004, 76, 639–645.

[134] Gravesen, P.; Branebjerg, J.; Jensen, O. S. J. Micromech. Microeng. 1993, 3, 168–182.

[135] The Lee Company. Lee Visco-Jet Micro Mixer. http://www.theleeco.com/electro-fluidic-systems/special-products/visco-jet-micro-mixer/visco-jet-micro-mixer.cfm. Last accessed September 8, 2014.

[136] Hypershear HPLC Mixers. http://www.tecdevexpress.com/PDF/Mixers2003_NP.pdf. Last accessed October 8, 2014.

[137] Kuban, P.; Berg, J.; Dasgupta, P. K. Anal. Chem. 2003, 75, 3549–3556.

[138] Gobby, D.; Angeli, P.; Gavriilidis, A. J. Micromech. Microeng. 2001, 11, 126–132

[139] Hessel, V.; Hardt, S.; Löwe, H.; Schönfeld, F. AIChE J. 2003, 49, 566–577.

[140] Bessoth, F. G.; DeMello, A. J.; Manz, A. Anal. Commun. 1999, 36, 213–215.

[141] Ehrfeld, W.; Golbig, K.; Hessel, V.; Löwe, H.; Richter, T. Ind. Eng. Chem. Res. 1999, 38, 1075–1082.

[142] Mengeaud, V.; Josserand, J.; Girault, H. H. Anal. Chem. 2002, 74, 4279–4286

[143] Hardt, S.; Penneman, H.; Schönfeld, F. Microfluid Nanofluid 2006, 2, 237–248

[144] Stroock, A. D.; Dertinger, S. K.; Ajdari, A.; Mezic, I.; Stone, H. A.; Whitesides, G. M. Science 2002, 295, 647–651.

[145] Stroock, A. D.; Dertinger, S. K.; Whitesides, G. M.; Ajdari, A. Anal. Chem. 2002, 74, 5306–5312.

[146] Bhagat, A. A. S.; Peterson, E. T. K.; Papautsky, I. J. Micromech. Microeng. 2007, 17, 1017–1024.

[147] Kim, D. S.; Lee, S. W.; Kwon, T. H.; Lee, S. S. J. Micromech. Microeng. 2004, 14, 798–805.

[148] Kim, D. S.; Lee, S. W.; Kwon, T. H.; Cho, D. W. J. Micromech. Microeng. 2004, 14, 1294–1301.

[149] Fournier, M. C.; Falk, L.; Villermaux J. Chem. Eng. Sci. 1996, 51, 5053–5064.

[150] Guichardon, P.; Falk, L.; Villermaux J. Chem. Eng. Sci. 2000, 55, 4245–4253.

[151] Cassidy, R. M.; Elchuk, S.; Dasgupta, P. K. Anal. Chem. 1987, 59, 85–90.

[152] Thermo Scientific/Dionex Corp. ICS-5000+ CD conductivity detector. http://www.dionex.com/en-us/products/ion-chromatography/ic-rfic-modules/detectors/ics5000-cd/lp-72689.html. Last accessed September 8, 2014.

[153] Waiz, S.; Cedillo, B. M.; Jambunathan, S.; Hohnholt, S. G.; Dasgupta, P. K.; Wolcott, D. K. Anal. Chim. Acta 2001, 428, 163–171.

[154] Al-Horr, R.; Dasgupta, P. K.; Adams, R. L. Anal. Chem. 2001, 73, 4694–4703.

[155] Liao, H.; Dasgupta, P. K.; Srinivasan, K.; Liu, Y. Anal. Chem. 2015, 87, 793–800.

[156] Li, L.; Rose, P.; Moore, P. K.Annu. Rev. Pharmacol. Toxicol. 2011, 51, 169–187.

[157] Kuban, V.; Dasgupta, P. K.Anal. Chem. 1992, 64, 1106–1112.

[158] Lottermoser, B.Mine Wastes. Characterization, Treatment and Environmental Impacts; Springer: New York, 2010.

[159] Kuban, V.; Dasgupta, P. K.; Marx, J. N. Anal. Chem. 1992, 64, 36–43.

[160] Caliendo, G.; Cirino, G.; Santagada, V.; Wallace, J. L. J. Med. Chem. 2010, 53, 6275–6286.

[161] Ma, J.; Dasgupta, P. K. Anal. Chim. Acta 2010, 673, 117–125.

[162] Yang, X.; Du, J.; Li, Y. Talanta 2015, 141, 207–211.

[163] Ma, J.; Dasgupta, P. K.; Blackledge, W.; Boss, G. R. Anal. Chem. 2010, 82, 6244–6250.

[164] Giuriati, C.; Cavalli, S.; Gorni, A.; Badocco, D.; Pastore, P. J. Chromatogr. A 2004, 1023, 105–112.

[165] NIST Webbook. http://webbook.nist.gov/cgi/cbook.cgi?ID=C7783064&Mask=10#Solubility (accessed Feb 19, 2015).

[166] Ma, J.; Dasgupta, P. K.; Blackledge, W.; Boss, G. R. Environ. Sci. Technol. 2010, 44, 3028–3034.

[167] Takeuchi, M.; Ishimine, K.; Miki, N.; Miyazaki, Y.; Tanaka, H. Presented at the 19th International Conference on Flow Injection Analysis and Related Techniques, Fukuoka, Japan, Nov 30–Dec 5, 2014; Abstract 401.

[168] Kadjo, A. F.; Dasgupta, P. K. Anal. Chim. Acta 2013, 773, 1–8.

[169] Ohira, S. I.; Kuhara, K.; Kudo, M.; Kodama, Y.; Dasgupta, P. K.; Toda, K. Anal. Chem. 2012, 84, 5421–5426.

[170] Liao, H.; Kadjo, A. F.; Dasgupta, P. K. Anal. Chem. 2015, 87, 8342-8346.

[171] Liu, Y.; Srinivasan, K.; Pohl, C.; Avdalovic, N. J. Biochem. Biophys. Methods 2004, 60, 205-232.

[172] Růžička, J.; Hansen, E. H., Mosbaek, H. Anal. Chim. Acta 1977, 92, 235-249.

[173] Rhee, J.-S.; Dasgupta, P. K. Mikrochim. Acta 1985, 87, 107-122.

[174] Dasgupta, P. K.; Chen, Y.; Serrano, C. A.; Guiochon, G.; Liu, H.; Fairchild, J. N.; Shalliker, R. A. Anal. Chem. 2010, 82, 10,143-10,150.

[175] Zini, Q.; Buldini, P. L.; Morettini, L. Microchem. J. 1985, 32, 148-152.

[176] American Society for Testing and Materials. Standard Specification of Reagent Water. ASTM D1193-06 (Reapproved 2011). www.astm.org/Standards/D1193.htm.

[177] Li, Y.; Muo, Y.; Xie, H. Anal. Chim. Acta 2002, 455, 315-325.

[178] Sabarudin, A.; Oshima, M.; Ishii, N.; Motomizu, S. Talanta 2003, 60, 1277-1285.

[179] Ma, J.; Adornato, L.; Byrne, R. H.; Yuan, D. TrAC, Trends Anal. Chem. 2014, 60, 1-15.

[180] Amornthammarong, N.; Zhang, J. Talanta 2009, 79, 621-626.

[181] Rimmelin-Maury, P.; Moutin, T.; Queguiner, B. Anal. Chim. Acta 2007, 587, 281-286.

[182] Ma, J.; Byrne, R. H. Talanta 2012, 88, 484-489.

[183] Hioki, A.; Lam, J. W. H.; Mclaren, J. W. Anal. Chem. 1997, 69, 21-24.

[184] Li, H.; Chen, F. J. Chromatogr. A 2000, 874, 143-147.

[185] Kadnar, R. J. Chromatogr. A. 1999, 850, 289-295.

[186] Lundberg, R. E.; Reynolds, W. C.; Kays, W. M. NASA Technical Note D-1972. National Aeronautics and space Administration, Washington D. C., 1972.

[187] Dasgupta, P. K. ACS Adv. Chem. Ser. 1993, 232, 41-90.

[188] Berg, J. M., James, D. L., Berg, C. F.; Toda, K.; Dasgupta, P. K. Anal. Chim. Acta 2010, 664, 56-61.

Biographical Information

Hongzhu Liao got his B.S. in chemistry from Ocean University of China in 2010. After that, He became a PhD student at University of Texas at Arlington (UTA) in 2010 fall semester. He was interested in organic chemistry and thus joined Dr. Marty Pomerantz's group. After Dr. Pomerantz had retired, Hongzhu switched to Dr. Purnendu K. Dasgupta's group in summer 2011, because he had more enthusiasm on building portable inexpensive analytical devices. Under Dr. Dasgupta's supervision, Hongzhu mainly worked on conductometric detection of very weak acids ($pK_a \geq 7.0$) in ion chromatography. He built three effective passive mixers for post-column reactions, developed volatile analyte transfer device (VATD) and permeative amine introduction device (PAID) for sensitive determination of very weak acids. During his time at UTA, Hongzhu earned 2014 summer ORISE fellowship at CDC and 2015 summer dissertation fellowship from UTA college of Science. He also earned 2015 ISCC (International Symposium on Capillary Chromatography) poster award.